Performance Comparison of Harmonically Tuned Power Amplifiers at 28 GHz in SiGe BiCMOS

Diem Thanh Phan

Thesis submitted to the faculty of the Virginia Polytechnic Institute and State University
in partial fulfillment of the requirements for the degree of

Master of Science
In
Electrical Engineering

Kwang-Jin Koh
Dong S. Ha
Sanjay Raman

Feb 02, 2017
Blacksburg, VA

Keywords: 5G, 28 GHz, class-AB, class-F, class-F^{-1}, harmonic tuned power amplifier, SiGe PA, linearity.

Performance Comparison of Harmonically Tuned Power Amplifiers at 28 GHz in SiGe BiCMOS

Diem Thanh Phan

Abstract

As the demand for wireless electronics is increasing, more and more gadgets are connected wirelessly and devices are being improved constantly. The need of the new research and development for advance electronics with high performances is the priority. The data transfer rates are improved for faster communication and better efficiency is to reduce the battery consumption in handheld devices.

This thesis presents three single-stage power amplifiers (PAs): class-AB, class-F and inverse class-F (class-F^{-1}) at 28 GHz. The PAs have identical input networks: input matching, base DC feed, and base stabilizing networks. At the load side, there is a different load network for each PA. Class-AB PA load network has a single inductor with a parasitic capacitor to create a resonance at 28GHz. Class-F PA load network is composed of a parallel network (one LC tank in series with an inductor) and a series network (one $3f_0$-resonance LC tank in series with a capacitor) to create a multi-resonance load network. Class-F^{-1} load network is composed of a parallel network (two LC tank in series with an inductor) and a series network (one $2f_0$-resonance LC tank in series with a capacitor) to have a multi-resonance network. The main purpose of using multi-resonance load networks in class-F and class-F^{-1} is to shape the collector currents and voltages in order to achieve the highest efficiency possible.

The chosen bias point is V_{CE}=2.3V and I_{CE}~12mA. As the results, class-AB PA achieves the peak PAE of 44%, 15 dBm OP_{-1dB}, >19 dBm P_{sat} , and 10 dB G_p. Class-F PA achieves the peak PAE of 46%, 14.5 dBm OP_{-1dB}, ~18 dBm P_{sat} , and 10 dB G_p. Class-F^{-1} PA achieves the peak PAE of 45%, 15.1 dBm OP_{-1dB}, >18 dBm P_{sat} , and 10 dB $G_{p.}$. In order to compare the linearity performances among three PA classes, a two-tone signal and a modulated signal with different modulation schemes (QPSK, 16QAM, 64QAM, and 256QAM) are applied to the PAs to produce IM3, ACPR, and EVM. After the analysis and comparison on efficiency and linearity, class-F PA gives the highest efficiency but has the worst linearity while class-AB has the best linearity but has the worst efficiency among three. Class-F^{-1} PA results lies in the middle of two other classes in term of efficiency and linearity.

Performance Comparison of Harmonically Tuned Power Amplifiers at 28 GHz in SiGe BiCMOS

Diem Thanh Phan

General Audience Abstract

As the demand for wireless electronics is increasing, more and more gadgets are connected wirelessly and devices are being improved constantly. The data transfer rates are improved for faster communication and better efficiency is to reduce the battery consumption in handheld devices.

A power amplifier is a very essential component in many microwave and millimeter-wave systems. This thesis presents the designs of three different RF power amplifiers (PAs), which belongs to three different types of PAs: class-AB PA, class-F PA, and inverse class-F (class-F^{-1}) PA. Each PA is designed to show distinct behaviors at a very high frequency around 28 GHz. Some portions of the designs are very identical among three classes. Three PAs have different circuit portions at the output side, which affect the performances of the PAs. There exists a capacitance from the transistor architecture, so called parasitic capacitance (C_P). In class-AB PA output, a single inductor is used to create a resonance with C_P. In class-F and class-F^{-1} PA outputs, the combination of inductors and capacitors results in resonances at fundamental frequency (f_0), second harmonic ($2f_0$), and third harmonic ($3f_0$) depending on the impedance requirements of each PA. The main purpose is to shape the voltage and current waveforms in order to obtain the highest performances possible.

The voltage and current supplied to the PA are chosen to achieve high power and efficiency at the output of the PAs. The most important parameters in PA design are efficiency and linearity. Efficiency is the effectiveness of the DC power conversion process from supplies into microwave power, which can be expressed as the ratio between output power and supplied DC power. Linearity is a term synonymous with fidelity in an audio amplifier. The term refers to the essential job of an amplifier to increase the power level of an input signal without otherwise altering the content of the signal. After the analysis and comparison on power efficiency and linearity, class-F PA gives the highest efficiency but has the worst linearity while class-AB has the best linearity but has the worst efficiency among three. Class-F^{-1} PA results lies in the middle of two other classes in term of efficiency and linearity.

Acknowledgements

I would like to express my sincere appreciation to my advisor, Dr. Kwang-Jin Koh, whose encouragement, guidance, and support throughout my work have been invaluable. I also would like to thank Dr. Dong S. Ha and Dr. Sanjay Raman for serving on my defense committee.

I am thankful for the supporting work and resources provided by my colleagues and friends in the Multifunctional Integrated Circuits and Systems (MICS) group. I would like to thank everyone in the RFIC group from Dr. Koh's for listening and giving feedbacks during weekly meetings and helping me along the way. Especially I would like to thank Dr. Dong Ho Lee and Seyed Yahya Mortazavi for giving me guidance and support throughout all my works. The path to this completion could be much more difficult without these people.

I would like to dedicate my achievements to my parents for their overwhelming love and kindness during these early years of my life. Special thanks to my brothers and sisters for supporting me working towards my degree. Last but not least, I would like to thank my friends for their support academically and personally. I don't know how I can achieve it without at least one of you.

Table of Contents

List of Figures

List of Tables

Chapter 1

Introduction

Contents

1.1 Overview of RF Front End in Wireless Systems

In order to communicate wirelessly, a radio transceiver (a combination of a transmitter and a receiver) are required as shown in Fig. 1.1. As referring to millimeter-wave (mm-w), the frequency range is identified from 30 GHz to 300 GHz, where the wavelengths range from 10 mm to 1 mm, respectively.

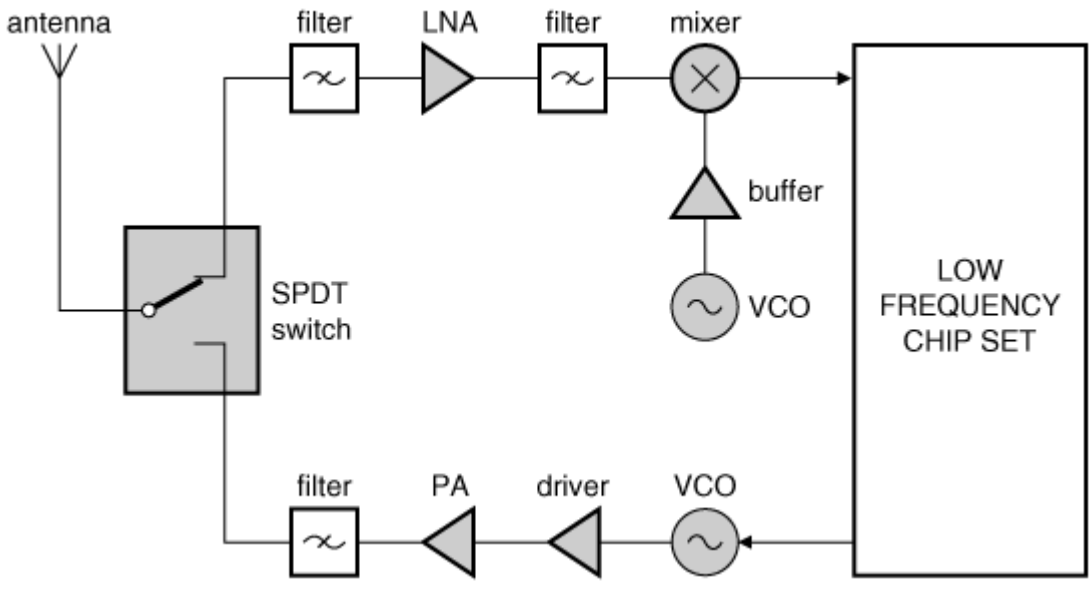

Fig. 1.1. RF generic front-end in wireless communications system [1].

Before transmitting, the data signal is modulated and mixed to a carrier frequency supplied by a local oscillator. This mixed signal is then amplified by the power amplifier and filtered before transmitted by the antenna. On the receiver side, the signal is picked up by an antenna. Due to the loss during the transmission of the signal, a noise amplifier is necessary to reduce noise and amplify the signal. This signal is then filtered and down-converted by a mixer. After being modulated, the signal should be the same as the data signal that was started on the transmitter side.

1.2 Motivation

The explosive demands on higher data-rate wireless communications lead the innovation of a next-generation of wireless communications system called 5G cellular network. The expectation for the new wireless communications systems is to provide high value of content with high quality and with interruption free data transfer. The main purpose of 5G is planned to design the best wireless world that is free from limitations and hindrance of the previous generations. 5G is going to change the way most high-bandwidth users access their mobile radio communication [2]. In addition, the potential communications systems will require to operate at very high frequencies well into the GHz ranges called millimeter wave (mm-wave) spectrum. 28 GHz and 38 GHz bands are the potential candidates for these new-generation systems as employing steerable directional antennas at both base stations and mobile devices [3]. The new wireless communications can successfully fulfill customers' expectations in handsets with and longer battery life, smaller size, and more functionalities.

With digital and high frequency capabilities, SiGe is an ideal substrate for module integration. In order to achieve higher performance (in terms of f_T), SiGe HBT's is chosen over SiGe BJT, with more details in Section 2.1. However, there is a trade off in transistor breakdown voltage when considering the complex interactions between impact-ionization and avalanche-induced [4].

Power amplifier is one of the key components in the RF chain of wireless communications systems. Designing high efficiency silicon power amplifiers for the mm-wave communication is very challenging due to the trade-off between the breakdown voltage and the maximum frequency of operation of semiconductor devices. In order to

achieve the highest efficiency, switching class amplifiers like class-F PA are highly considered. At mm-wave frequencies, a major challenge for switching amplifiers is to preserve the non-overlapping voltage and current waveforms for efficient switching mode operation [5]. It is very important to pay attention to the power efficiency of power amplifiers since PAs consume the most of the energy in telecommunication equipment's. However, wireless communication standards also impose stringent requirements on linearity performance of PAs [6].

The trade-off between efficiency and linearity in PA designs is a big challenge for RFIC design engineers. This triggered me and became my motivation to study on the performance (especially efficiency) and linearity of different PA classes. This thesis presents design procedures, compressive analysis, and the comparisons on the performance and linearity amongst three classes of PAs: class-AB, class-F, inverse class-F (class-F^{-1}) based on simulation results.

1.3 Research Goals

In this work, the target is to design three PA classes AB, F, and F^{-1} using the same bias condition including base DC supply and collector DC supply, identical input matching network, identical topology for base DC feed network. Each load network is designed for each PA based on its classification.

The first goal is to achieve high efficiency with these high frequency PAs while still carrying out other core specifications such as output power, power gain, and s-parameters. Based on the specifications, all three PAs are integrated in 8HP 0.13 μm SiGe BiCMOS technology at a high frequency, 28 GHz. Since the load network is the only different among three amplifiers, it is fair the compare the performances of classes. The comparison is focused on power efficiencies since it is the most important parameter in PA design which measures how much improvement of a designed PA. This thesis includes both theoretical analysis and simulated results on efficiency for all three PAs. The purpose is to find out which PA has the highest efficiency among three and identify some limiting factors that degrades the PA's efficiency.

The second main goal is to analyze and compare the linearity parameters of three PAs based on the simulation results. After collecting the data from 1-tone, 2-tone, modulated signal simulations, the nonlinear parameters are analyzed and estimated using different

nonlinear analysis techniques and modelling such as 50-Ω Volterra series for IP_{-1dB} and IIP_3 estimation. In order to have fair comparison on linearity among three PAs, ACPR and EVM simulations are being conducted along with intermodulation (IMD) simulation.

1.4 Thesis Organization

The thesis is organized as follows:

Chapter 1 covers the overview of the research.

Chapter 2 gives background information on the technology and the fundamental parameters in power amplifier design.

Chapter 3 describes the circuit design of the power amplifiers to achieve high efficiency along with other design requirements.

Chapter 4 covers the post-simulation review on the main performances, especially the efficiencies. Also, the performance comparison is included to evaluate the improvement in PAE from three PAs.

Chapter 5 is all about analysis and comparison on linearity based on the simulation data. By estimating and calculating some very important parameters, each amplifier shows its non-linear behaviors.

Chapter 6 concludes the thesis. Conclusions are drawn and futures works are recommended.

Chapter 2

Background

Contents

2.1 Process Technology – The SiGe HBT

Silicon (Si) is hardly the ideal semiconductor from a device designer's perspective. Si-based technologies are preferred over III-V devices (e.g., GaAs or InP) in many RF and microwave applications because of the enormous yield, lower cost, and manufacturing advantages associated with conventional Si fabrication. However, Si has small carrier mobility and the maximum velocity that these carriers can attain under high electric fields is limited to about 10^7 cm/sec under normal conditions. Si is identified as a "slow" semiconductor for this reason [7].

With all of these tradeoffs, the combination of Si and Ge is introduced with the idea of using the SiGe alloys to practice bandgap engineering in the Si material system. This is because Ge has larger lattice constant than Si so the energy bandgap of Ge is smaller than that of Si (0.66 eV vs 1.12 eV), and therefore SiGe will have a bandgap smaller than that of Si. SiGe heterojunction bipolar transistor (SiGe HBT) contains n-Si/p-SiGe emitter-base heterojunction and a p-SiGe/n-Si base-collector heterojunction shown in Fig. 3.1. The SiGe HBT represents the first practical bandgap-engineered transistor in the Si material system. SiGe HBT can be easily teamed with best-of-breed Si CMOS to form a monolithic SiGe HBT BiCMOS technology. SiGe HBT BiCMOS technologies enable system-on-a-chip

solutions across a very broad market base for both wired and wireless applications at an acceptable cost [7].

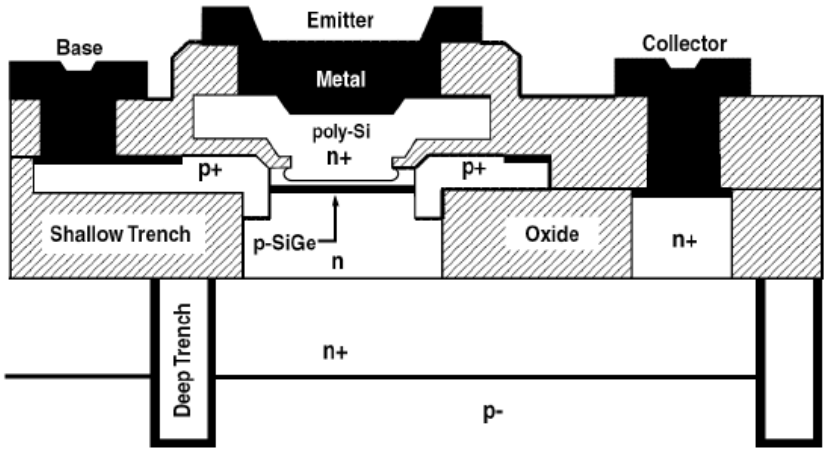

Fig. 2.1. Schematic cross section of the SiGe HBT [8].

2.2 High Frequency Harmonic Tuned Power Amplifiers

2.2.1 Class-AB Power Amplifier Classification

Class-AB PAs can be identified as power amplifiers with reduced conduction angle. Since the class-A amplifier is on the entire conduction angle, the power dissipation is more and the efficiency is capped at 50%. The class-B amplifier operates as the transistor turned off half of a period that allow the amplifier to achieve 78.5% in efficiency. As shown in Table 2.1, class-AB has the conduction angle somewhere between class-A's and class-B's and in which the output transistor turn-off for less than half of a period. From another perspective, a class AB PA is less linear than a class-A stage and more linear than a class B stage. This is usually accomplished by reducing the input voltage swing and hence backing off from the 1-dB compression point.

Table 2.1. Conduction angle and efficiency of several power amplifier classes.

Class	Conduction Angle	Collector Efficiency (%)
A	2π	50
AB	π - 2π	50 - 78.5
B	π	78.5
C	0 - π	100

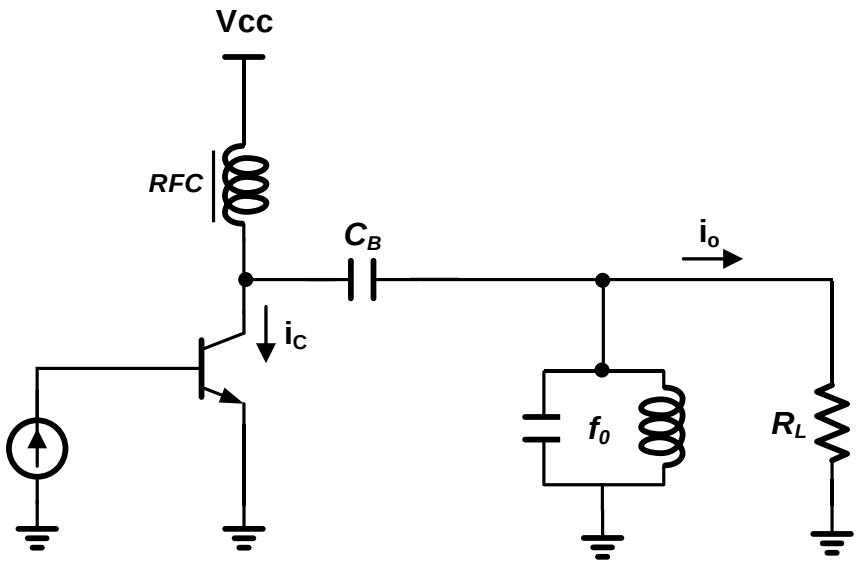

Fig. 2.2. Ideal class-AB power amplifier.

2.2.2 Class-F Power Amplifier Classification

The class-F power amplifiers utilize multiple harmonic resonators in the output network to shape the collector voltage (V_{CE}) such that the transistor switching loss is reduced and the efficiency is increased. The collector current flows when the collector voltage is low, and the collector voltage is high when the collector current is zero. Thus the result of the collector current and the collector voltage is low is reducing the power dissipation in the transistor.

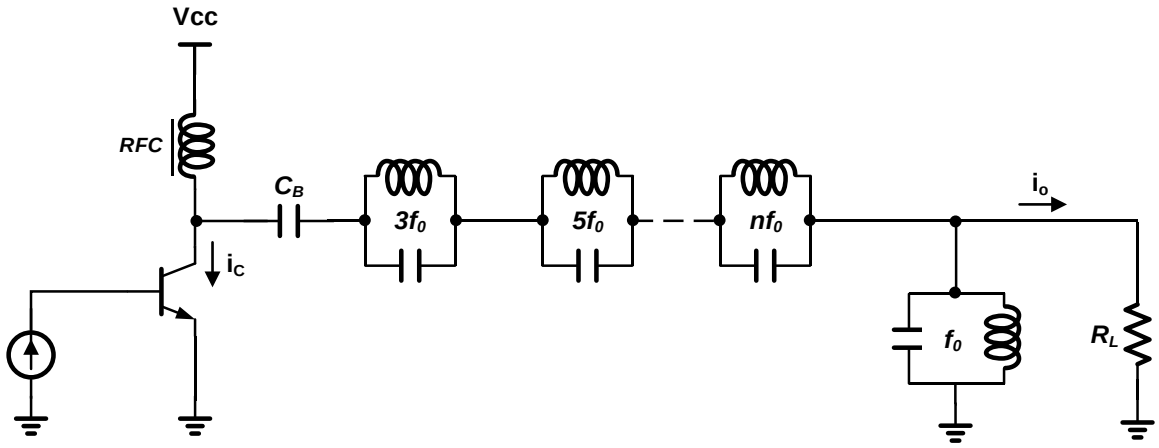

Fig. 2.3. Ideal class-F power amplifier.

In a class-F amplifier with odd harmonics, the collector voltage contains only odd harmonics and the collector current contains only even harmonics. Therefore, the input impedance of the load network is high and represents an open circuit at odd harmonics. The input impedance of the load network is low and represents a short circuit at even harmonics. The collector voltage of class F amplifiers with odd harmonics is symmetrical for the lower and upper half of the cycle, resulting a square waveform and the collector current will be a half-sine waveform as shown in Fig. 2.4 (a) [9].

The v_{CE} of odd harmonics is given by

$$v_{CE} = V_{DC} - V_1 cos\omega_0 t + \sum_{n=3,5.7,..}^{\infty} V_n \cos n\omega_0 t \quad (2.1)$$

The collector current i_C given by

$$i_C = I_{DC} - I_1 cos\omega_0 t + \sum_{n=2,4.6,..}^{\infty} I_n \cos n\omega_0 t \quad (2.2)$$

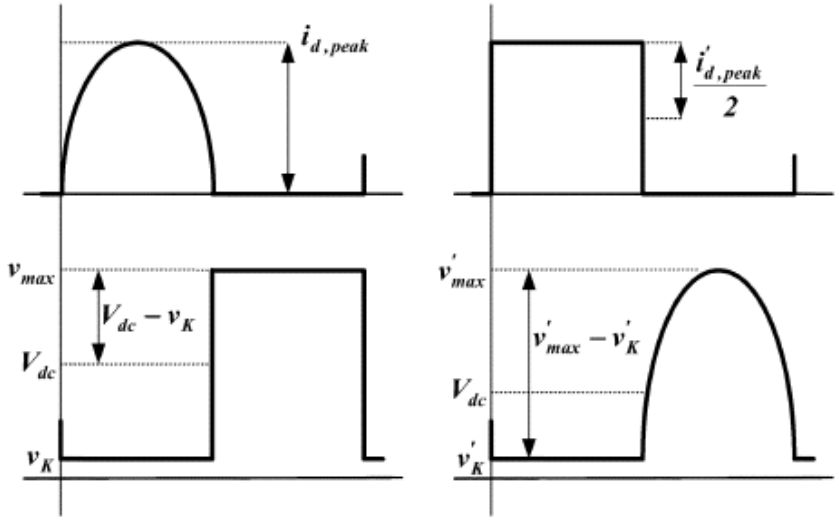

(a) (b)

Fig. 2.4. Ideal current and voltage waveforms for: (a) class-F amplifier and (b) inverse class-F amplifier [9].

2.2.3 Class-F^{-1} Power Amplifier Classification

In inverse class-F PAs, the collector voltage and current are inverted from class-F case. The collector voltage contains only even harmonics, and the collector current contains only odd harmonics. Thus, the load network represents an open circuit with high impedance at even harmonics and a short circuit with low impedance at odd harmonics. The collector of class-F amplifiers with odd harmonics is not symmetrical for the lower and upper half of the cycle.

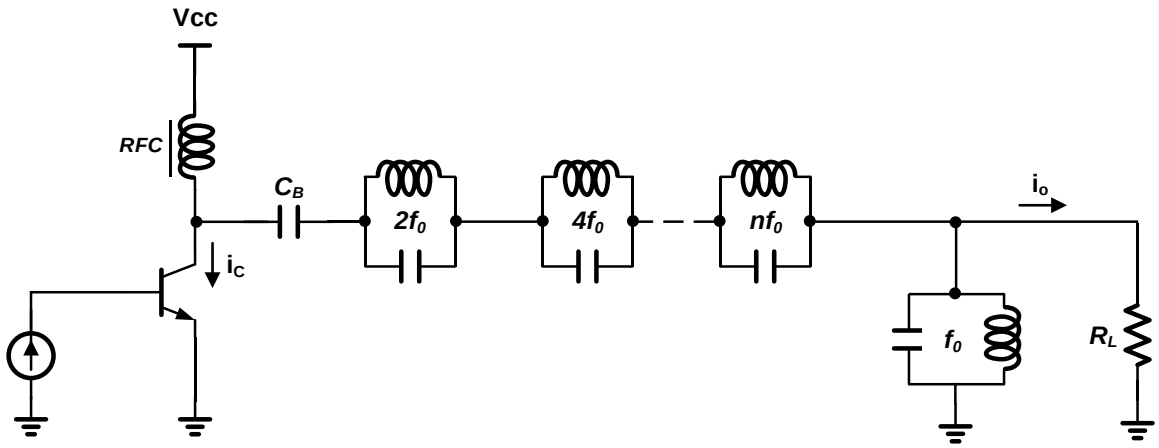

Fig. 2.5. Ideal inverse class-F power amplifier.

The even harmonics is tuning instead odd to shape the collector current to be a square waveform and the collector voltage will be a half-sine waveform as shown in Fig. 2.4 (b) [9].

The v_{CE} of even harmonics is given

$$v_{CE} = V_{DC} - V_1 cos\omega_0 t + \sum_{n=24.6,..}^{\infty} V_n \cos n\omega_0 t \tag{2.3}$$

The collector current i_C given by

$$i_C = I_{DC} - I_1 cos\omega_0 t + \sum_{n=3,5.7,..}^{\infty} I_n \cos n\omega_0 t \tag{2.4}$$

More in-depth theoretical analysis and calculations on efficiency performance and limiting factors are expressed for both class-F and inverse class-F later in Section 4.1.

2.3 Definition of Power Amplifier Parameters

2.3.1 Input power, Output Power, and Power Gain (G_p)

In a power amplifier, the input power P_{in} is the available input power at the specified frequency f in a frequency band$[f_L, f_H]$, expressed as:

$$P_{in}(f) = \frac{1}{2} Re\{V_{in} \cdot I_{in}^*\} \tag{2.5}$$

The output power P_{out} is the power delivered to the external load (50 ohm) at the same frequency,

$$P_{out}(f) = \frac{1}{2} Re\{V_{in} \cdot I_{in}^*\} \tag{2.6}$$

The PA power gain G is defined as the ratio between output power and input power:

$$G(f) = \frac{P_{out}(f)}{P_{in}(f)} \tag{2.7}$$

Power quantities are usually expressed in logarithmic scale due to the broad dynamic range of the signals involved in a PA. Power levels are usually expressed in decibels over 1 mW (dBm) by assuming 1 mW as s reference [10].

$$P_{dBm} = 10 \cdot \log_{10}\left(\frac{P}{1mW}\right) = 10 \cdot \log_{10}(P_{mW}) = 10 \cdot \log_{10}(P_{mW}) + 30$$
$$P_{mW} = 10^{\frac{P_{dBm}}{10}} \tag{2.8}$$

Power gain is expected to show its value in logarithmic scale as follows,

$$G = 10 \cdot \log_{10}(G) = P_{out,dBm} - P_{in,dBm} \tag{2.9}$$

2.3.2 -1dB Gain Compression Point (P_{-1dB})

Using power sweep (input power), output power and power gain can be graphically represented as functions of the input power in logarithmic scale. As shown in Fig. 2.6, the power gain decreases from its linear value G_L (small signal regime) down to -∞ in dB scale. This is because of nonlinear phenomena in large signal regime referred to as gain compression [10]. The point where there is a 1dB deviation in output power from the ideal linear behavior called the -1dB compression point. Input $P_{in,-1dB}$ and output $P_{out,-1dB}$ powers are clearly related through the linear power gain G_L by:

$$P_{out,-1dB} = (G_{L,dB} - 1) \cdot P_{in,-1dB} \tag{2.10}$$

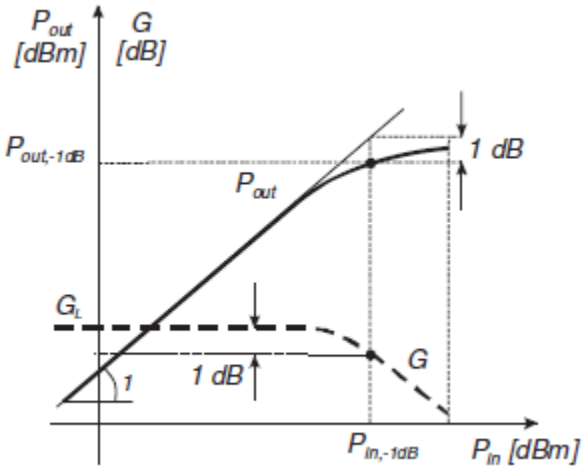

Fig. 2.6. Sample $P_{in} - P_{out}$ power sweep (continuous line) and corresponding amplifier power gain G (dashed line). From both P_{-1dB} can be derived [10].

2.3.3 Efficiency (η) and Power Added Efficiency (PAE)

Along with input power and output power, PA may be regarded to be the component to convert DC power (P_{DC}) from supplies into microwave power (P_{out}). A voltage supply can be assumed,

$$P_{DC} = V_{bias} \cdot \frac{1}{T} \cdot \int_0^T I_{bias}(t) \cdot dt \tag{2.11}$$

The effectiveness of this conversion process is measured as refering to the efficiency of an amplifier (η) which can be expressed as the ratio between output RF power and supplied DC power:

$$\eta = \frac{P_{out}}{P_{DC}} = \frac{G \cdot P_{in}}{P_{DC}} = \frac{G}{1000 \cdot P_{DC}} \cdot 10^{\frac{P_{in,dBm}}{10}} \tag{2.12}$$

As frequency increases, the PA gain decreases, as a result of its active constituents gain roll-off behaviour. The contribution to the output power coming directly from the input drive cannot therefore be neglected, since it constitutes, at microwave frequencies and beyond, a significant portion of the total. As a consequence, the added power, Padd, i.e. the net increase in the signal power from the PA input to its output, is defined as:

$$P_{add} = P_{out} - P_{in} = P_{out} \cdot \left(1 - \frac{1}{G}\right) \tag{2.13}$$

From this, a more meaningful and familiar parameter can be obtained, the *Power-Added Efficiency* (PAE). It is defined as the ratio between the added power and the supplied DC power [10]:

$$PAE = \frac{P_{add}}{P_{DC}} = \frac{P_{out} - P_{in}}{P_{DC}} = \frac{P_{out} \cdot \left(1 - \frac{1}{G}\right)}{P_{DC}} = \eta \cdot \left(1 - \frac{1}{G}\right) = \eta_{add} \tag{2.13}$$

2.3.4 Scattering Parameters

At high RF and microwave frequencies, direct measurement of Y-, Z-, or H- parameters is difficult due to unavailability of equipment to measure RF/MW total current and voltage, difficulty of obtaining perfect opens/shorts, and active devices may be unstable under open/short conditions [11].

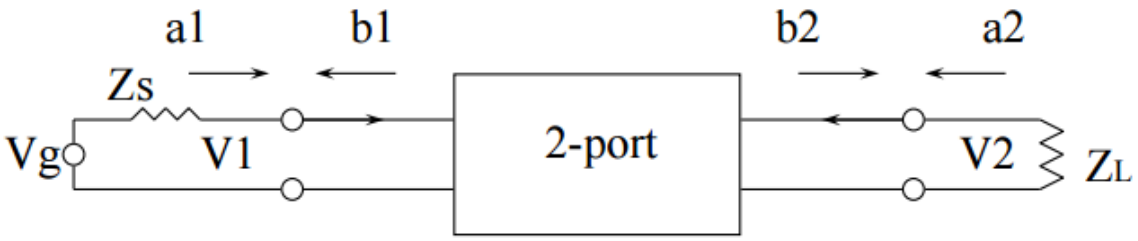

Fig. 2.7. Two-port network representation of s-parameters [11].

In two-port device there are four S-parameter S_{11}, S_{21} S_{12}, and S_{22} with a_1, a_2 are incident waves and b_1, b_2 are reflected waves as shown in Fig. 2.7. S-parameters can be arranged as follow,

$$\left.\begin{matrix} b_1 = s_{11}a_1 + s_{12}a_2 \\ b_2 = s_{21}a_1 + s_{22}a_2 \end{matrix}\right\rangle \rightarrow \begin{bmatrix} b_1 \\ b_2 \end{bmatrix} = \begin{bmatrix} s_{11} & s_{12} \\ s_{21} & s_{22} \end{bmatrix} \begin{bmatrix} a_1 \\ a_2 \end{bmatrix} \tag{2.14}$$

S-parameters can be determined from here,

$$s_{11} = \frac{b_1}{a_1}|_{a_2=0} = \frac{\text{Input reflecion coefficient } \Gamma\text{in}}{\text{for case of } Z_L = Z_0} \tag{2.15}$$

$$s_{21} = \frac{b_2}{a_1}|_{a_2=0} = \frac{\text{Forward transmission (insertion)gain}}{\text{for case of } Z_L = Z_0} \tag{2.16}$$

$$s_{12} = \frac{b_1}{a_2}|_{a_1=0} = \frac{\text{Reverse transmission (insertion)gain}}{\text{for case of } Z_S = Z_0} \tag{2.17}$$

$$s_{22} = \frac{b_2}{a_2}|_{a_1=0} = \frac{\text{Output reflecion coefficient } \Gamma\text{out}}{\text{for case of } Z_S = Z_0} \tag{2.18}$$

S-parameters can be expressed in decibels (dB), and each of them has its own meaning and can be interpret as follows,

- $s_{11} = 20\log_{10}|s_{11}|$, corresponds to the algebraic negative of the input return loss of a 2-port with a R_0 termination on the opposite port.
- $s_{12} = 20\log_{10}|s_{12}|$, is reverse isolation (active device or amplifier), or algebraic negative of the insertion loss (I.L.) for a passive device, with R_0 at ports 1 and 2.
- $s_{21} = 20\log_{10}|s_{21}|$, is power gain (active device or amplifier), or algebraic negative of the insertion loss (I.L.) for a passive device, under matched R_0 at ports 1 and 2.
- $s_{22} = 20\log_{10}|s_{22}|$, corresponds to the algebraic negative of the output return loss of a 2-port with a R_0 termination on the opposite port [11].

2.3.5 Stability Factor (k)

Stability is caused by negative resistances either at the input or output port, leading the oscillation in the circuit. Oscillation will occur if a net negative real part exists ($\mathrm{Re}\{Z_S + Z_{in}\}$ or $\mathrm{Re}\{Z_{out} + Z_L\} < 0$).

For unconditional stability:

$$\left.\begin{matrix}|\Gamma_S| < 1)\\ |\Gamma_L| < 1)\end{matrix}\right\} \text{for any passive source and load}$$

Then $|\Gamma_S\Gamma_{in}| < 1$ and $|\Gamma_L\Gamma_{out}| < 1$ in order to avoid net negative resistance, also

$$|\Gamma_{in}| = \left|s_{11} + \frac{s_{12}s_{21}\Gamma_L}{1 - s_{22}\Gamma_L}\right| < 1 \tag{2.19}$$

$$|\Gamma_{out}| = \left|s_{22} + \frac{s_{12}s_{21}\Gamma_S}{1 - s_{11}\Gamma_S}\right| < 1 \tag{2.20}$$

At high frequency (millimeter-wave), a method is needed to determine the regions in Γ_S and Γ_L that are stable. In order to make the circuit unconditionally stable, it is necessary to avoid the unstable region or modify the transistor with resistive loading [12].

For Conditional Stability:
It is also known as potentially unstable which is a usual case in circuit design where $\mathrm{Re}\{Z_{in}\}$ and $\mathrm{Re}\{Z_{out}\} > 0$ for some $|\Gamma_S| \leq 1$ and $|\Gamma_L| \leq 1$ at some specific frequencies.

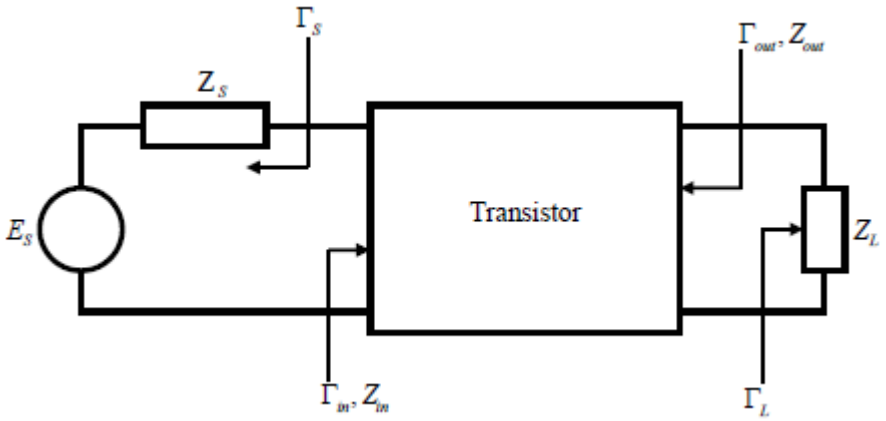

Fig. 2.8. Representation of reflection coefficients at input and output of a transistor [12].

Stability Factor (k):

$$k = \frac{1 + |s_{11}s_{22} - s_{12}s_{21}|^2 - |s_{11}|^2 - |s_{22}|^2}{2|s_{12}||s_{21}|} > 1 \tag{2.21}$$

$$\text{and} \quad |\Delta| = |s_{11}s_{22} - s_{12}s_{21}| = \det(s) < 1$$

will guarantee unconditional stability if:

- A transistor is potentially unstable, typically $|\Delta|$ <1 and 0< k <1.
- Negative k values can occur, but result in most of the Smith Chart producing instability.
- Checking for stability at all frequencies for which device has a k<1 [12].

2.4 Important Distortion Parameters in PA Design

Nonlinear behavior in a PA obviously introduces a distortion on the output voltage and current waveforms, thus degrading the quality of the information content to be transmitted. Several indicators of PA linearity have been used, depending on the system specifications and modulation schemes. Therefore, a simple third-order approximation of the PA transfer characteristic is commonly adopted,

$$y(t) = \alpha_1 x(t) + \alpha_2 x^2(t) + \alpha_3 x^3(t) \tag{2.22}$$

where $x(t)$and $y(t)$ are the input and output signal to the amplifier, α_1 is the small-signal voltage (or current) gain, and α_2, α_3 are the first two coefficients of a McLaurin series expansion of the PA transfer characteristic, truncated to third order.

Furthermore, α_1, α_2, and α_3 corresponding to the first three orders of Volterra kernels. If a single-tone excitation is assumed as the input signal with amplitude X and frequency f

$$x(t) = Xcos(2\pi f_1 t) = Xcos(\omega t) \tag{2.23}$$

Then, the output signal would become:

$$y(t) = \frac{\alpha_2 X^2}{2} + \left(\alpha_1 X + \frac{3\alpha_3 X^3}{4}\right) cos\omega t + \frac{\alpha_2 X^2}{2} cos2\omega t + \frac{\alpha_3 X^3}{4} cos3\omega t \tag{2.24}$$

2.4.1 Harmonic Distortion

The harmonic distortion due to the n-th output harmonic component, HD_{nf}, is defined in a straightforward manner by:

$$HD_{nf} = \frac{P_{out,nf}}{P_{out,f}} \tag{2.25}$$

This leads to a total harmonic distortion (THD) is defined summing up all harmonic distortion components in the output signal as:

$$THD = \sum_{n\geq 2} \frac{P_{out,nf}}{P_{out,f}} \tag{2.26}$$

Typically, these quantities are expressed in logarithmic units (decibels) over the carrier power (dBc).

2.4.2 Two-tone Intermodulation

Since the input signals to the PA is usually modulated signals rather than single-tone signals, the single-tone test is not really sufficient. Therefore, a two-tone test is used to simulate two different signals and analyze their mutual interaction in the nonlinear PA. This test also presents an insight of how the interference occurs which leads the distortion at the output. Two-tone test is much more complex than single-tone test.

In two-tone test, the input signal is given as two tones with a very close spacing at frequencies f_1 and f_2 ($f_1 < f_2$) with the amplitudes of X_1 and X_2 respectively:

$$\begin{aligned} x(t) &= X_1 \cos(2\pi f_1 t) + X_2 \cos(2\pi f_2 t) \\ &= X_1 \cos(\omega_1 t) + X_2 \cos(\omega_2 t) \end{aligned} \tag{2.27}$$

Substitute this input signal into the PA expansion in (2.22), the output signal becomes:

$$\begin{aligned} y(t) = {} & \frac{\alpha_2 {X_1}^2}{2} + \frac{\alpha_2 {X_2}^2}{2} + \left[\alpha_1 X_1 + \frac{3\alpha_3 {X_1}^3}{4} + \frac{3\alpha_3 X_1 {X_2}^2}{2}\right] \cos(\omega_1 t) \\ & + \left[\alpha_1 X_2 + \frac{3\alpha_3 {X_2}^3}{4} + \frac{3\alpha_3 {X_1}^2 X_2}{2}\right] \cos(\omega_2 t) \\ & + \frac{\alpha_2 {X_1}^3}{2} \cos(2\omega_1 t) + \frac{\alpha_2 {X_2}^2}{2} \cos(2\omega_2 t) \\ & + \alpha_2 X_1 X_2 \{\cos[(\omega_2 - \omega_1)t] + \cos[(\omega_2 + \omega_1)t]\} \\ & + \frac{\alpha_3 {X_1}^3}{4} \cos(3\omega_1 t) + \frac{\alpha_3 {X_2}^3}{4} \cos(3\omega_2 t) \\ & + \frac{3\alpha_3 {X_1}^2 X_2}{4} \{\cos[(2\omega_1 + \omega_2)t] + \cos[(2\omega_1 - \omega_2)t]\} \\ & + \frac{3\alpha_3 X_1 {X_2}^2}{4} \{\cos[(2\omega_2 + \omega_1)t] + \cos[(2\omega_2 - \omega_1)t]\} \end{aligned} \tag{2.28}$$

Table 2.2. Output components in a two-tone test grouped by the originating term in the truncated series expansion [10].

Originating Term	Output Frequencies	Corresponding Amplitude	Nomenclature
$x(t)$	$f_1,\ f_2$	$X_1,\ X_2$	*Linear term*
	$2 \cdot f_1,\ 2 \cdot f_2$	$X_1^2,\ X_2^2$	*Second harmonic*
	$dc\ (from\ f_1),\ dc\ (from\ f_2)$	$X_1^2,\ X_2^2$	*Rectified component*
$x^2(t)$	$f_1 - f_2$	$X_1 \cdot X_2$	*Second-order intermodulation*
	$f_1 + f_2$	$X_1 \cdot X_2$	*Second-order intermodulation*
	$f_1,\ f_2$	$X_1^3,\ X_2^3$	*Compression*
	$f_1,\ f_2$	$X_1 \cdot X_2^2,\ X_1^2 \cdot X_2$	*Suppression*
	$3 \cdot f_1,\ 3 \cdot f_2$	$X_1^3,\ X_2^3$	*Third harmonic*
$x^3(t)$	$2 \cdot f_1 - f_2,\ 2 \cdot f_2 - f_1$	$X_1^2 \cdot X_2,\ X_1 \cdot X_2^2$	*Third-order intermodulation*
	$2 \cdot f_1 + f_2,\ 2 \cdot f_2 + f_1$	$X_1^2 \cdot X_2,\ X_1 \cdot X_2^2$	*Third-order intermodulation*

Some output frequency components are summarized in Table 2.2. They are grouped by the term in the expansion, linear, quadratic or cubic. In order to visualize the collation of each component Fig. 2.9 displays a clear overall picture of the intermodulation products.

The latter contributions, giving rise to out-of-band and in-band components, actually exhibit a power level increase by 3 dB per dB increase of the single tones' power as shown in Table 2.2.

The most concerned issue is the harmonic contributions of the fundamental together and the second-order intermodulation. The terms at $2f_2 + f_1$ and $2f_1 + f_2$ can be eliminated by filters since they are for away from the desired parts of the output at f_1 and f_2. However, the two terms located at $2f_2 - f_1$ and $2f_1 - f_2$, called third-order intermodulation components, give a rise to Intermodulation Distortion (IMD) at the input signal frequencies f_1 and f_2 (in-band distortion). This is given by the compression and suppression terms:

$$IMD = P_{out}\left(2f_{2n(2m)} - f_{m(n)}\right) \qquad n, m = 1, 2 \tag{2.29}$$

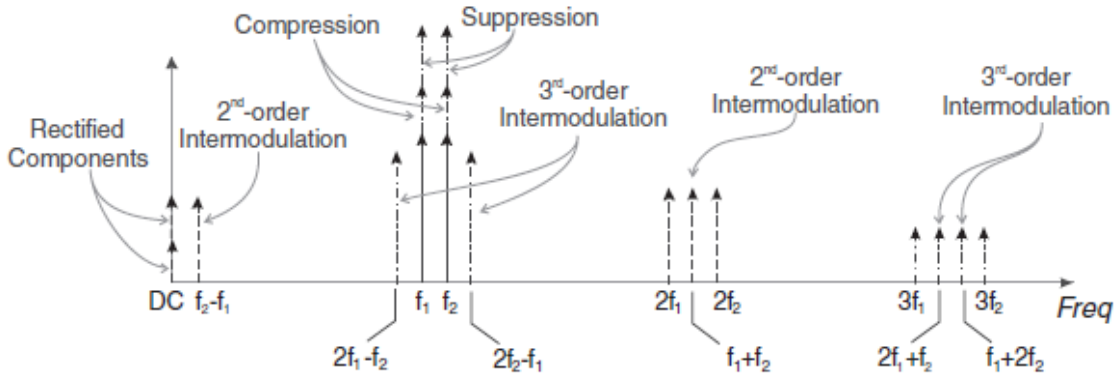

Fig. 2.9. Frequency allocation of the output components originated in a two-tone test [10].

2.4.3 Intercept Point IPn

The n-order intercept point (IPn) is defined as the input (IPnin) or output (IPnout) power level at which the n-order IMD component level equals the ideal linear output power of the PA as one of two n-order intermodulation components is sweeping one of the input tone's power as illustrated in Fig. 2.10.

The definition of IPn consists of both output signal components rising by 1dB and n dB per dB increase in input power respectively. IPn can be determined by the derivations using mathematic expressions from the parameters in Fig. 2.10 as follow:

$$\frac{n}{1} = \frac{OIPn - P_{out} + \Delta P}{OIPn - P_{out}} \tag{2.30}$$

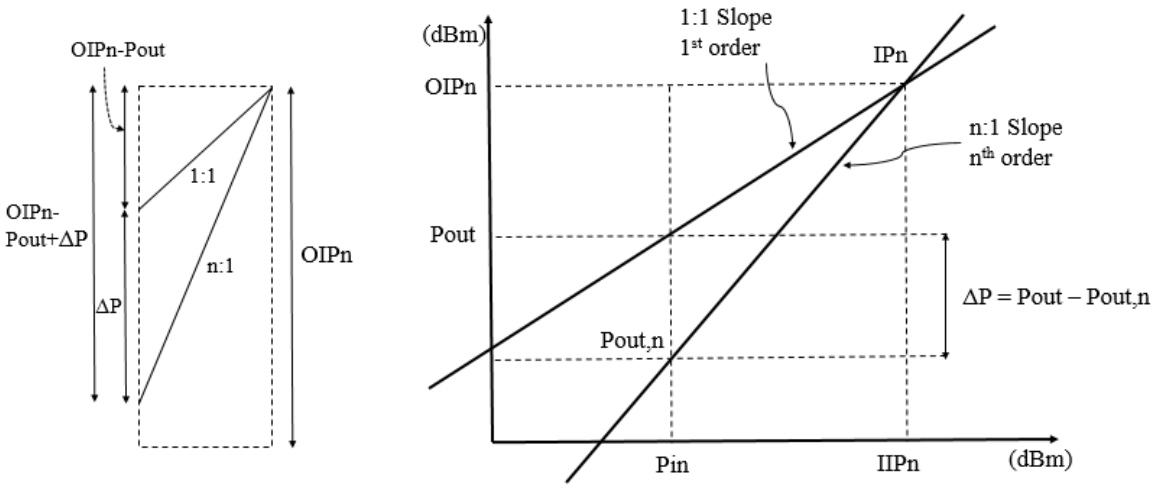

Fig. 2.10. Representation of n-order intercept point.

By rearranging (2.30), the n-order output intercept can be obtained,

$$OIPn = P_{out} + \frac{\Delta P}{n-1} \tag{2.31}$$

From here, the n-order input intercept is simply determined using the relationship between the powers and the power gain,

$$\left.\begin{matrix} P_{out} = P_{in} + G \\ OIPn = IIPn + G \end{matrix}\right\} \rightarrow IIPn = P_{in} + \frac{\Delta P}{n-1} \tag{2.32}$$

In the case that power amplifiers can be made by several cascaded stages, the total IPn can be estimated using the sum of all the terms that include the power gain (G_n) and the previous intercepts (IPn). The total IP2 and IP3 can be demonstrated as:

$$\frac{1}{IIP3_{total}^2} \approx \frac{1}{IIP3_1^2} + \frac{G_1^2}{IIP3_2^2} + \frac{G_1^2 G_2^2}{IIP3_3^2} + \frac{G_1^2 G_2^2 G_3^2}{IIP3_4^2} + \cdots + \frac{G_1^2 G_2^2 \ldots G_{n-1}^2}{IIP3_n^2} \tag{2.33}$$

$$\frac{1}{IIP2_{total}} \approx \frac{1}{IIP2_1} + \frac{G_1}{IIP2_2} + \frac{G_1 A_2}{IIP2_3} + \frac{G_1 G_2 G_3}{IIP2_4} + \cdots + \frac{G_1 G_2 \ldots G_{n-1}}{IIP2_n} \tag{2.34}$$

2.4.4 Adjacent Channel Power Ratio

In order to account for signal distortion and the related spectral regrowth in the case of band-limited input signals, an Adjacent Channel Power Ratio (ACPR) is introduced.

The total ACPR ($ACPR_{tot}$) is defined as the ratio between the total power in the signal bandwidth and the total power in adjacent channels as shown in Fig. 2.11 [10]:

$$ACPR_{tot} = \frac{P_{in-band}}{P_{adjacent-channels}} = \frac{\int_B P_{out}(f)df}{\int_{LS} P_{out}(f)df + \int_{US} P_{out}(f)df} \tag{2.35}$$

Since it is important to know ACPR of a single sideband, a Lower-Sideband ACPR ($ACPR_{LS}$) and an Upper-Sideband ACPR ($ACPR_{US}$) can be defined,

$$ACPR_{LS} = \frac{\int_B P_{out}(f)df}{\int_{LS} P_{out}(f)df} \tag{2.36}$$

$$ACPR_{US} = \frac{\int_B P_{out}(f)df}{\int_{US} P_{out}(f)df} \tag{2.37}$$

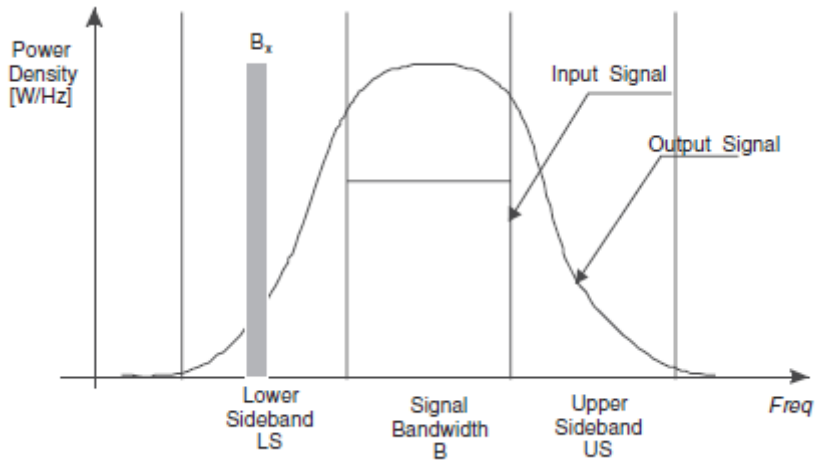

Fig. 2.11. Input and output power spectral densities for adjacent channel power ratio definitions [10].

2.4.5 Error Vector Magnitude (EVM)

The Error Vector Magnitude (EVM) is a measure used to quantify the performance of a digital radio transmitter or receiver. A signal sent by an ideal transmitter or received by a receiver would have all constellation points precisely at the ideal locations, however various imperfections in the implementation (such as carrier leakage, low image rejection ratio, phase noise etc.) cause the actual constellation points to deviate from the ideal locations as shown in Fig. 2.12.

EVM is basically a measure of the deviation of captured encoded data symbols from their ideal locations within the I/Q constellation. The root mean square EVM is a comprehensive measurement that is degraded by any imperfection in the RF signal or device. It is defined in EVM in dB as:

$$EVM\ (dB) = 10\log_{10}\left(\frac{P_{error}}{P_{ref}}\right) \tag{2.38}$$

where P_{error} is the RMS power of the error vector and P_{ref} is the outermost point in the reference signal constellation for single carrier modulations.

EVM can also defined in percentage as:

$$EVM\ (\%) = \sqrt{\frac{P_{error}}{P_{ref}}} \times 100\% \tag{2.39}$$

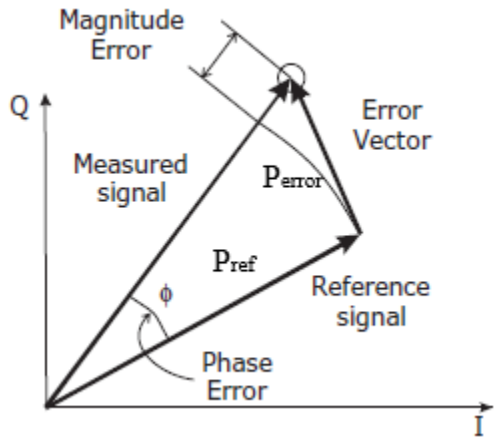

Fig. 2.12. Error vector magnitude and related quantities [10].

2.5 Load Pull and Impedance Matching

2.5.1 Introduction to Load-Pull Measurements

Fig. 2.13 shows a relationship between the output power and output impedance. Thus, a load-pull measurement can be performed to collect more than two data points. A simple load-pull set up could be the device under test with a calibrating tuner on its input and output. Source-pull can also be formed, but it shows less effective for increasing the maximum power than the load-pull [13].

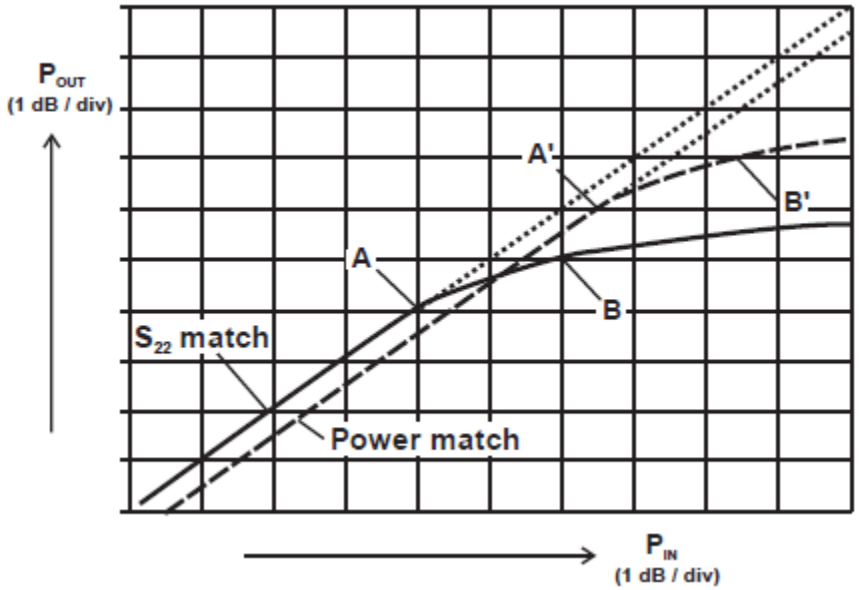

Fig. 2.13. Compression characteristics for conjugate (S_{22}) match (solid curve) and power match (dashed curve) [13].

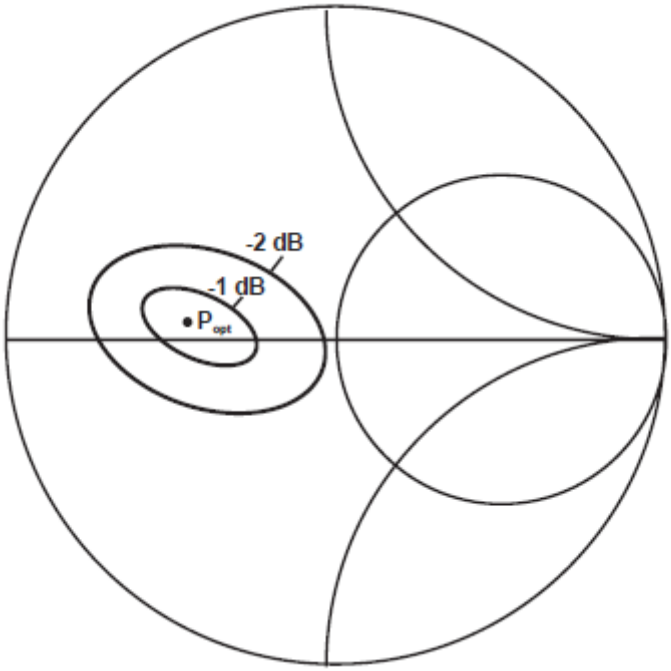

Fig. 2.14. The load-pull contours indicating the optimal output impedance on a Smith chart [13].

A typical set of load-pull data is shown in Fig. 2.14. This result shows the constant power contours indicating the specified power level on a Smith chart. The PA designers is mainly concerned with the contours which give the optimum power output such as 1dB and 2 dB contours.

Load-pull is very useful in RF and microwave power amplifier design. It gives the PA designers better ideas on what impedances to target to get the optimum performances. In power amplifier designs, two very important requirements are the output power and efficiency (PAE). Load-pull is used to find out not only the impedance at which the output power is maximum, but also the impedance where the PA can achieve its highest maximum PAE. Load-pull can be simulated in either Advance Design System (ADS) or Cadence Virtuoso.

2.5.2 Smith Chart and Impedance Matching

2.5.2.1 Smith Chart

The chart was originally conceived back in the 1930s by a Bell Laboratories engineer named Phillip Smith, who wanted an easier method of solving the tedious repetitive

equations that often appear in RF theory. His solution, appropriately named the Smith Chart, is still widely in use.

A Smith Chart is a combination of a family of circles and a family of arcs of circles. The circles of Fig. 2.15 (a) are the circles of constant resistance, where the unity circle is zero ohms. Each point on constant resistance circle has the same resistance as any other point on the circle. As the radius decreases and the center of the circle moves to the right, the resistance increases. At the rightmost point of the Smith chart, an infinite resistance can be plotted. The arcs of circles of Fig. 2.15 (b) are the circles of constant reactance. All arcs above the centerline of the chart represent +jX, or inductive reactances, and all arcs below the centerline represent −jX, or capacitive reactances. As the magnitude of the reactive component increases (−jX or +jX), the radius of each circle decreases, and the center of each circle moves closer and closer to the extreme right side of the chart. Infinite resistance and infinite reactance are represented by the same point on the chart [14].

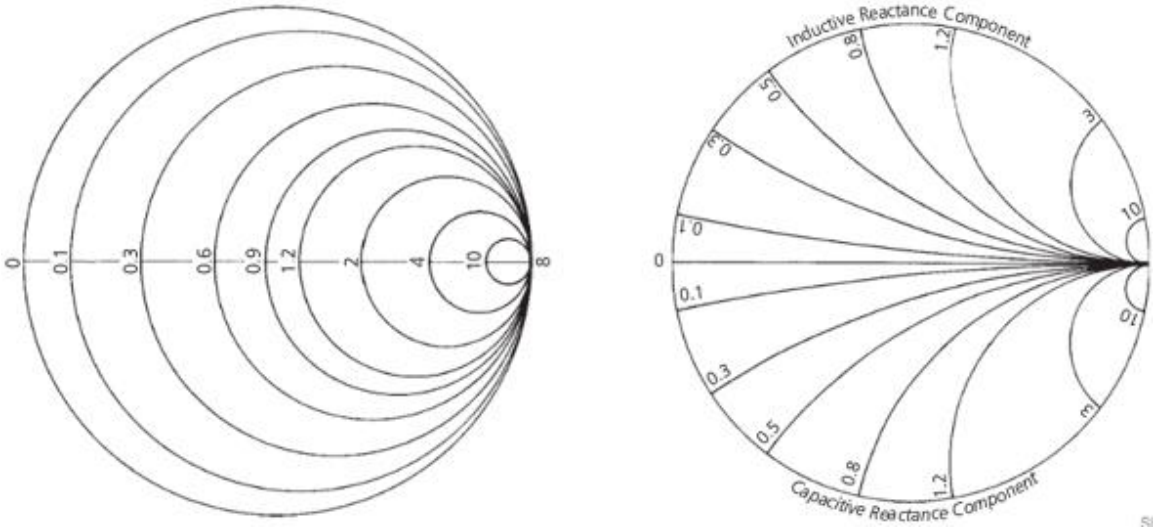

(a) (b)

Fig. 2.15. Smith Chart, (a) Constant resistance circles, (b) Constant reactance circles [14].

2.5.2.2 Impedance Matching

Since losses often occur when the radio frequency signals go through the PAs, there should be solutions to reduce these losses. In order to deliver the maximum power from the source to the load, the source resistance should equal to the load resistance according

to the maximum power transfer theorem in DC. Also, the source impedance should equal to the complex conjugate of the load impedance in AC.

Conjugate matching is considered to maximize the output delivered to the load. In RF design, this method can be applied to both the input and the output. There are two cases being considered in impedance matching.

If the impedances are purely resistive where $Z_S = R_S$ and $Z_L = R_L$. as shown in Fig. 2.16, the power delivered to the load is given by:

$$P_L = I^2 R_L = \frac{{V_S}^2 R_L}{(R_S + R_L)^2} = \frac{{V_S}^2}{\frac{R_S}{R_L} + 2R_S + R_L} \tag{2.40}$$

In order to find R_L for the maximum power $P_{L,max}$, (2.40) is differentiated with respect to R_L as:

$$\frac{\partial P_L}{\partial R_L} = \frac{\partial}{\partial R_L}\left[\frac{V^2}{\frac{R_S}{R_L} + 2R_S + R_L}\right] = 0 \tag{2.41}$$

This is only true when $R_S = R_L$. If the impedances are complex where $Z_S = R_S + X_S$ and $Z_L = R_L + X_L$, the average power delivered to the load is given by:

$$P_L = \frac{1}{2}\left(\frac{|V_S|}{|Z_S + Z_L|}\right)^2 \cdot R_L = \frac{1}{2}\frac{|V_S|^2 R_L}{(R_S + R_L)^2 + (X_S + X_L)^2} \tag{2.42}$$

Clearly the maximum power is delivered when the reactances cancel out each other ($X_S = -X_L$) with minimized loss in (2.42). If this is the case, the remaining expression is the same as in (2.40) which is purely resistive. Thus, conjugate matching ($Z_S = {Z_L}^*$) is needed to make sure the maximum possible power being delivered from a source to a load.

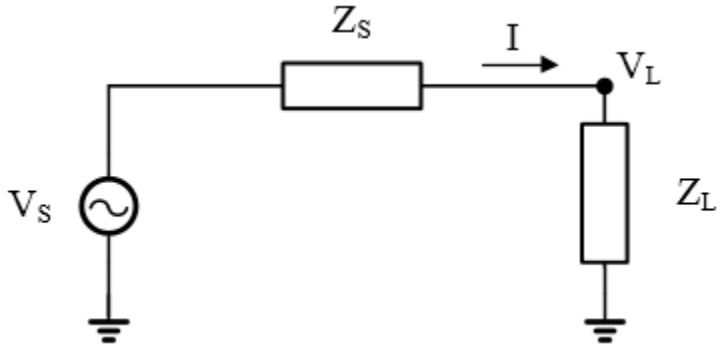

Fig. 2.16. Simple representation of source and load impedance network.

2.6 Power Efficiency Limiting Factor

2.6.1 Class-F^{-1} Power Efficiency Limiting Factors

In theory, Class-F^{-1} PA can be designed to achieve up to 100% efficiency. This can be proved with calculations. In order to form the expression for the collector voltage and current waveforms, v_n and i_n are defined to be the peak of fundamental voltage and current components at the nth harmonic. V_{DC} and I_{DC} are DC voltage and current. As in Fig. 2.17 (a), $i_1/I_{DC} = 4/\pi$ is the ratio of the ideal non-overlapped rectangular current to DC current, and $v_1/V_{DC} = \pi/2$ is the ratio of the ideal non-overlapped half-sinusoidal voltage to DC voltage. Thus, the collector efficiency can be obtained as:

$$\eta_c = \frac{1}{2}\left(\frac{i_1}{I_{DC}}\right)\left(\frac{v_1}{V_{DC}}\right) \times 100\% = \frac{1}{2}\left(\frac{4}{\pi}\right)\left(\frac{\pi}{2}\right) \times 100\% = 100\% \tag{2.38}$$

2.6.1.1 Class-F^{-1} Finite Number of Harmonics

The series expansion of the voltage and current waveforms can be expressed with an infinite number of harmonics in the ideal condition. However, the number of harmonics is limited in practical situation due to the limited band, leading to the overlaps of voltage and current as shown in Fig. 2.17(b). The components at the harmonic higher than the third harmonic do not have much contribution in the waveform shaping. Therefore, the voltage and current waveforms are illustrated using sinusoidal expressions up to the third harmonic for the maximum efficiency [15, 16].

$$v_C(\varphi) = V_{DC}\left(1 - \sqrt{2}cos\varphi + \frac{1}{2}cos2\varphi\right) \tag{2.39}$$

and

$$i_C(\varphi) = I_{DC}\left(1 - \frac{2}{\sqrt{3}}cos\varphi + \frac{1}{3\sqrt{3}}cos3\varphi\right) \tag{2.40}$$

From the equations (2.39) and (2.40), the maximum efficiency is calculated as:

$$\eta_{c,max} = \frac{1}{2}\left(\frac{i_1}{I_{DC}}\right)\left(\frac{v_1}{V_{DC}}\right) = \frac{1}{2} \times \frac{2}{\sqrt{3}} \times \sqrt{2} = 0.816. \tag{2.41}$$

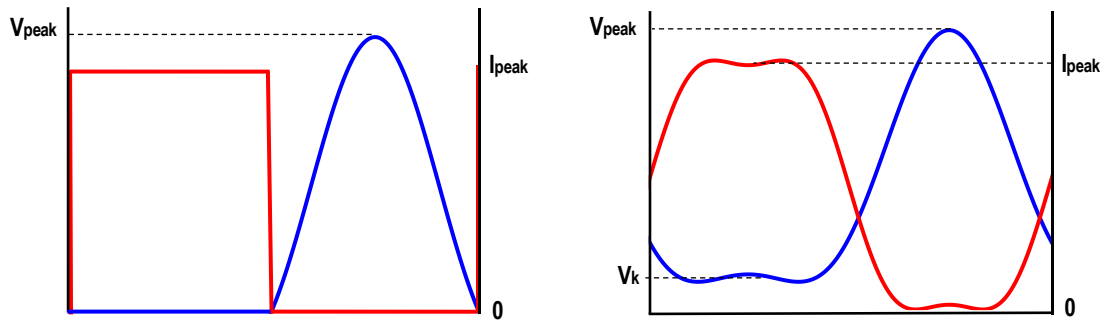

(a) (b)

Fig. 2.17. (a) Class-F^{-1} ideal non-overlapped IV waveforms. (b) Class-F^{-1} overlapped IV waveforms with finite number of harmonic control and finite knee voltage.

2.6.1.2 Class-F^{-1} Knee Voltage, V_k

The knee voltage (V_k) is one of the factors limiting the efficiency of amplifiers in Fig. 2.17.(b). In order to analyze the effect of V_k on the efficiency, the equation (2.39) can be rewritten as follow:

$$v_C(\varphi) = V_{DC} - v_1 cos\varphi + v_2 cos2\varphi \tag{2.42}$$

The half-sinusoidal voltage waveform can achieve the maximum flatness when the minimum points represent the knee voltage points. This implies the minimum collector voltage $v_{C,min}(\varphi) = V_k$. Assume φ_0 is the angle where the collector voltage reaches in minimum points, the equation (2.42) can be expressed as follow:

$$V_{DC} - v_1 cos\varphi_0 + v_2 cos2\varphi_0 = V_k \tag{2.43}$$

The minimum points of the collector voltage need to satisfy the following condition:

$$\frac{\partial v_C(\varphi)}{\partial \varphi} = 0 \; at \; \varphi = \varphi_0 \text{ where } -\pi \le \varphi_0 \le \pi$$

$$\rightarrow v_1 sin\varphi_0 - 2v_2 sin2\varphi_0 = 0 \rightarrow \begin{cases} cos\varphi_o = \dfrac{v_1}{4v_2}, & if \dfrac{v_2}{v_1} > \dfrac{1}{4} \\ \varphi_o = 0, & if \dfrac{v_2}{v_1} < \dfrac{1}{4} \end{cases} \tag{2.44}$$

Substituting (2.44) into (2.43) obtains

$$\begin{cases} V_{DC} - v_1 \dfrac{v_1}{4v_2} + 2v_2 \left(\dfrac{v_1}{4v_2}\right)^2 - v_2 = V_k, \\ V_{DC} - v_1 + v_2 = V_k, \end{cases} \rightarrow \begin{cases} 1 - \dfrac{V_k}{V_{DC}} = \dfrac{V_1}{V_{DC}} \left(\dfrac{v_1}{8v_2} + \dfrac{v_2}{v_1}\right), if \dfrac{v_2}{v_1} > \dfrac{1}{4} \\ 1 - \dfrac{V_k}{V_{DC}} = \dfrac{V_1}{V_{DC}} \left(1 - \dfrac{v_2}{v_1}\right), \quad if \dfrac{v_2}{v_1} < \dfrac{1}{4} \end{cases}$$

$$\rightarrow \begin{cases} \frac{V_1}{V_{DC}} = \left(1 - \frac{V_k}{V_{DC}}\right)\left(\frac{v_1}{8v_2} + \frac{v_2}{v_1}\right)^{-1}, & if\ \frac{v_2}{v_1} > \frac{1}{4} \\ \frac{V_1}{V_{DC}} = \left(1 - \frac{V_k}{V_{DC}}\right)\left(1 - \frac{v_2}{v_1}\right)^{-1}, & if\ \frac{v_2}{v_1} < \frac{1}{4} \end{cases} \quad (2.42)$$

The collector efficiency η_c becomes

$$\eta_c = \frac{1}{2} \times \frac{2}{\sqrt{3}} \times \begin{cases} \left(1 - \frac{V_k}{V_{DC}}\right)\left(\frac{v_1}{8v_2} + \frac{v_2}{v_1}\right)^{-1}, & if\ \frac{v_2}{v_1} > \frac{1}{4} \\ \left(1 - \frac{V_k}{V_{DC}}\right)\left(1 - \frac{v_2}{v_1}\right)^{-1}, & if\ \frac{v_2}{v_1} < \frac{1}{4} \end{cases} \quad (2.43)$$

When $v_2/v_1 = 1/2\sqrt{2}$, the maximum efficiency $\eta_{c,max}$ occurs

$$\eta_{c,max} = 0.816 \times \left(1 - \frac{V_k}{V_{DC}}\right) \quad (2.44)$$

As the results, the collector voltage waveforms with the knee voltage will be

$$v_C(\varphi) = V_{DC}\left\{1 - \sqrt{2}\left(1 - \frac{V_k}{V_{DC}}\right)cos\varphi + \frac{1}{2}\left(1 - \frac{V_k}{V_{DC}}\right)cos2\varphi\right\} \quad (2.45)$$

In this thesis, the supply voltage $V_{DC} = 2.3\ V$ is applied to the collector of the transistor. The process technology being used has the knee voltage $V_k \approx 0.4\ V$. Thus, the theoretical maximum collector efficiency becomes $\eta_{c,max} \approx 67.4\%$.

2.6.1.3 Class-F^{-1} Transistor Breakdown Voltage, V_{BK}

Beside the knee voltage, the breakdown voltage of the device could affect the efficiency of the amplifiers. This breakdown voltage create an upper-bound of the collector voltage, corresponding to the maximum points of the waveforms. From (2.42), the collector voltage reaches the maximum at $\varphi = \pm\pi$ (V_{BK}).

$$v_{C,max} = V_{DC} + v_1 + v_2 = V_{BK} \quad (2.46)$$

In order to find the relationship among the knee voltage, breakdown voltage and the collector voltage, both side of (2.46) can be subtracted by V_k

$$V_{DC} + v_1 + v_2 - V_k = V_{BK} - V_k$$

$$\rightarrow 1 - \frac{V_k}{V_{DC}} = \frac{V_{BK}}{V_{DC}}\left(1 - \frac{V_k}{V_{BK}}\right) - \frac{v_1}{V_{DC}}\left(1 + \frac{v_2}{v_1}\right) \quad (2.47)$$

The maximum collector efficiency occurs when $\frac{v_1}{V_{DC}} = \sqrt{2}\left(1 - \frac{V_k}{V_{DC}}\right)$ and $\frac{v_2}{v_1} = \frac{1}{2\sqrt{2}}$.. (2.47) becomes

$$1-\frac{V_k}{V_{DC}}=\frac{V_{BK}}{V_{DC}}\left(1-\frac{V_k}{V_{BK}}\right)-\left(1-\frac{V_k}{V_{DC}}\right)\left(\sqrt{2}+\frac{1}{2}\right)$$

$$\rightarrow 1-\frac{V_k}{V_{DC}}=\frac{1}{\sqrt{2}+\frac{3}{2}}\times\frac{V_{BK}}{V_{DC}}\left(1-\frac{V_k}{V_{BK}}\right)\approx 0.343\times\frac{V_{BK}}{V_{DC}}\left(1-\frac{V_k}{V_{BK}}\right) \quad (2.48)$$

Substituting (2.48) into (2.44) gives

$$\eta_{c,max}=0.816\times 0.343\times\frac{V_{BK}}{V_{DC}}\left(1-\frac{V_k}{V_{BK}}\right)=0.28\times\frac{V_{BK}}{V_{DC}}\left(1-\frac{V_k}{V_{BK}}\right) \quad (2.49)$$

Similar to the estimation in the previous section 2.6.1.2, the maximum collector efficiency with the effect of knee voltage ($V_k \approx$ 0.4V) and breakdown voltage (V_{BK} =5.9V) becomes $\eta_{c,max} \approx$ 67%.

2.6.1.4 Class-F^{-1}Load Network Losses

The passive components used in the load network are real components from the library of the given technology. The parasitic resistances due to high Q in the passive components can causes losses in the load network. R_p and R_s are defined as the resistances in the parallel load network and the series load network respectively. These resistances cause losses in both voltage and current, leading to the dissipated power or power loss (P_{loss}). Assuming the optimum load resistance is R_{opt}, the power loss can be expressed as

$$P_{loss}=\text{current loss}\times\text{voltage loss}=\left(\frac{R_p}{R_p+R_s+R_{opt}}\right)\times\left(\frac{R_{opt}}{R_s+R_{opt}}\right) \quad (2.50)$$

As the result, the maximum collector efficiency becomes $\eta_{c,max}\times P_{loss}$.

2.6.1.5 Class-F^{-1} Effects of Higher-order Harmonics

Observing the IV waveforms and the spectrums in section 4.1.3, the collector current shows the noticeable fifth-harmonic component. As the suggestion from [17], the collector current can be express the following in order to achieve the maximally flat waveform.

$$i_C(\varphi)\cong I_{DC}(1-1.207\cdot cos\varphi+0.28\cdot cos3\varphi-0.073\cdot cos5\varphi) \quad (2.51)$$

In this current expression, the fundamental to DC current component ratio i_1/I_{DC} = 1.207 instead of $2/\sqrt{3}$ or 1.155 as in (2.40) and the maximum collector efficiency becomes $\eta_{c,max} \approx$ 70 % instead of 67%.

2.6.2 Class-F Power Efficiency Limiting Factors

As in class-F^{-1} PA, class-F can achieve up to 100% efficiency ideally. As in Fig. 2.18 (a), $i_1/I_{DC} = \pi/2$ is the ratio of the ideal non-overlapped half-sinusoidal current to DC current, and $v_1/V_{DC} =$ is the ratio of the ideal non-overlapped rectangular voltage to DC voltage. Thus, the collector efficiency can be obtained as:

$$\eta_c = \frac{1}{2}\left(\frac{i_1}{I_{DC}}\right)\left(\frac{v_1}{V_{DC}}\right) \times 100\% = \frac{1}{2}\left(\frac{\pi}{2}\right)\left(\frac{4}{\pi}\right) \times 100\% = 100\% \tag{2.52}$$

2.6.2.1 Class-F Finite Number of Harmonics

The number of harmonics is limited in practical situation due to the limited band, leading to the overlaps of voltage and current as shown in Fig. 2.18(b). The voltage and current waveforms are illustrated using polynomial expressions up to the third harmonic for the maximum efficiency [15, 16].

$$v_C(\varphi) = V_{DC}\left(1 - \frac{2}{\sqrt{3}}cos\varphi + \frac{1}{3\sqrt{3}}cos3\varphi\right) \tag{2.53}$$

and

$$i_C(\varphi) = I_{DC}\left(1 - \sqrt{2}cos\varphi + \frac{1}{2}cos2\varphi\right) \tag{2.54}$$

From the equations (2.39) and (2.40), the maximum efficiency is calculated as:

$$\eta_{c,max} = \frac{1}{2}\left(\frac{i_1}{I_{DC}}\right)\left(\frac{v_1}{V_{DC}}\right) = \frac{1}{2} \times \sqrt{2} \times \frac{2}{\sqrt{3}} = 0.816. \tag{2.55}$$

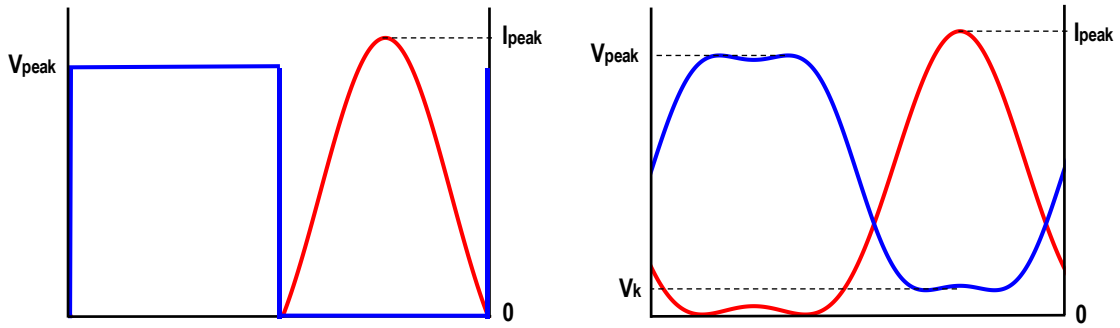

(a) (b)

Fig. 2.18. (a) Class-F ideal non-overlapped IV waveforms. (b) Class-F overlapped IV waveforms with finite number of harmonic control and finite knee voltage.

2.6.2.2 Class-F Finite Knee Voltage, V_k

In order to analyze the effect of V_k on the efficiency of class-F PA, the equation (2.53) can be rewritten as follow:

$$v_C(\varphi) = V_{DC} - v_1 cos\varphi + v_3 cos3\varphi \tag{2.56}$$

The rectangular voltage waveform can achieve the maximum flatness when the minimum points represent the knee voltage points. This implies the minimum collector voltage $v_{C,min}(\varphi) = V_k$. Assume φ_0 is the angle where the collector voltage reaches in minimum points, the equation (2.56) can be expressed as follow:

$$V_{DC} - v_1 cos\varphi_0 + v_3 cos3\varphi_0 = V_k \tag{2.57}$$

The minimum points of the collector voltage need to satisfy the following condition:

$$\frac{\partial v_C(\varphi)}{\partial \varphi} = 0 \; at \; \varphi = \varphi_0 \text{ where } -\pi \le \varphi_0 \le \pi$$

$$\rightarrow v_1 sin\varphi_0 - 3v_2 sin3\varphi_0 = 0$$

$$\rightarrow \begin{cases} cos\varphi_o = \left[\frac{1}{12}\left(3 + \frac{v_1}{v_3}\right)\right]^{1/2}, & if \frac{v_3}{v_1} > \frac{1}{9} \\ \varphi_o = 0, & if \frac{v_3}{v_1} < \frac{1}{9} \end{cases} \tag{2.58}$$

Substituting (2.58) into (2.57) gives

$$\begin{cases} 1 - \frac{V_k}{V_{DC}} = \frac{v_1}{V_{DC}} \left\{ \left[\frac{1}{12}\left(3 + \frac{v_1}{v_3}\right)\right]^{\frac{1}{2}} - \frac{v_3}{v_1}\left(4 \times \left[\frac{1}{12}\left(3 + \frac{v_1}{v_3}\right)\right]^{3/2} - 3 \times \left[\frac{1}{12}\left(3 + \frac{v_1}{v_3}\right)\right]^{1/2}\right) \right\}, \\ V_{DC} - v_1 + v_3 = V_k, \end{cases}$$

$$\rightarrow \begin{cases} 1 - \frac{V_k}{V_{DC}} = \frac{v_1}{V_{DC}} \left[\frac{1}{12}\left(3 + \frac{v_1}{v_3}\right)\right]^{1/2} \left(\frac{2}{3} + 2\frac{v_3}{v_1}\right), if \frac{v_3}{v_1} > \frac{1}{9} \\ 1 - \frac{V_k}{V_{DC}} = \frac{V_1}{V_{DC}}\left(1 - \frac{v_3}{v_1}\right), \quad if \frac{v_3}{v_1} < \frac{1}{9} \end{cases}$$

$$\rightarrow \begin{cases} \frac{v_1}{V_{DC}} = \left(1 - \frac{V_k}{V_{DC}}\right)\left[\left[\frac{1}{12}\left(3 + \frac{v_1}{v_3}\right)\right]^{1/2} \left(\frac{2}{3} + 2\frac{v_3}{v_1}\right)\right]^{-1}, if \frac{v_3}{v_1} > \frac{1}{4} \\ \frac{v_1}{V_{DC}} = \left(1 - \frac{V_k}{V_{DC}}\right)\left(1 - \frac{v_3}{v_1}\right)^{-1}, \quad if \frac{v_3}{v_1} < \frac{1}{4} \end{cases} \tag{2.59}$$

The maximum efficiency happens when v_2/v_1=1/6, thus (2.58) becomes

$$\frac{v_1}{V_{DC}} = \left(1 - \frac{V_k}{V_{DC}}\right)\left[\left(\frac{3}{4}\right)^{1/2}\right]^{-1} = \frac{2}{\sqrt{3}}\left(1 - \frac{V_k}{V_{DC}}\right) \tag{2.60}$$

The maximum collector efficiency $\eta_{c,max}$ becomes

$$\eta_{c,max} = \frac{1}{2} \times \sqrt{2} \times \frac{2}{\sqrt{3}}\left(1 - \frac{V_{knee}}{V_{DC}}\right) = 0.816 \times \left(1 - \frac{V_{knee}}{V_{DC}}\right) \tag{2.61}$$

As the results, the collector voltage waveforms with the knee voltage will be

$$v_C(\varphi) = V_{DC}\left\{1 - \frac{2}{\sqrt{3}}\left(1 - \frac{V_k}{V_{DC}}\right)cos\varphi + \frac{1}{3\sqrt{3}}\left(1 - \frac{V_k}{V_{DC}}\right)cos3\varphi\right\} \tag{2.62}$$

In this thesis, the supply voltage $V_{DC} = 2.3\,V$ is applied to the collector of the transistor. The process technology being used has the knee voltage $V_k \approx 0.4\,V$. Thus, the theoretical maximum collector efficiency becomes $\eta_{c,max} \approx 67.4\%$.

2.6.2.3 Class-F Maximum Collector Voltage Swing, $V_{C,\,max}$

Beside the knee voltage, the breakdown voltage of the device could affect the efficiency of the amplifiers. This breakdown voltage creates an upper-bound of the collector voltage, corresponding to the maximum points of the waveforms. From (2.56), the collector voltage reaches the maximum at $\varphi = 2\pi/3$.

$$v_{C,max} = V_{DC} + \frac{1}{2}v_1 + v_3 \tag{2.63}$$

In order to find the relationship among the knee voltage, breakdown voltage and the collector voltage, both side of (2.46) can be subtracted by V_k

$$V_{DC} + v_1 + v_2 - V_k = v_{C,max} - V_k$$

$$\rightarrow 1 - \frac{V_k}{V_{DC}} = \frac{v_{C,max}}{V_{DC}}\left(1 - \frac{V_k}{v_{C,max}}\right) - \frac{V_1}{V_{DC}}\left(\frac{1}{2} + \frac{v_3}{v_1}\right) \tag{2.64}$$

The maximum collector efficiency occurs when $\frac{v_1}{V_{DC}} = \frac{2}{\sqrt{3}}\left(1 - \frac{V_k}{V_{DC}}\right)$ and $\frac{v_3}{v_1} = 1/6$, then (2.64) becomes

$$1 - \frac{V_k}{V_{DC}} = \frac{v_{C,max}}{V_{DC}}\left(1 - \frac{V_k}{v_{C,max}}\right) - \frac{4}{3\sqrt{3}}\left(1 - \frac{V_k}{V_{DC}}\right)$$

$$\rightarrow 1 - \frac{V_k}{V_{DC}} = \frac{3\sqrt{3}}{3\sqrt{3} + 4} \times \frac{v_{C,max}}{V_{DC}}\left(1 - \frac{V_k}{v_{C,max}}\right) \approx 0.565 \times \frac{v_{C,max}}{V_{DC}}\left(1 - \frac{V_k}{v_{C,max}}\right) \tag{2.65}$$

Substituting (2.65) into (2.61) gives

$$\eta_{c,max} = 0.816 \times 0.565 \times \frac{v_{C,max}}{V_{DC}}\left(1 - \frac{V_k}{v_{C,max}}\right)$$
$$= 0.461 \times \frac{v_{C,max}}{V_{DC}}\left(1 - \frac{V_k}{v_{C,max}}\right). \quad (2.66)$$

Unlike in class-F^{-1}, the maximum collector voltage swing $v_{C,max}$ of class-F PA will be smaller the breakdown voltage because the maximum efficiency can exceed 100% at $v_{C,max} = V_{BK}$. This leads to a conclusion that class-F has limited voltage swing due to the waveform shaping. The maximum swing can be referred back to the result in the expression (2.60) since the there is no effect of the breakdown voltage in this class-F design.

2.6.2.4 Class-F Load Network Losses

The passive components used in the load network are real components from the library of the given technology. The parasitic resistances due to high Q in the passive components can causes losses in the load network. R_p and R_s are defined as the resistances in the parallel load network and the series load network respectively. These resistances cause losses in both voltage and current, leading to the dissipated power or power loss (P_{loss}). Assume the optimum load resistance is R_{opt}, the power loss can be expressed as

$$P_{loss} = \text{current loss} \times \text{voltage loss} = \left(\frac{R_p}{R_p + R_s + R_{opt}}\right) \times \left(\frac{R_{opt}}{R_s + R_{opt}}\right) \quad (2.67)$$

As the result, the maximum collector efficiency becomes $\eta_{c,max} \times P_{loss}$.

2.6.2.5 Class-F Effects of Higher-order Harmonics

Observing the IV waveforms and the spectrums in section 4.2.3, the collector current shows the noticeable fifth-harmonic component. As the suggestion from [17], the collector current can be express the following in order to achieve the maximally flat waveform.

$$i_C(\varphi) \cong I_{DC}(1 - 1.5 \cdot cos\varphi + 0.583 \cdot cos2\varphi - 0.083 \cdot cos4\varphi) \quad (2.68)$$

In this current expression, the fundamental to DC current component ratio i_1/I_{DC} = 1.5 instead of $\sqrt{2}$ or 1.414 as in (2.54) and the maximum collector efficiency becomes $\eta_{c,max} \approx$ 71.5 % instead of 67.4%.

2.6.3 Class-AB Power Efficiency Limiting Factors

2.6.3.1 Class-AB Finite Knee Voltage, V_k

As two other classes, the maximum efficiency of class-AB also gets affected by the knee voltage, leading to the expression [13]:

$$\eta_c = \left(1 - \frac{V_k}{V_{DC}}\right)\eta_{ideal} \tag{2.69}$$

2.6.3.2 Class-AB Conduction Angle

The output current waveform can be expanded into its Fourier series components:

$$i_C(\varphi) = I_{DC} + I_1 cos\varphi + I_2 cos2\varphi + I_3 cos3\varphi \tag{2.70}$$

The expansion coefficients I_n as illustrated in Fig. 2.19. are given by

$$I_n = \begin{cases} \frac{I_{max}}{2\pi}.\frac{2\sin\left(\frac{\alpha}{2}\right) - \alpha\cos\left(\frac{\alpha}{2}\right)}{1-\cos\left(\frac{\alpha}{2}\right)} & \text{when } n = 0 \\ \frac{I_{max}}{2\pi}.\frac{\alpha - \sin(\alpha)}{1-\cos\left(\frac{\alpha}{2}\right)} & when\ n = 1 \\ \frac{2I_{max}}{2\pi}.\frac{\sin\left(n\frac{\alpha}{2}\right)\cos\left(\frac{\alpha}{2}\right) - n\sin\left(\frac{\alpha}{2}\right)cos\left(n\frac{\alpha}{2}\right)}{n(n^2-1)[1-\cos\left(\frac{\alpha}{2}\right)]} & when\ n \geq 2 \end{cases} \tag{2.71}$$

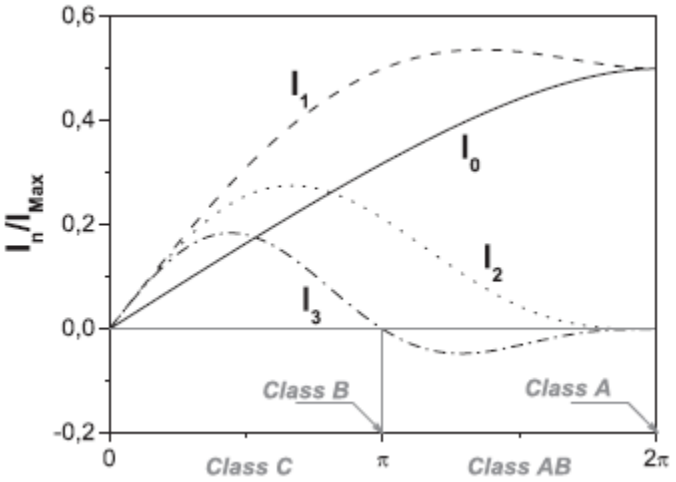

Fig. 2.19. Current components normalized to the device maximum current as functions of conduction angle α.

$$i_C(\varphi) = I_{DC} + I_1 cos\varphi + I_2 cos2\varphi + I_3 cos3\varphi \tag{2.70}$$(2.70)

As suggested in [10], the DC power P_{DC}, the output power at the fundamental frequency P_{RF} and collector efficiency η_c for class-A PA are expressed

$$P_{DC,A} = V_{DC}.\frac{I_{Max}}{2} \tag{2.71}$$

$$P_{RF,A} = \frac{1}{2}.\frac{I_{Max}}{2}(V_{DC} - V_k) \tag{2.72}$$

$$\rightarrow \eta_{c,A} = \frac{1}{2}\left(1 - \frac{V_k}{V_{DC}}\right) \tag{2.73}$$

The collector efficiency of class-AB PA depends on the conduction angle. As normalized to the class-A reference values, the collector efficiency expression can be constructed based on (2.71) - (2.73) and in term of the conduction angle α:

$$P_{DC} = V_{DC}.I_{DC} = \frac{P_{DC,A}}{\pi}.\frac{2\sin\left(\frac{\alpha}{2}\right) - \alpha\cos\left(\frac{\alpha}{2}\right)}{1 - \cos\left(\frac{\alpha}{2}\right)} \tag{2.74}$$

$$P_{RF} = \frac{I_1 V_1}{2} = \frac{P_{RF,A}}{\pi}.\frac{\alpha - \sin(\alpha)}{1 - \cos\left(\frac{\alpha}{2}\right)} \tag{2.75}$$

$$\rightarrow \eta_c = \frac{P_{RF}}{P_{DC}} = \eta_{c,A}.\frac{\alpha - \sin(\alpha)}{2\sin\left(\frac{\alpha}{2}\right) - \alpha\cos\left(\frac{\alpha}{2}\right)} \tag{2.76}$$

With the conduction angle values between π to 2π, the collector efficiency of class-AB η_c varies from 50% to 78.5% as also shown in Table 2.1. Usually the bias point of class-AB is chosen to be close to class-B bias point which is close to the conduction angle π in order to get higher efficiency [10].

2.7 Literature Survey

Fig. 2.20. shows the recent PAs with high PAE performance in 0.13 μm SiGe BiCMOS, and Table 2.3 summarizes the measured performance of these PAs.

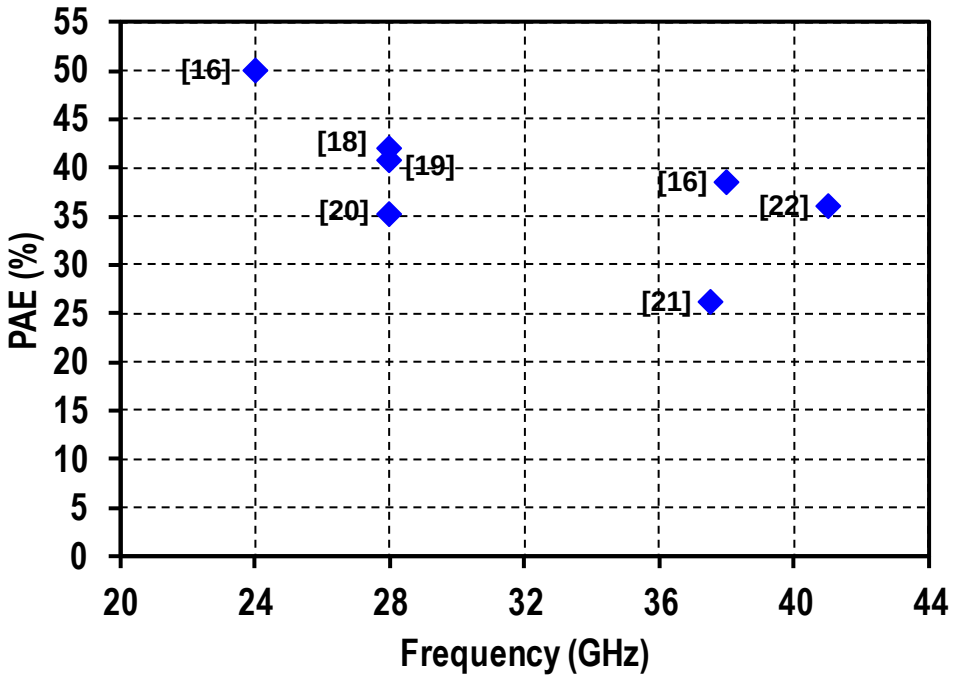

Fig. 2.20. Recent High PAE PAs in 0.13 μm SiGe BiCMOS.

Table 2.3. The measured PAs performance summary with recent state-of-the-art integrated silicon.

Authors	Freq.(GHz)	PAE(%)	P_{sat}(dBm)	OP_{-1dB}(dBm)	Gain(dB)	Supply(V)	Technology	Feature
JSSC 2016]	24	50	18	16	21	2.3	0.13 μm SiGe	2-stage Class-F^{-1}
	38	38.5	16.5	15	16.5	2.4		
CICC 2015 [18]	28	42	17.1	15	21.2	2.4	0.13 μm SiGe	2-stage Class-F^{-1}
ISSCC 2014 [19]	28	40.7	17.1	15	10.3	2.2	0.13 μm SiGe	1-stage Class-F^{-1}
SiRF 2014 [20]	28	35.3	18.6	15.5	15.3	3.6	0.13 μm SiGe	2-stage Class-F^{-1}
BCTM 2011 [21]	37.5	26.2	14.8	NA	5.6	2.5	0.13 μm SiGe	2-stage Class-B
JSSC 2014 [22]	41	36	18.1	NA	21.2	2.4	0.13 μm SiGe	1-stage Class-E

Chapter 3

Power Amplifier Design

Contents

3.1 Design Specifications

The designs target the next generation high-speed wireless communications at mm-wave. Even this work primarily focuses on the comparison on the performances (particularly efficiency and linearity) among Class-AB, Class-F, and Class- F^{-1} PAs, these designs should follow some standards and requirements to be suitable to the communication systems. After reviewing some of the requirements of the system and the recent state-of-art integrated works in silicon and III-V technologies, several important designed specifications are determined for three PAs as shown in Table 3.1 below. For linearity, the EVM required for 28GHz in 5G system is 5.5% which is equivalent to -25 dBc [23].

Table 3.1. Proposed Design Specifications for Class-AB, Class-F, and Class- F^{-1} PAs.

Design Parameter	Proposed Specification
Frequency	$28\ GHz$
PAE	$> 40\ \%$
Gain	$\sim 10\ dB$
OP_{-1dB}	$15\ dBm$
P_{sat}	$\geq 17\ dBm$
EVM	$< 5.5\ \%\ (-25dBc)$

3.2 Device Selection

3.2.1 0.13 µm SiGe BiCMOS-8HP Technology

The BiCMOS-8HP technology used in this work offers Regular High Performance (HP) vertical NPN bipolar transistors. The specifications for the Regular process option devices are given in Table 3.2. Supported layouts consist of single emitter stripe devices with a fixed emitter (EX) width of 0.12 um. The emitter length can be scaled to obtain the desired current rating with a minimum length equal to 0.52 um and a maximum length of 18 µm. The Regular High Performance (HP) device is offered in both CBEBC and CBE configurations. To handle higher current densities, the p-cell permits an increase in the number of collector contact rows as well as the base metal width. All NPNs have polysilicon emitters with a non-self-aligned extrinsic base.

Table 3.2. Key Parameters for Regular High Performance (HP) NPN (0.12 um x 2.5 um) [24].

Parameter	Minimum	Maximum	Maximum	Unit
V_{BE}	0.703	0.728	0.753	Volts
Beta	100	460	900	
f_T (peak)	180	210	240	GHz
BV_{CEO}	1.5	1.8	2.5	Volts
BV_{CBO}	5.5	6.0	7.0	Volts
BV_{EBO}	1.2	2.3	4.0	Volts
BV_{CSO}	20	50		Volts

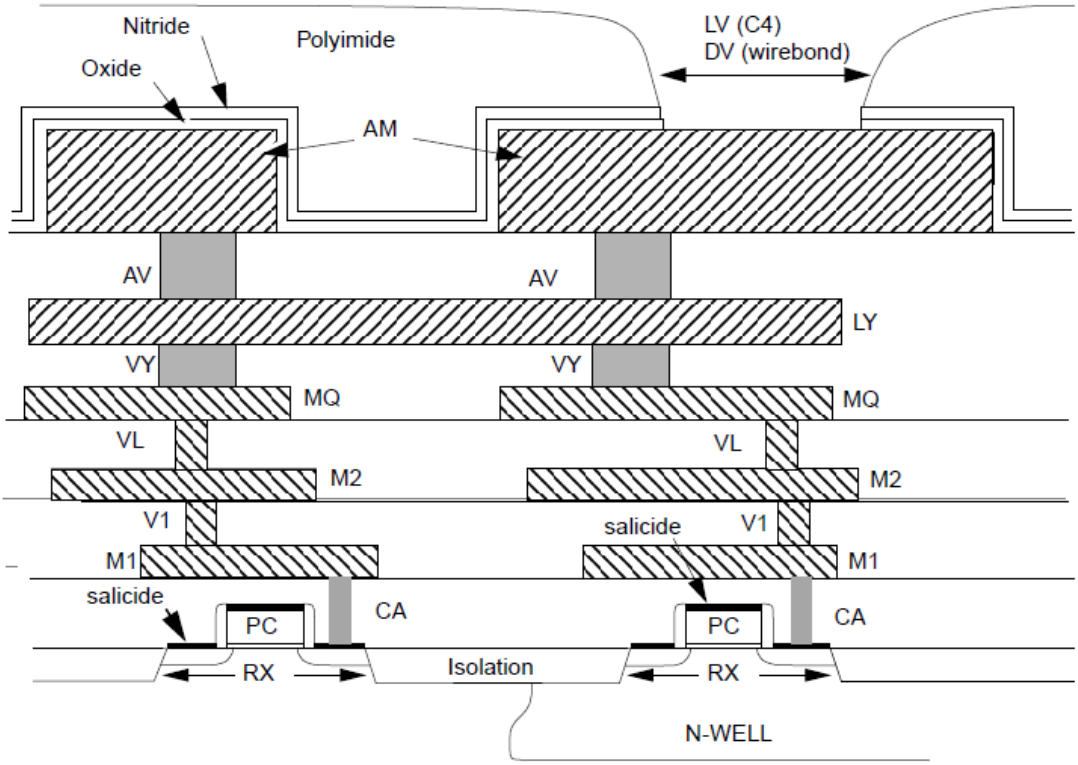

Fig. 3.1. Cross Section of the 5 Level of Metal BEOL Option (2 Thin Mx; x=1, 2 and 1 Thick= MQ and Analog Metal = LY, AM) with either DV or LV Final Passivation [24].

3.2.2 Device Size Selection

A very first and important step in PA design is to determine the size of transistor that can satisfy the output power required for the system. With optimization, this output power can be obtained with carefulness in order to achieve the highest efficiency possible. In this thesis, the Q_1 emitter length of l_e=2×16 μm is chosen to have an optimal current density of 1.4 mA/μm for a peak 180 GHz f_T at the 1-dB compression point.

3.3 Bias Point Selection

In order to determine the bias point for the PA, DC IV characteristic curves is generated using Keysight's Advanced Design System (ADS). The collector voltage is swept from 0 V to 7 V with a step of 10 mV, and the base voltage is swept from 0.7 V to 1.0 V with a step of 10 mV in Fig. 3.2. Each red curve represents the relationship between I_{CE} and V_{CE} at a specific base voltage (corresponding with the base current). In order to have a fair comparison in performance among three PAs, a class-AB bias point is chosen. Since the BV_{CEO} and BV_{CBO} of the given SiGe HBT technology are 1.8 V and 6 V respectively, the supply voltage of Vcc is chosen to be 2.3 V to achieve the power level of ~ 15 dBm at 1-dB compression. The base is biased at a voltage V_B of ~0.83 V conduct a quiescent collector current of ~12 mA. The black dot in Fig. 3.2 indicates the location of the class-AB bias point (V_{CE}=2.3V, I_{CE}=12mA) on the IV characteristic curves where the required power level and high efficiency can be achieved.

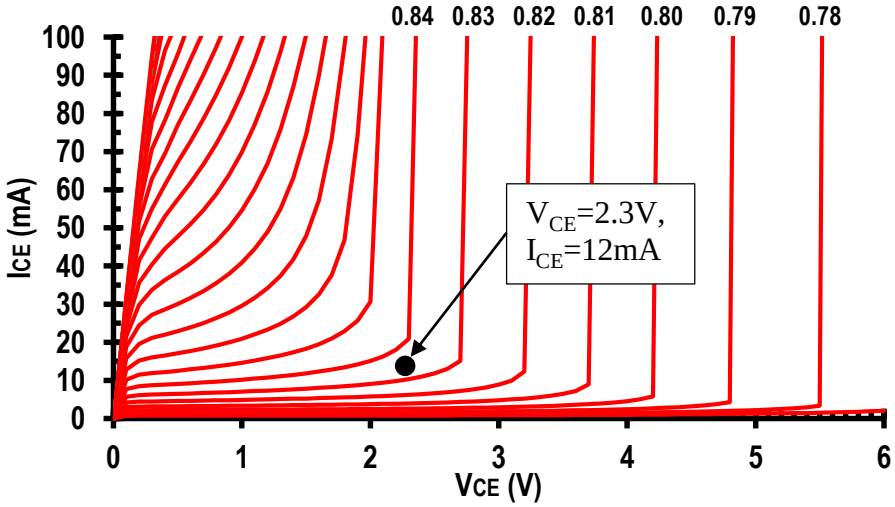

Fig. 3.2. DC IV characteristic curves (I_{CE} vs. V_{CE}) with the Q_1 emitter length of l_e=2×16 μm.

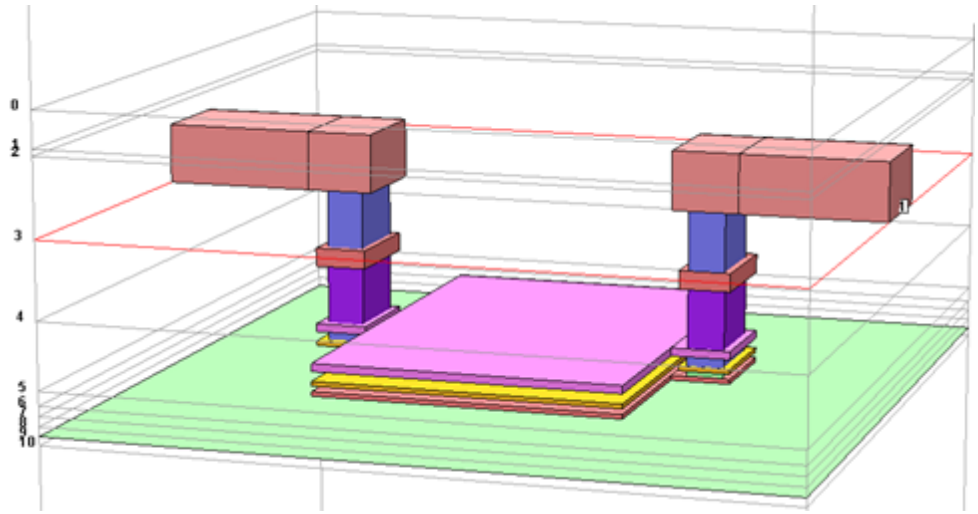

Fig. 3.3. A screenshot of a 130 fF MOM capacitor created for EM simulation in Sonnet.

3.4 Passive Component Selection

Resistors: Resistors (model kqres) from the BiCMOS-8HP library are used for the designs. Due to losses, resistors are carefully used in the circuit designs and mainly used in the base bias network.

Inductors: T-line inductors from the library are used. The Q for these inductors is observed to be about 35 for all bands.

Capacitors: The Nitride MIM capacitors given in the library models are used in some parts of the designs. Since these MIM capacitors have a low Q at the target mm-wave bands [24], the MOM capacitors are custom made using the BEOL lower metal layers and silicon dioxide as a dielectric in order to get better Q. This brings Q to at least about 65 at the fundamental frequency and > 20 up to third harmonic band around 84 GHz.

3.5 Stabilizing and DC Feed Network Design

Stability is one of biggest challenge in PA design since the PAs have to operate at very high frequencies with a wide range in many of applications. Every technology exhibits different stability behaviors due to the transistor's physical structure, semiconductor materials, and so on. Since the demand of achieving high performances, designers have to compensate the oscillation caused by instability of the circuit at different frequencies. In order to reduce or eliminate this oscillation, some kinds of stabilizing networks need to be applied to ensure the stability at all frequencies

In this work, the SiGe HBT technology is used for the designs in a beyond-BV_{CEO} operation. There are two main types of instability existing in the designs of this technology. First, large-signal S-parameters show sub-harmonic tones are generated in the circuit due to hard switching of the device's large nonlinear base-emitter capacitance [22]. In order to mitigate this sub-harmonic tones, a harmonic trap in Fig. 3.4① is used. The different values of C_{BB} are utilized for each PA as shown in Table 3.3. in order to help stabilize the circuits due to different sub-harmonic tones and other stability behaviors. The second main type of instability is caused by the reversal of the base current due to the beyond BV_{CEO} operation of SiGe HBT's which results in a negative real part of input impedance. This phenomenon leads to small signal oscillations at low frequencies [22]. The base bias path provides < 250 Ω of DC resistance to mitigate the effect of this base current reversal at large collector swings. Also, L_{BB} = 500 pH is used to isolates the bias circuit from Q_1 in AC wise [19].

In addition, a base network as illustrated in Fig. 3.4 ② is included to ensure the stability for all frequencies especially at low frequencies.

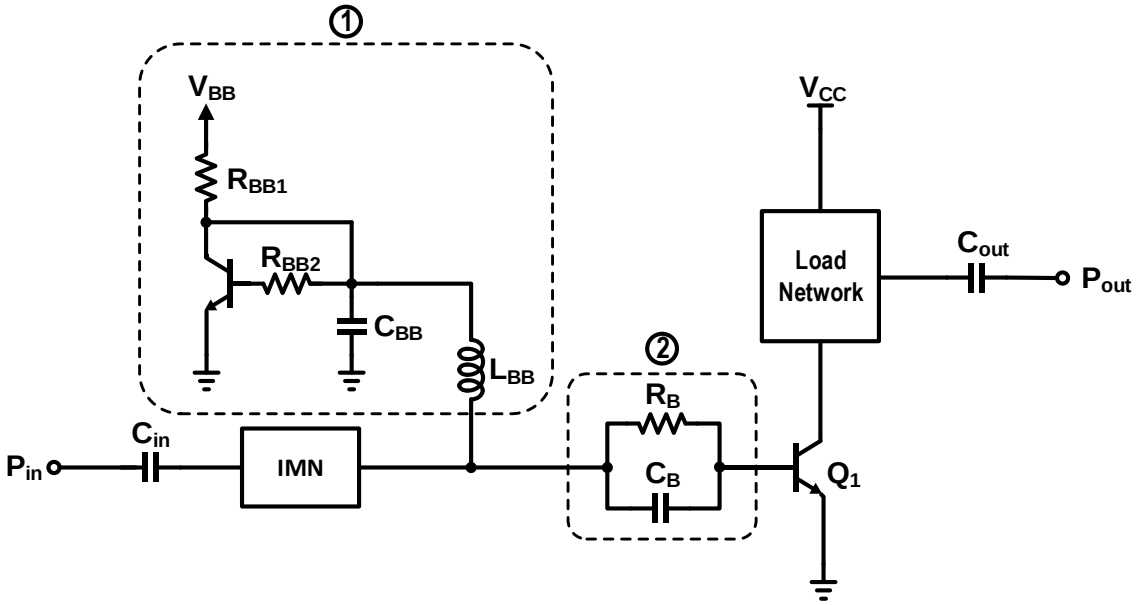

Fig. 3.4. Base DC feed and stabilizing circuits.

Table 3.3. Summary of the passive values of base DC feed and stabilizing circuits.

R_{BB1} (Ω)	R_{BB2} (Ω)	C_B (fF)	R_B (Ω)	L_{BB} (pH)	C_{BB} (fF)		
195	1500	1000	7	500	350 (F^{-1})	84 (F)	500 (AB)

3.6 Matching and Load Network Design

3.6.1 Input Matching Network

The intention of this study is to have identical input networks and different load networks for three PAs in order to have a fair comparison on their performances. The input matching network is conjugated match to deliver maximum power possible. A pi-type LC network is used to match 50 Ω source and to achieve high efficiency.

The matching process is done using Smith Chart tool in ADS. The impedance looks from the source is $\sim 9.5 - j5\ \Omega$ and matched to the source of 50 Ω at 28 GHz. Since finite Qs exist in passive elements (i.e. inductors and capacitors), the values of capacitors and inductors obtained from matching tool need to be tuned eventually. After tuning, the values of the components are L_{IM} = 113 pH, C_{IM1} = 297 fF, and C_{IM2} = 325 fF.

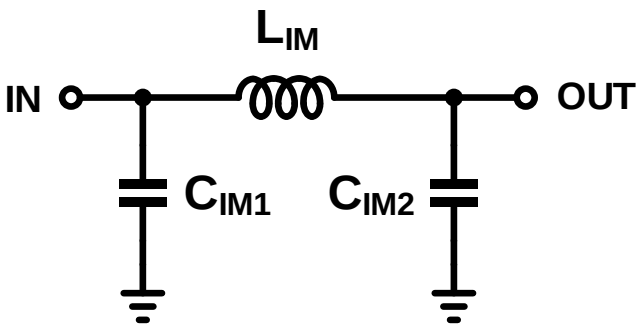

Fig. 3.5. Pi-type LC input matching network for all three PAs.

3.6.2 Transistor Parasitic Capacitance Extraction

Transistor parasitic capacitance extraction is extremely significant in the design process since all the load networks are designed based on the result of this capacitance. The parasitic capacitance is extracted from load-pull simulation result. Load-pull is performed in Cadence virtuoso using portAdapter (a component used in load-pull simulation) to

sweep the angle theta with the parameter sweep of gamma. This simulation goes through many possible points of load impedance on the Smith Chart where the optimal output power can be achieved.

At the end, the results can be plotted as power contours as shown in Fig. 3.6 and Fig. 3.7. In order to estimate the parasitic capacitance, the point that represents the optimal output power should be close to the real axis as possible. This means a value of the inductance is needed to cancel out the capacitance. The value of the inductor Lp can be adjusted to resonate the capacitance to bring this point close to the real axis on the Smith Chart. Then the parasitic capacitance can be determined through a simple calculation $C_P = 1/(\omega L_P)$ at 28 GHz. This capacitance turns out to be ~60 fF.

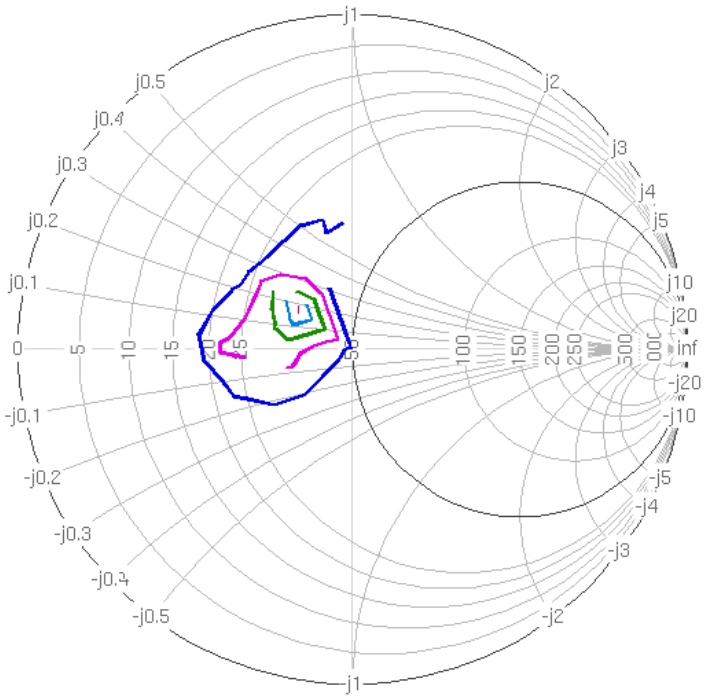

Fig. 3.6. Output power contours from load-pull simulation without a finite inductance.

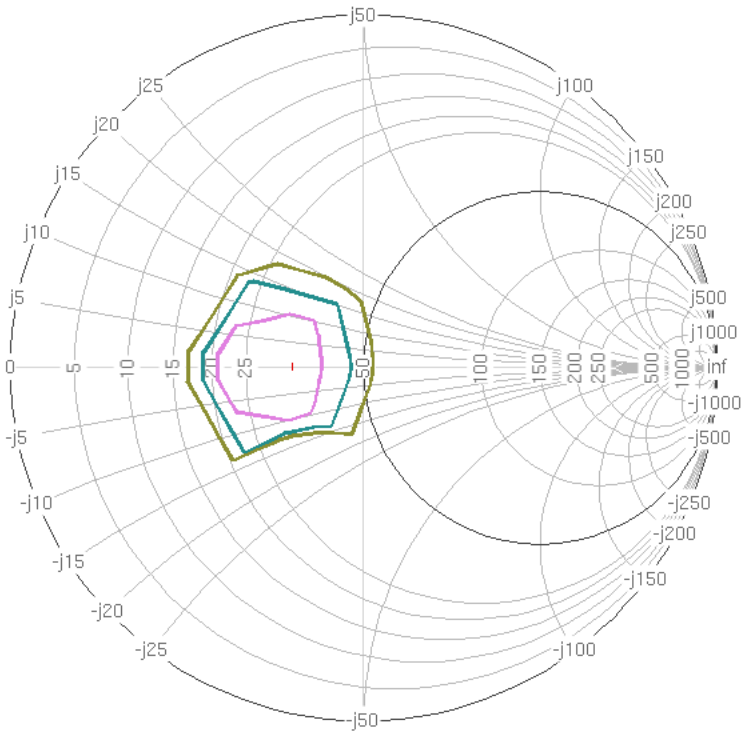

Fig. 3.7. Output power contours from load-pull simulation with the tuned finite inductance.

3.6.3 Load Network for Class-AB Power Amplifier

Class-AB load network simply consists of an inductor L_P which can resonate the parasitic capacitor, C_P as illustrated in Fig. 3.8. As referring to the previous section 3.6.2, the parasitic capacitor extracted from the transistor is ~60 fF. In order to resonate this capacitance at 28 GHz, the value of the shun inductor can be found as $L_P = 1/(\omega C_P) = 538$ pH.

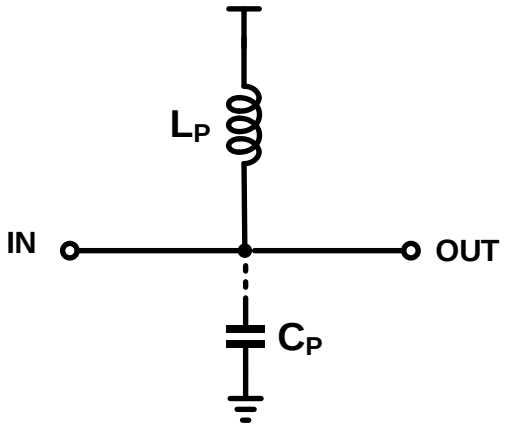

Fig. 3.8. Class-AB load network with the resonant tank L_P-C_P.

3.6.4 Load Network for Class-F Power Amplifier

In order to shape class-F voltage and current waveforms, a load network composes of a parallel multi-resonance network and a series dual-resonance network is used to provide the optimum impedance of 50 Ω at the ω_o-band, low impedance of <10 Ω at the $2\omega_o$-band, and high impedance of >150 Ω at the $3\omega_o$-band [19].

3.6.4.1 Multi-resonance Parallel Load Network

This network consists of an L_{P1}-C_{P1} tank, an inductor L_{P1}, and the transistor parasitic capacitor C_P as illustrated in Fig. 3.9①. The goal of creating this LC network is to create high impedance at the f_o-band, low impedance at the $2f_o$-band, and high impedance at the $3f_o$-band. The ideal value of the elements in the network are determined through mathematical expressions and calculations as demonstrated below.

The impedance of L_{P1}-C_{P1} tank can be obtained,

$$\frac{j\omega L_{P1} \times \frac{1}{j\omega C_{p1}}}{j\omega L_{P1} + \frac{1}{j\omega C_{p1}}} = \frac{j\omega L_{P1}}{1 - \omega^2 L_{P1} C_{P1}} \tag{3.1}$$

This L_{P1}-C_{P1} tank is connected with a series inductor L_{P2} to ensure that the branch will resonate the parasitic capacitor C_P to create open or high impedances at the ω_o-band and the $3\omega_o$-band and short or low impedance at the $2\omega_o$-band.

$$\frac{j\omega L_{P1}}{1 - \omega^2 L_{P1} C_{P1}} + j\omega L_{P2} = \frac{j\omega(L_{P1} + L_{P2} - \omega^2 L_{P1} L_{P2} C_{P1})}{1 - \omega^2 L_{P1} C_{P1}} \tag{3.2}$$

In order to meet the load impedance requirement of class-F PA, the expression (3.2) has to satisfy these conditions at first, second and third harmonic.

At the ω_o-band,

$$\frac{L_{P1} + L_{P2} - {\omega_0}^2 L_{P1} L_{P2} C_{P1}}{1 - {\omega_0}^2 L_{P1} C_{P1}} = \frac{1}{{\omega_0}^2 C_P}$$

$$\rightarrow\ 1 - {\omega_0}^2 L_{P1} C_{P1} - {\omega_0}^2 C_P (L_{P1} + L_{P2} - {\omega_0}^2 L_{P1} L_{P2} C_{P1}) = 0 \tag{3.3}$$

At the $2\omega_o$-band,

$$\frac{L_{P1} + L_{P2} - 4{\omega_0}^2 L_{P1} L_{P2} C_{P1}}{1 - 4{\omega_0}^2 L_{P1} C_{P1}} = 0$$

$$\rightarrow\ L_{P1} + L_{P2} = 4{\omega_0}^2 L_{P1} L_{P2} C_{P1} \tag{3.4}$$

At the $3\omega_o$-band,

$$\frac{L_{P1}+L_{P2}-9\omega_0{}^2L_{P1}L_{P2}C_{P1}}{1-9\omega_0{}^2L_{P1}C_{P1}}=\frac{1}{9\omega_0{}^2C_P}$$

$$\rightarrow\ 1-9\omega_0{}^2L_{P1}C_{P1}-9\omega_0{}^2C_P(L_{P1}+L_{P2}-\omega_0{}^2L_{P1}L_{P2}C_{P1})=0 \quad (3.5)$$

Substituting (3.4) into (3.3) and (3.5), the expressions becomes

$$1-\omega_0{}^2L_{P1}C_{P1}-3\omega_0{}^2C_P(\omega_0{}^2L_{P1}L_{P2}C_{P1)}=0 \quad (3.6)$$

$$1-9\omega_0{}^2L_{P1}C_{P1}+45\omega_0{}^2C_P(\omega_0{}^2L_{P1}L_{P2}C_{P1})=0 \quad (3.7)$$

From (3.6) and (3.7),

$$\frac{1-\omega_0{}^2L_{P1}C_{P1}}{3}=\frac{1-9\omega_0{}^2L_{P1}C_{P1}}{-45}\rightarrow\omega_0{}^2L_{P1}C_{P1}=\frac{2}{3} \quad (3.8)$$

Substituting (3.8) into (3.4),

$$L_{P1}+L_{P2}=\frac{8}{3}L_{P2}\rightarrow L_{P2}=\frac{3}{5}L_{P1} \quad (3.9)$$

Then from (3.6), (3.8), and (3.9), the expressions of L_{P1} and L_{P2} in terms of C_P can be obtained as follows,

$$1-\frac{2}{3}-3\omega_0{}^2C_P\left(\frac{2}{3}L_{P2}\right)=0\rightarrow L_{P2}=\frac{1}{6\omega_0{}^2C_P}\ \text{and}\ L_{P1}=\frac{5}{18\omega_0{}^2C_P} \quad (3.10)$$

Substituting $L_{P1}=\frac{5}{18\omega_0{}^2C_P}$ into (3.8), the capacitance C_{P1} is calculated in terms of C_P,

$$C_{P1}=\frac{2}{3}\times\frac{1}{\omega_0{}^2L_{P1}}=\frac{12}{5}C_P \quad (3.10)$$

From the results of this mathematic development, the value of the ideal passive components can be determined based on the parasitic capacitance of the transistor C_P [10]. In this design, C_P is estimated to be ~60 fF. Based on this value of C_P, all the values of ideal components are calculated. Fig. 3.10(a) shows that the impedance magnitude of class-F PA with the ideal components in the load network. As the result, the impedance is very high and close to infinity at the ω_o-band, zero at the $2\omega_o$-band, and very high at the $3\omega_o$-band (red line) as illustrated in Fig 3.10(a).

However, the design utilizes the real passive components with the quality factors (Q) varied depending on the operating frequency. Since low-Q components can produce losses to the circuits, lowering the Qs in the passive components is extremely needed. Using tools in ADS and EM simulation from Sonnet, Q is ~35 for T-line inductors for all bands. However, the MIM capacitors given in the library have very low Q. Therefore, the MOM capacitors are custom made using the BEOL lower metal layers and silicon dioxide as a

dielectric. An example of a MOM capacitor is illustrated in Fig. 3.3. As mentioned, this can bring Q to about 60 at the fundamental frequency and >20 up to third harmonic band around 84 GHz. After optimization, real passive components are obtained and shown in Table 3.4. As the result, the impedances of the parallel load network (red line) are captured with >700 Ω at the ω_o-band, <3 Ω at the $2\omega_o$-band, and >500 Ω at the $3\omega_o$-band as illustrated in Fig 3.10(b) [19].

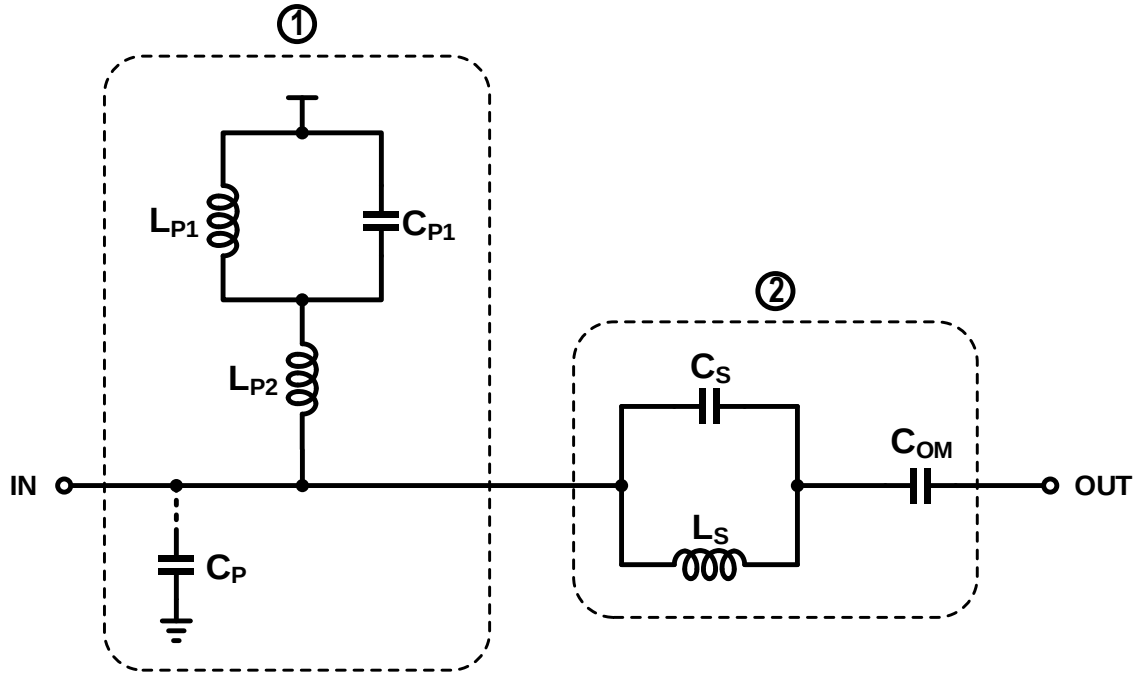

Fig. 3.9. Class-F load network with ① a parallel multi-resonance network (Z_P) and ② a series dual-resonance network (Z_S).

Table 3.4. Summary of the passive values of the class-F load network.

C_P (fF)	L_{P1} (pH)	L_{P2} (pH)	L_S (pH)	C_{P1} (pH)	C_S (pH)	C_{OM} (fF)
60	158	86	142	134	25	315

Table 3.5. Summary of the equivalent resistances of the class-F load network.

R_P (Ω) @f_o	R_P (Ω) @$2f_o$	R_P (Ω) @$3f_o$	R_S (Ω) @f_o	R_S (Ω) @$3f_o$
775	2.6	487	1.6	1432

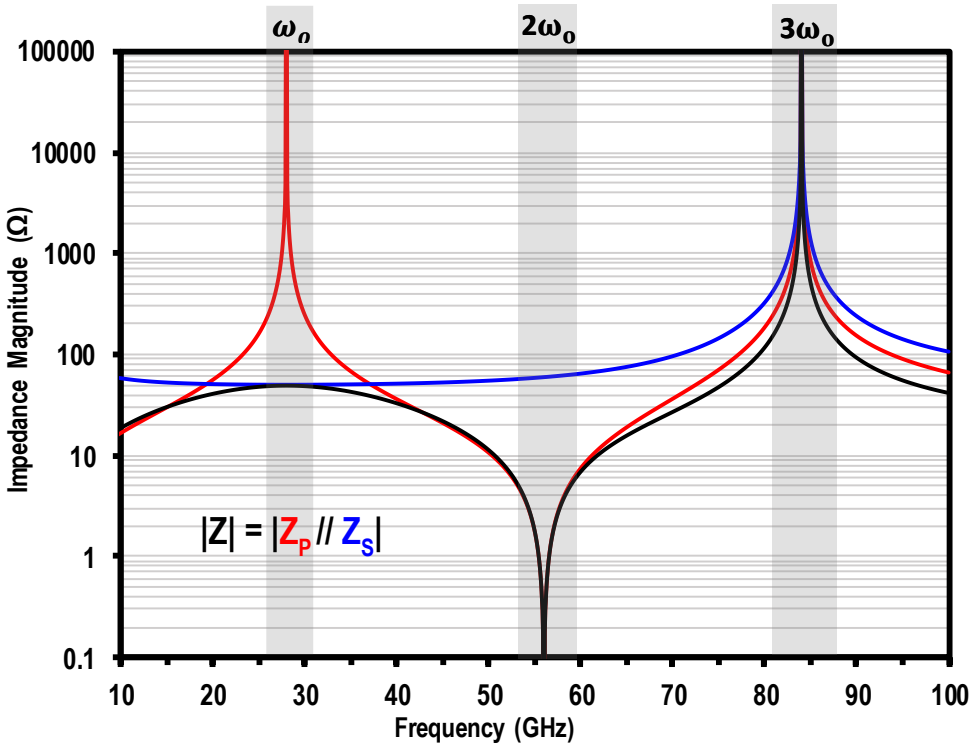

(a)

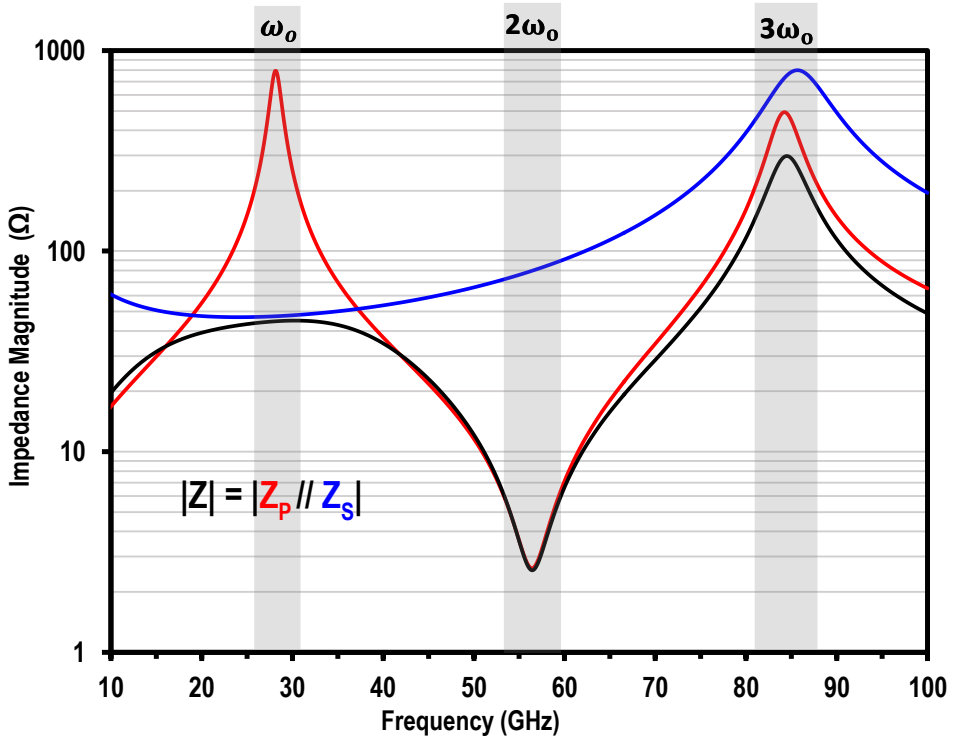

(b)

Fig. 3.10. Impedance magnitude of class-F load network (a) ideal components (b) real components.

3.6.4.2 Dual-resonance Series Load Network

The dual-resonance series load network is designed to have a parallel resonance at the $3\omega_o$-band by utilizing a LC tank (L_S-C_S) to provide high impedance. The L_S-C_S tank becomes inductive to cancel out the parasitic capacitor in order to bring the impedance to the optimum 50 Ω at the fundamental frequency band. As the result, the series network in Fig. 3.9 ② provides close to 50 Ω resistance at the ω_o-band and high impedance (783 Ω) at the $3\omega_o$-band (blue line in Fig. 3.10(b))

The overall impedance of the multi-resonance load network can be obtained with Z_P// Z_S as shown (black line) in Fig. 13.10. As the result, the load network provides ~50-Ω optimum resistance at the ω_o-band, low impedance (2.6 Ω) at the $2\omega_o$-band, and high impedance (283 Ω) at the $3\omega_o$-band.

3.6.5 Load Network for Class-F^{-1} Power Amplifier

Using the similar idea of multi-resonance load network as in class-F, class-F^{-1} load network consists of two LC tanks with a series inductor for the multi-resonance parallel network and a LC tank with a series capacitor for the dual-resonance series network. The load network design idea is influenced by the works from reference papers [16, 18, 19, 25]. The design of the load network for class-F^{-1} is more tricky and challenging than that of class-F due to the complexity of the LC tank impedance at different frequency bands.

3.6.5.1 Multi-resonance Parallel Load Network

Since the complexity of the parallel network, the design approach is a slightly different from class-F's. The main idea is to have two LC tanks (L_{P1}-C_{P1} and L_{P2}-C_{P2}) that can resonate at different frequency bands to create inductive or capacitive impedance to satisfy the impedance requirements. Assuming the fundamental frequency is ω_0, the L_{P1}-C_{P1} tank resonates at ω_1 where ω_1 falls within the frequency band $(\omega_0, 2\omega_0)$ and the L_{P2}-C_{P2} tank resonates at ω_2 where ω_2 falls within the frequency band $(2\omega_0, 3\omega_0)$. In order to estimate the equivalent inductance and capacitance from each tank, the imaginary part of the impedance is evaluated. The equivalent inductance and capacitance for either tank can be expressed as follow:

$$L_{1,2}(\omega) = \frac{L_{P1,2}}{1 - \left(\frac{\omega}{\omega_{1,2}}\right)^2} \tag{3.11}$$

$$C_{1,2}(\omega) = C_{P1,2}\left[1 - \left(\frac{\omega_{1,2}}{\omega}\right)^2\right] \tag{3.12}$$

where $\omega_1 = \sqrt{\frac{1}{L_{P1}C_{P1}}}$ and $\omega_2 = \sqrt{\frac{1}{L_{P2}C_{P2}}}$.

At the ω_o-band, the operating frequencies of both tanks $\omega_{1,2}$ are greater than the fundamental frequency ω_0, leading to a positive in the denominator of (3.11). The L_{P1}-C_{P1} tank and the L_{P2}-C_{P2} tank become inductive and can be expressed with the equivalent inductances $L_1(\omega_0)$ and $L_2(\omega_0)$ respectively as in (3.11) and (3.12). The combination of these inductances and L_{P2} can resonate C_P and create a high impedance as the result.

$$L_1(\omega_0) = \frac{L_{P1}}{1 - \left(\frac{\omega_0}{\omega_1}\right)^2} \tag{3.13}$$

$$L_2(\omega_0) = \frac{L_{P2}}{1 - \left(\frac{\omega_0}{\omega_2}\right)^2} \tag{3.14}$$

At the $2\omega_o$-band, the L_{P1}-C_{P1} tank becomes capacitive since the frequency is twice of the fundamental frequency and greater than ω_1. The expression (3.12) can be used the equivalent capacitance of the L_{P1}-C_{P1} tank in (3.15). Meanwhile, the L_{P2}-C_{P2} tank still remains inductive since its operating frequency is still greater then $2\omega_0$. The excessive inductance combined with the capacitance C_P can create a parallel resonance to provide high impedance at the second harmonic band.

$$C_1(2\omega_0) = C_{P1}\left[1 - \left(\frac{\omega_1}{2\omega_0}\right)^2\right] \tag{3.15}$$

$$L_2(2\omega_0) = \frac{L_{P2}}{1 - \left(\frac{2\omega_0}{\omega_2}\right)^2} \tag{3.16}$$

At the $3\omega_o$-band, the operating frequencies of both tanks $\omega_{1,2}$ are smaller than the 3rd harmonic frequency. Therefore, both tanks produce equivalent capacitances to create a series resonance with L_{P3} for a short circuit to the ground or low impedance.

$$C_1(3\omega_0) = C_{P1}\left[1 - \left(\frac{\omega_1}{3\omega_0}\right)^2\right] \tag{3.17}$$

$$C_2(3\omega_0) = C_{P2}\left[1 - \left(\frac{\omega_2}{3\omega_0}\right)^2\right] \tag{3.18}$$

With a similar assessment with class-F, inverse class-F parallel network has to meet the requirements for the impedances with high impedance (>500 Ω) at the ω_o-band, high impedance (>150 Ω) at the $2\omega_o$-band, and low impedance (<10 Ω) at the $3\omega_o$-band [19]. Based on the inductance and capacitance expressions determined above, two parallel resonances expect to occur at the ω_o-band and the $3\omega_o$-band, and a series resonance occurs at the $2\omega_o$-band. The mathematical developments of these resonances can be expressed in the following equations at each frequency band.

At the ω_o-band:

$$L_1(\omega_0) + L_2(\omega_0) + L_{P3} = \frac{1}{{\omega_0}^2 C_P}$$

$$\rightarrow \frac{L_{P1}}{1 - \left(\frac{\omega_0}{\omega_1}\right)^2} + \frac{L_{P2}}{1 - \left(\frac{\omega_0}{\omega_2}\right)^2} + L_{P3} = \frac{1}{{\omega_0}^2 C_P} \tag{3.19}$$

At the $2\omega_o$-band:

$$C_1(2\omega_0) + L_2(2\omega_0) + L_{P3} = \frac{1}{4{\omega_0}^2 C_P}$$

$$\rightarrow C_{P1}\left[1 - \left(\frac{\omega_1}{2\omega_0}\right)^2\right] + \frac{L_{P2}}{1 - \left(\frac{2\omega_0}{\omega_2}\right)^2} + L_{P3} = \frac{1}{4{\omega_0}^2 C_P} \tag{3.20}$$

At the $3\omega_o$-band:

$$C_1(3\omega_0) + C_2(3\omega_0) + L_{P3} = 0$$

$$\rightarrow C_{P1}\left[1 - \left(\frac{\omega_1}{3\omega_0}\right)^2\right] + \frac{L_{P2}}{1 - \left(\frac{3\omega_0}{\omega_2}\right)^2} + L_{P3} = 0 \tag{3.21}$$

In order to satisfy these equations, the passive components are carefully chosen. The values of the component of the L_{P1}-C_{P1} tank are chosen to be < 200 pH for L_{P1} and < 200 fF C_{P1}. As the result, the resonance frequency ω_1 is 37 GHz and falls between ω_0 and $2\omega_0$ chosen to be 37 GHz after utilizing the optimization tool in ADS of ideal components L_{P1} and C_{P1}. The values of the components in the L_{P2}-C_{P2} tank are also chosen to have a resonance frequency between $2\omega_0$ and $3\omega_0$. With ideal components, the resonance frequency of the L_{P2}-C_{P2} tank is 67 GHz. The value of the remaining inductor L_{P3} is determined to meet all the impedance requirements at the first three harmonic bands. The

impedance magnitude after all ideal components being applied in the parallel network (redline) is illustrated in Fig. 3.13(a).

The next step is replacing the ideal components with real components. As mentioned in section 3.6.4 (which is about class-F load network design), both MIM and MOM (custom made by EM simulation tool Sonnets) capacitors are utilized in the parallel load network design for class-F^{-1} PA. The goal is to reduce the losses in both parallel and series paths due to high Q in the capacitors. With optimization and EM simulation, the values of the real passive components are obtained and shown in Table 3.6.

Fig. 3.12(a) shows the resonance frequency of the L_{P1}-C_{P1} tank to be ~35 GHz which is very close to the initial resonance frequency. The impedances of the L_{P1}-C_{P1} tank at three frequency bands shown Fig. 3.12(b) confirms the results where the tank is inductive at the ω_o-band and becomes capacitive at the $2\omega_o$-band and the $3\omega_o$-band. These results satisfy the equations (13.13), (13.15), and (13.17). Similarly, the L_{P1}-C_{P1} tank resonates at ~65.5 GHz which is 1.5 GHz from the initial frequency as illustrated in Fig. 3.12(c). Also, the impedances are inductive at the ω_o-band and the $2\omega_o$-band and capacitive at the ω_o-band which satisfy the equations (13.14), (13.16), and (13.18). The overall impedance of the parallel network (red line in Fig. 13.13 (b)) is obtained after two tanks and L_{P3} are connected in series and C_P in parallel. The network provides high impedance (800 **Ω**) at the ω_o-band, high impedance (208 **Ω**) at the $2\omega_o$-band, and low impedance (8 **Ω**) the $3\omega_o$-band.

3.6.5.2 Dual-resonance Series Load Network

The dual-resonance series load network is designed to have a parallel resonance at the $2\omega_o$-band by utilizing a LC tank (L_S-C_S) to provide high impedance. The L_S-C_S tank apparently becomes inductive at the fundamental frequency band. In order to cancel this excessive inductance and bring it to the optimum 50 **Ω**, a series capacitor C_{OM} is utilized toward the output side. As the result, the series network provides close to 50 **Ω** at the ω_o-band and high impedance (700 **Ω**) at the $2\omega_o$-band (blue curve in Fig. 13.13(b)).

The overall impedance of the multi-resonance load network can be obtained with Z_P// Z_S as shown (black line) in Fig. 13.13. As the result, the load network provides ~50-**Ω** optimum resistance at the ω_o-band, high impedance (158 **Ω**) at the $2\omega_o$-band, and low impedance (7.7 **Ω**) at the $3\omega_o$-band.

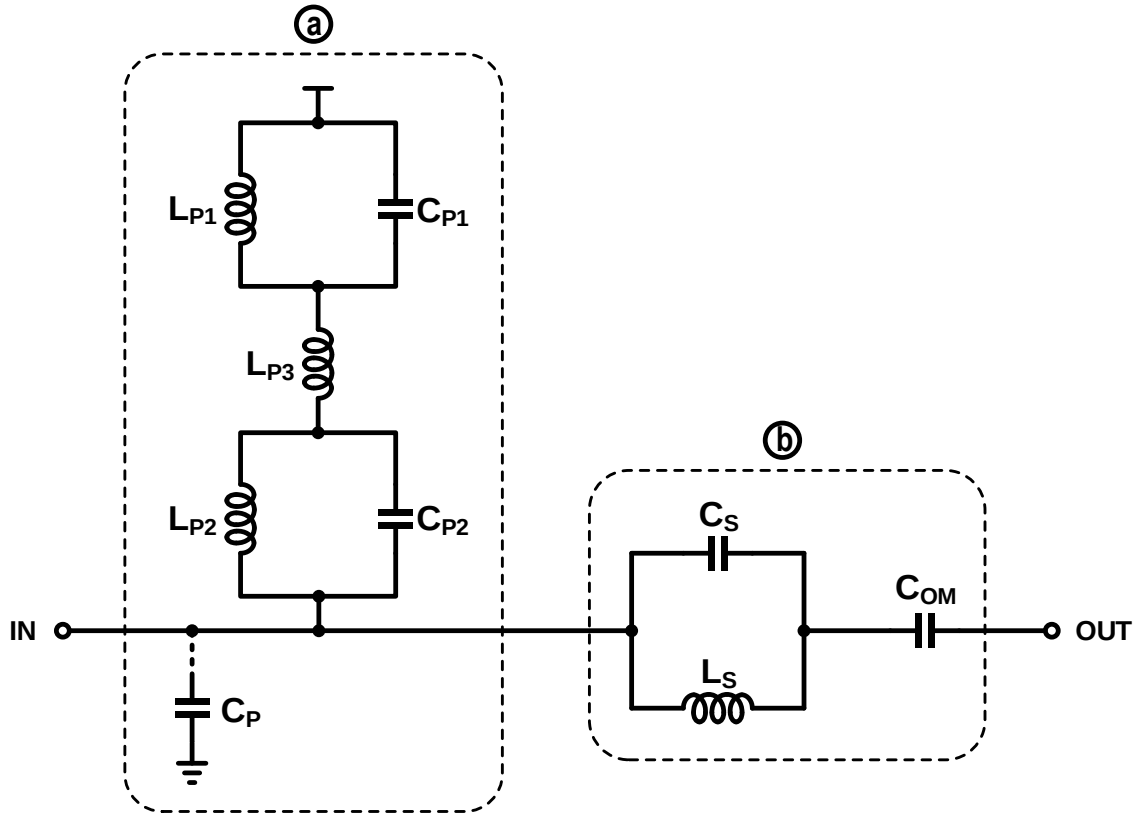

Fig. 3.11. Class-F load network with ⓐ a parallel multi-resonance network (Z_P) and ⓑ a series dual-resonance network (Z_S).

Table 3.6. Summary of the passive values of the class-F^{-1} load network.

C_P (fF)	L_{P1} (pH)	L_{P2} (pH)	L_{P3} (pH)	L_S (pH)	C_{P1} (fF)	C_{P2} (fF)	C_S (fF)	C_{OM} (fF)
60	149	57	67	115	140	115	84	500

Table 3.7. Summary of the equivalent parasitic resistances of the class-F^{-1} load network.

R_P (Ω) @f_o	R_P (Ω) @$2f_o$	R_P (Ω) @$3f_o$	R_S (Ω) @f_o	R_S (Ω) @$2f_o$
525	191	7.4	1.2	437

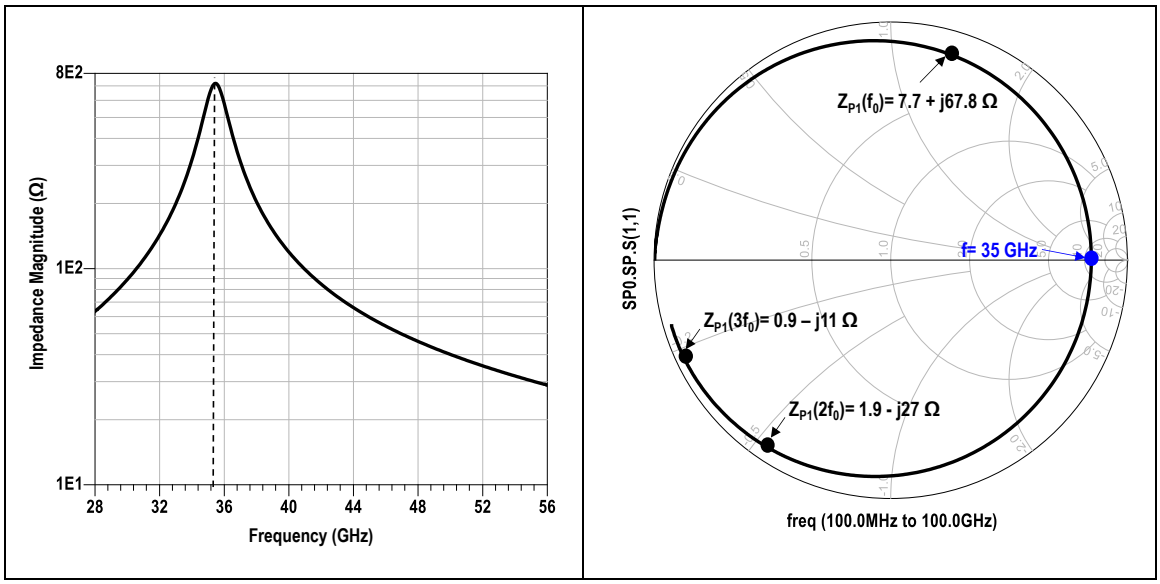

(a) (b)

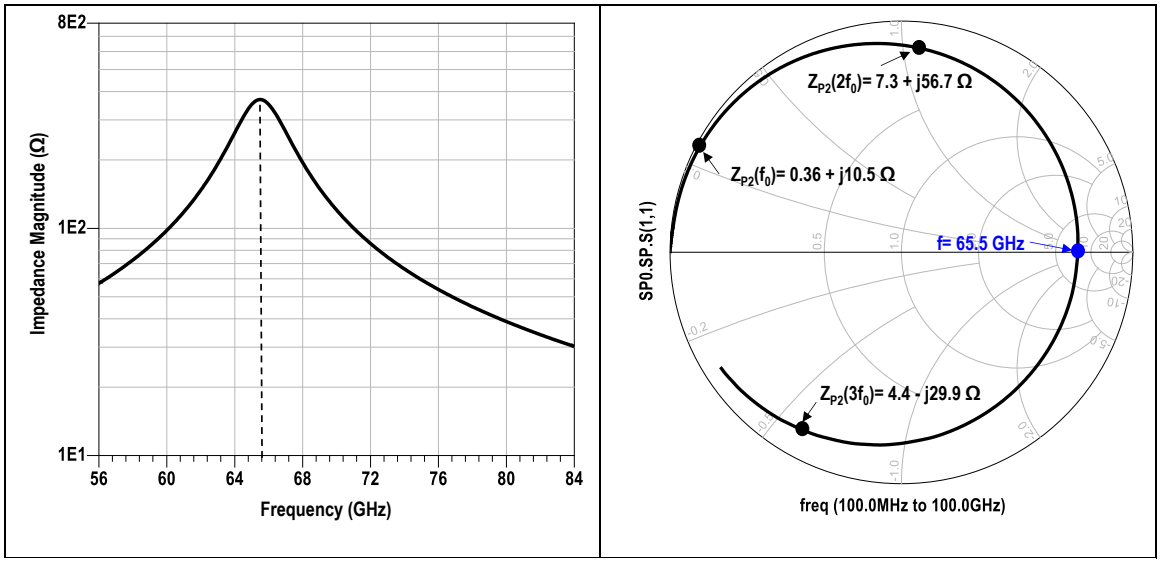

(c) (d)

Fig. 3.12. Class-F^{-1} (a) L_{P1}-C_{P1} tank impedance magnitude, (b) L_{P1}-C_{P1} tank impedances at f_0, $2f_0$, $3f_0$, (c) L_{P1}-C_{P1} tank impedance magnitude, (d) L_{P1}-C_{P1} tank impedances at f_0, $2f_0$, $3f_0$.

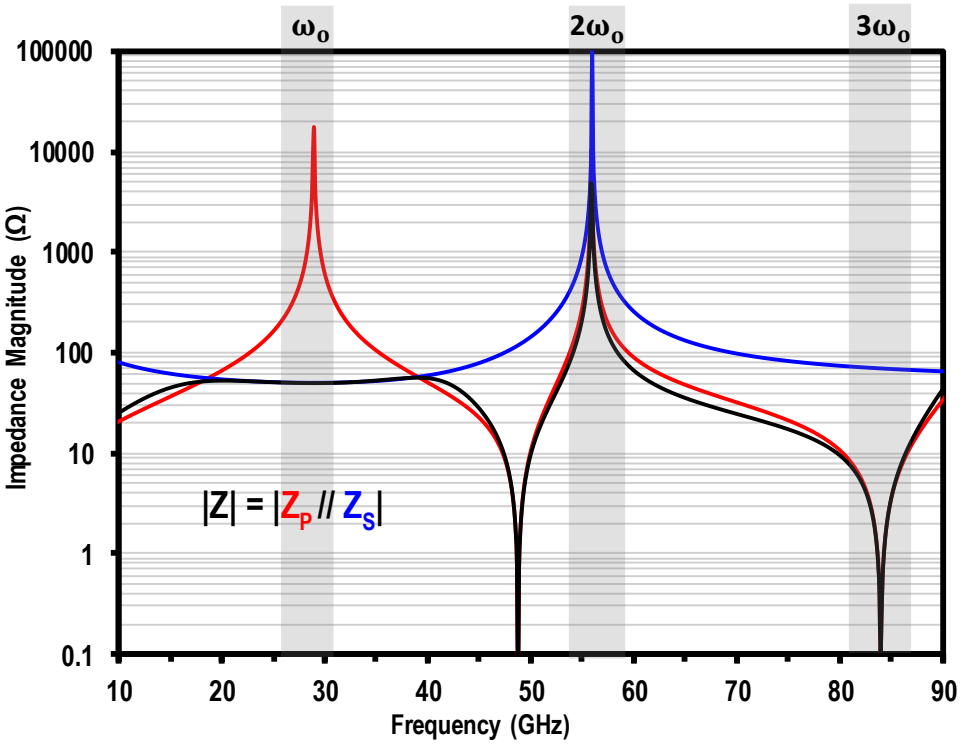

(a)

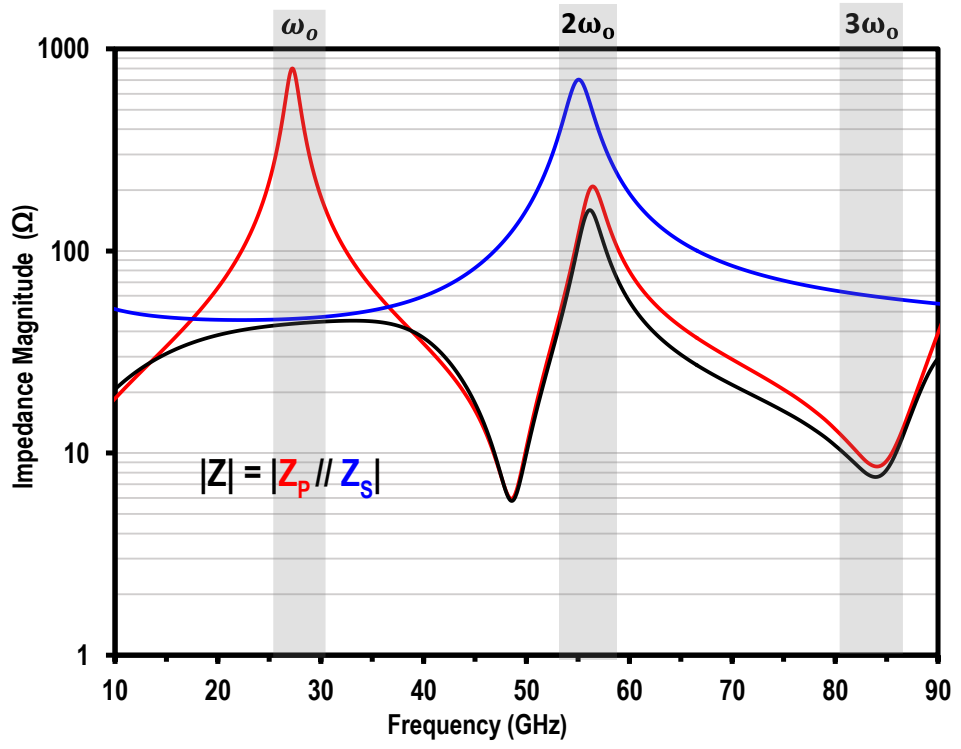

(b)

Fig. 3.13. Impedance magnitude of class-F load network (a) ideal components (b) real components.

3.7 Final Schematics

3.7.1 Class-AB Power Amplifier Final Schematic

Fig. 3.14 shows the final schematic of class-AB common emitter power amplifier, consisting of a pi-type input matching, a base DC feed used for both biasing and stabilizing the circuit, and a base stabilizing network at the input. The load network is a single inductor to cancel out the parasitic capacitor at the fundamental frequency of 28 GHz.

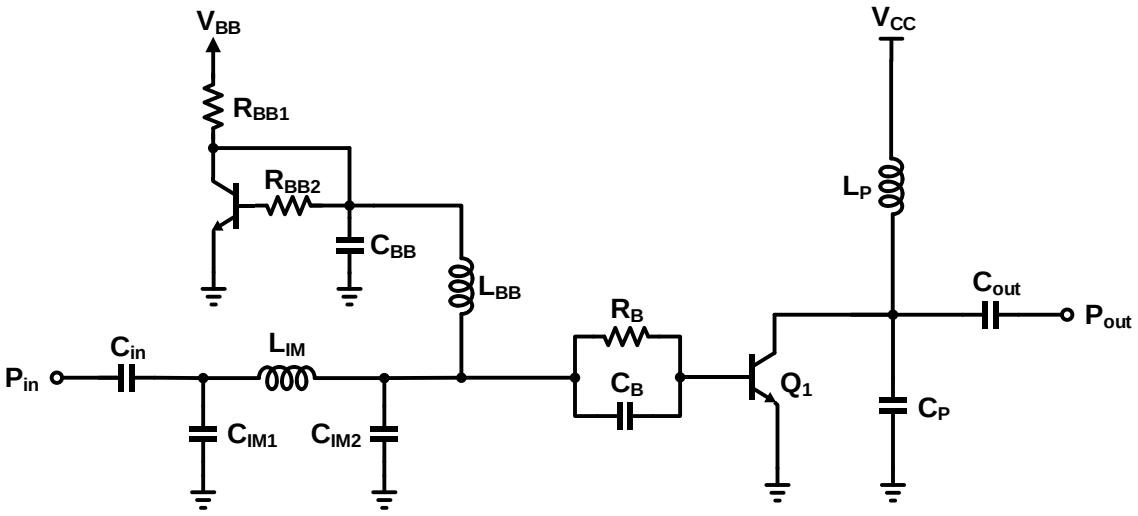

Fig. 3.14. Final schematic of class-AB power amplifier.

3.7.2 Class-F Power Amplifier Final Schematic

Fig. 3.15 shows the final schematic of class-F common emitter power amplifier, consisting of a pi-type input matching, a base DC feed used for both biasing and stabilizing the circuit, and a base stabilizing network at the input. The load network is a multi-resonance network, composing of a parallel network (a LC tank in series with an inductor) and a series network (a $3f_0$-resonance LC tank in series with a capacitor to bring the impedance to 50 Ω.)

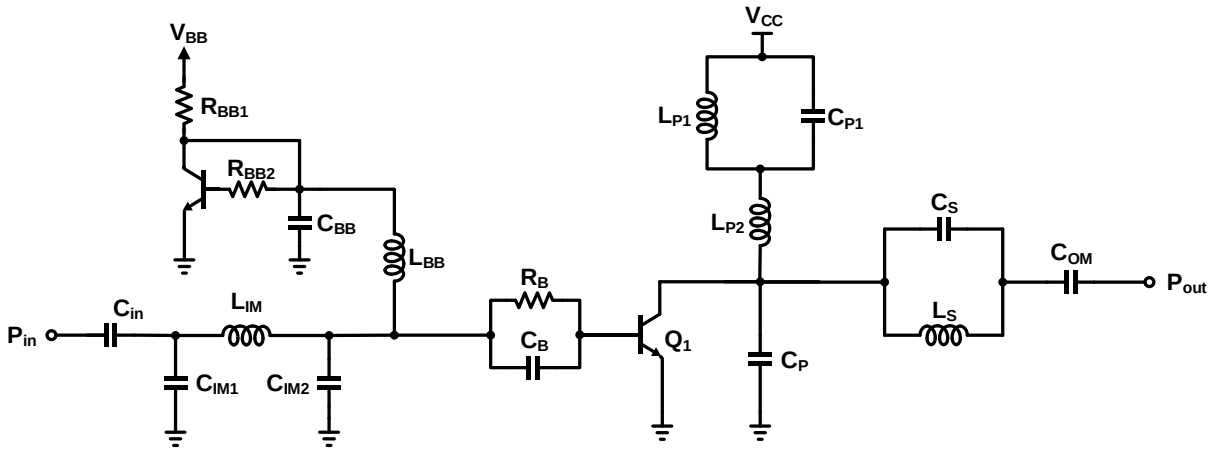

Fig. 3.15. Final schematic of class-F power amplifier.

3.7.3 Class-F^{-1} Power Amplifier Final Schematic

Fig. 3.16 shows the final schematic of class-F common emitter power amplifier, consisting of a pi-type input matching, a base DC feed used for both biasing and stabilizing the circuit, and a base stabilizing network at the input. The load network is a more complex multi-resonance network, composing of a parallel network (two LC tanks in series with an inductor) and a series network (a $2f_0$-resonance LC tank in series with a capacitor to bring the impedance to 50 Ω.)

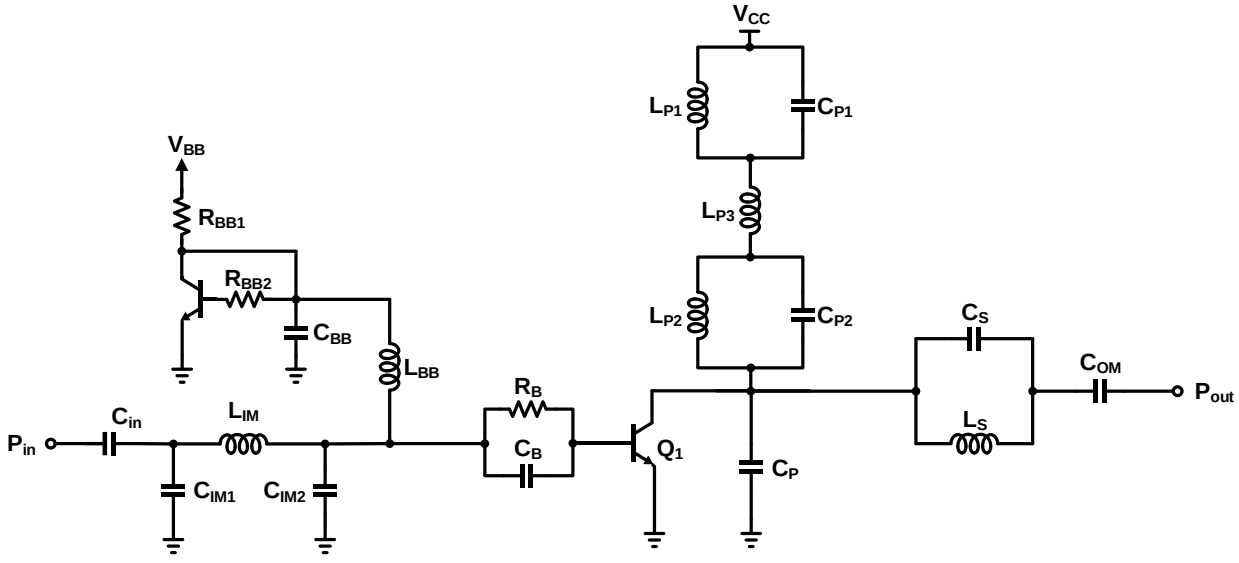

Fig. 3.16. Final schematic of inverse class-F power amplifier.

Chapter 4

Power Amplifier Performance

Contents

4.1 Class-F^{-1} Power Amplifier Performance

4.1.1 Class-F^{-1} Small-signal and Large-signal Stabilities

4.1.1.1 Class-F^{-1} Small-signal Stability

Small-signal stability is extremely important since the amplifier works at mm-wave frequency where the oscillation occurs frequently. With a careful design of the input and output networks, the stability factor (k) is guaranteed to be >1 at all frequencies as illustrated in Fig. 4.1.

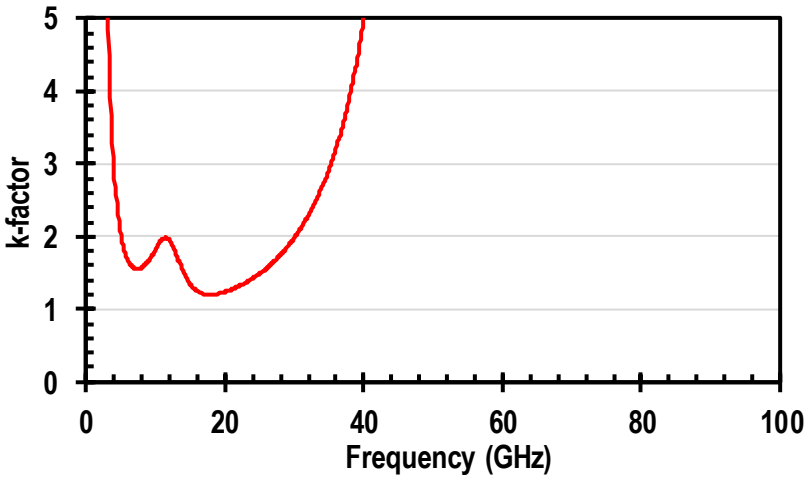

Fig. 4.1. Class-F^{-1} small-signal stability factor k.

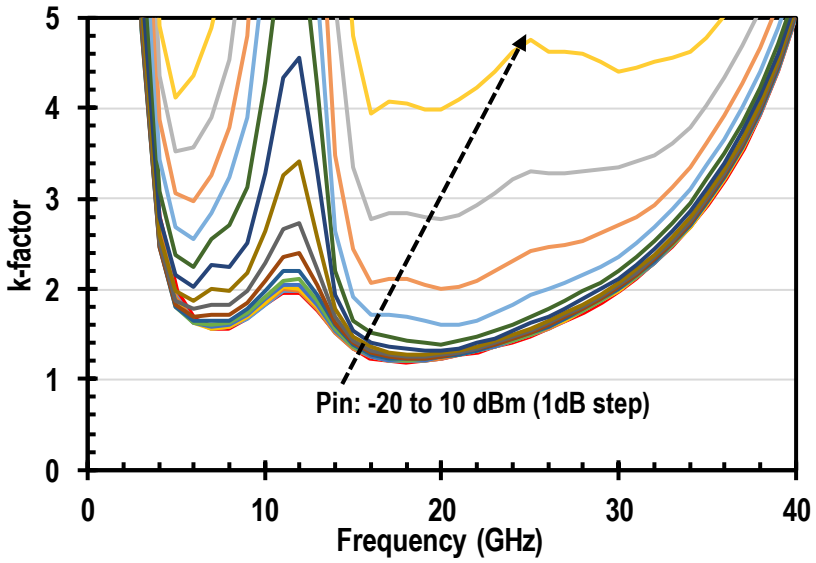

Fig. 4.2. Class-F^{-1} large-signal stability factor k.

4.1.1.2 Class-F^{-1} Large-signal Stability

The purpose of large-signal stability test is to make sure the amplifier not only stable at all frequencies but also stable at all input power levels. Fig. 4.2 shows the large-signal stability factor as sweeping the input power from -20 dBm to 10 dBm with 1dB step. As having a closer look at the stability factor at low power level, both results from small-signal and large-signal stability tests are very close.

4.1.2 Class-F^{-1} Scattering Parameters

Using a conjugate matching for the input matching, 50-Ω match is obtained to ensure the maximum power delivered from the source to the transistor. At the output, the multi-resonance load network is utilized to bring to optimum load close to 50 Ω at the fundamental frequency (28 GHz). From the small-signal and large-signal simulation results, the S-parameters are captured with S_{11} <-10 dB @25.5-30.5 GHz, S_{22} <-10 dB @15-30 GHz, and S_{21} =9-11.3 dB @25.5-30.5 GHz in Fig 4.3.

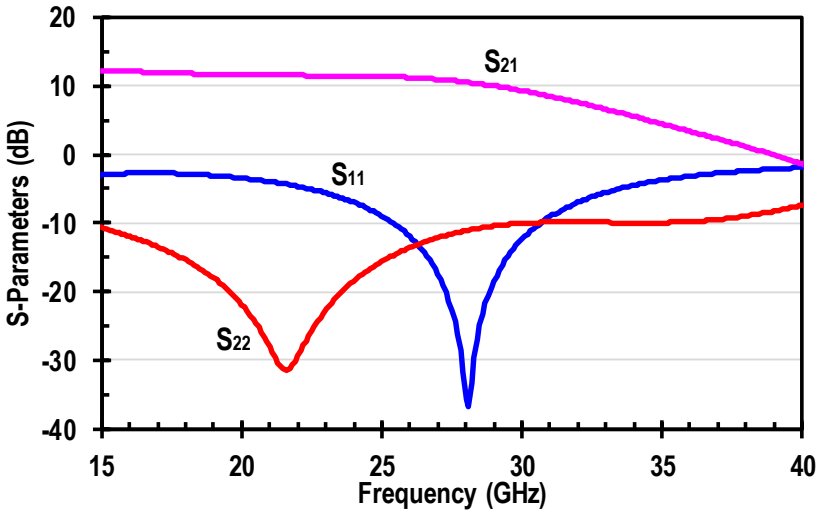

Fig. 4.3. Class-F^{-1} S-parameters (gain, input and output matching).

4.1.3 Class-F^{-1} Time-domain Simulation Waveforms

As mentioned in the design section, class-F^{-1} PA shows its bias point which is very close to class-B operation so called deep class-AB operation. AC load-line is utilized to show the relationship between collector current and voltage of class-F^{-1} PA as illustrated in Fig. 4.4(a). The shape of the load-line shows the behavior of the class-F^{-1} PA. The current and voltage swings and knee voltage can be estimated from the curve.

Using the same data for the fundamental current and voltage components, the time-domain IV waveforms are displayed in Fig. 4.4(b). This figure contains three different pieces of information presented in different color and line patterns to show how much different among the results of the waveforms in the ideal and real situations. In class-F^{-1}, the main goal is to obtain a rectangular current waveform and a half-sinusoidal voltage waveform to guarantee achieving highest efficiency possible.

In Fig. 4.4(b), the dash grey line represents the theoretic current and voltage waveforms based on the expressions in (2.45) and (2.51). The dash line in green color shows the current and voltage waveforms when the PA has all ideal passive components in the load network. Finally, when all real components used in the load network of the class-F^{-1} PA, the solid red line and blue line represent the rectangular collector current waveform and the half-sinusoidal voltage waveform respectively. By observing three cases, the differences in the waveforms show how far the real design is from the theoretical estimation. The losses in the design is caused by using the real passive components not only in the load network but

also in the input matching network, base DC feed network, etc. In order to maximize the magnitude of the current and voltage, a careful selection of the real components is required in the design process.

Fig. 4.4. (c) and (d) are the spectrums of collector current and voltage respectively. As the results, the ratio v_2/v_1 is ~0.2 compared to the optimal value of ~0.35, and the ratio i_3/i_1 is ~0.31 compared to the optimal value of ~0.232 from [17]. From the spectrum data, the collector efficiency becomes 63.2 %. Considering the power loss of P_{loss} = 0.759, the theoretical maximum collector efficiency is estimated as $\eta_{c,max} = 67\% \times P_{loss}$= 50.9 % while the actual collector efficiency is calculated to be η_c = 48 %.

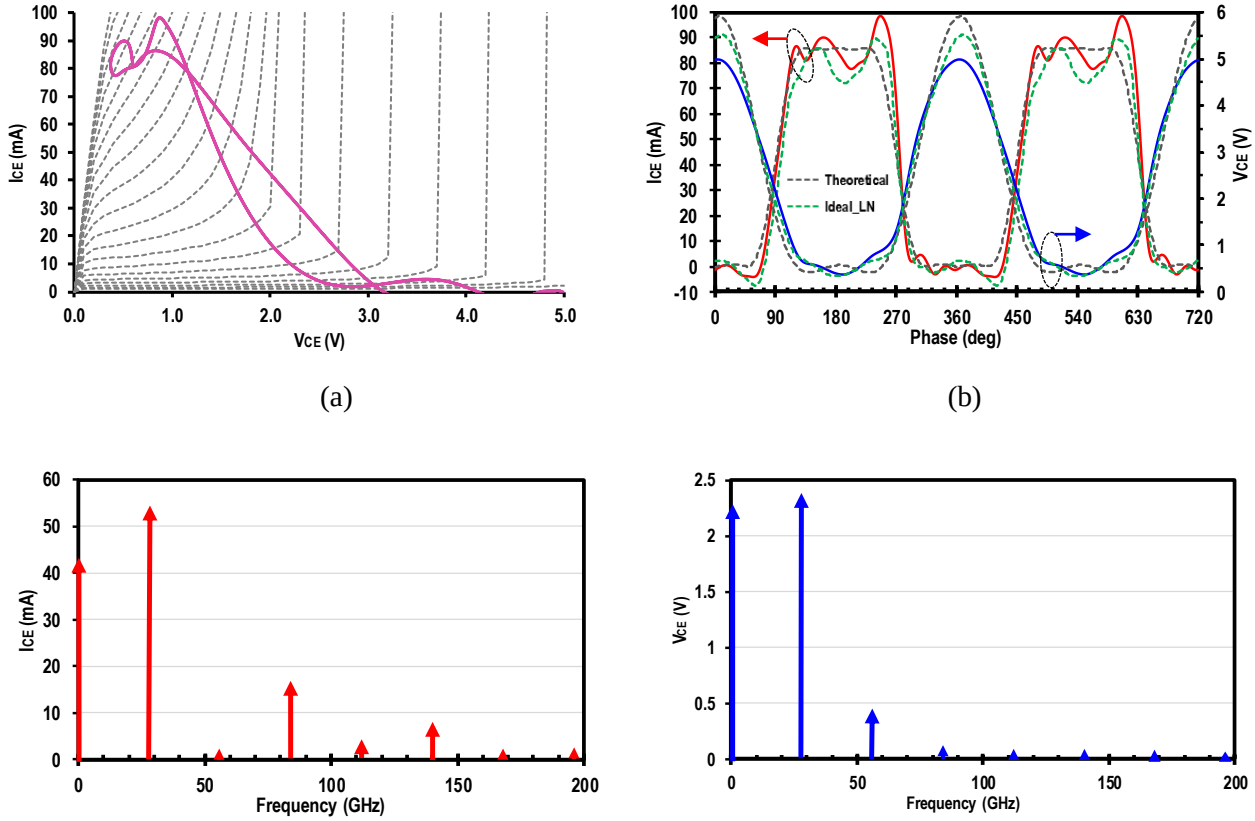

Fig. 4.4. Class-F^{-1} simulated time domain results at 28 GHz: (a) AC load line, and (b) collector voltage and current waveforms, (c) collector current spectrum, and (d) collector voltage spectrum. In (b), green dash line is for ideal load network, solid lines are for real load network, and grey dash line is for theoretical estimation based on (2.45) and (2.51).

4.1.4 Class-F^{-1} Power Gain, Output Power, and PAE

4.1.4.1 Class-F^{-1} Output Power

Class-F^{-1} PA operates at a class-AB bias point where the required output power can be achieved. Fig. 4.5 shows the output power of class-F^{-1} PA versus the input power sweep from -20dBm to 15dBm at 28 GHz. The pink dash line is the output power curve of the class-F^{-1} PA with all ideal components used in the load network, and the black line is the output power with all real components in the load network. As the result, the output power at 1 dB compression point (OP_{-1dB}) is achieved with 15.1 dBm. At the peak PAE, the corresponding output power is estimated to be 17.3 dBm. The PA reaches the saturated output power P_{sat} of >19 dBm.

4.1.4.2 Class-F^{-1} Power Gain

Fig. 4.6. shows the simulated result of the power gain of the class-F^{-1} PA with the ideal component load network (pink) and real component load network (blue). At 28 GHz, the PA achieves the power gain level of 10.9 dB. The peak PAE is achieved at the corresponding output power of ~7 dB.

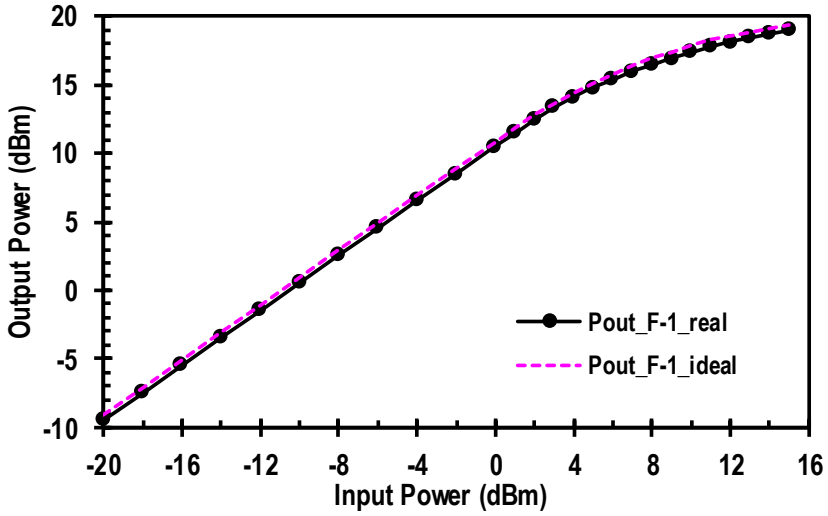

Fig. 4.5. Class-F^{-1} output power (P_{out}) vs. P_{in} at 28 GHz.

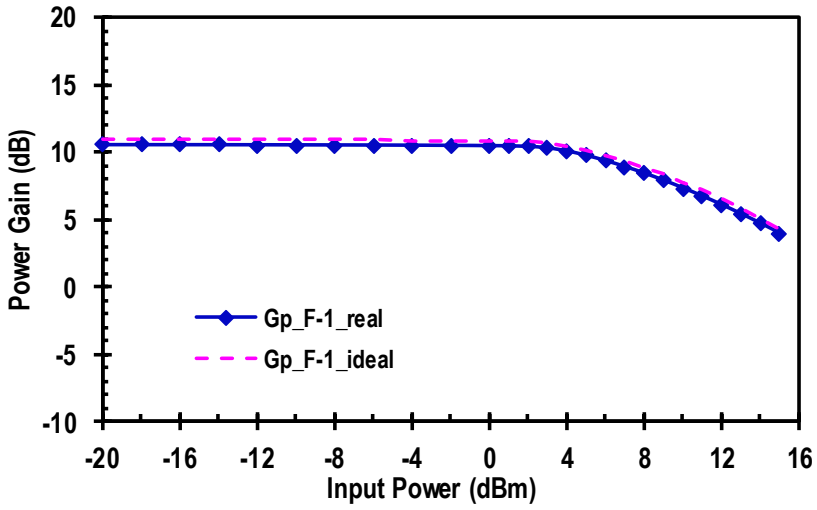

Fig. 4.6. Class-F^{-1} power gain (G_P) vs. P_{in} at 28 GHz.

4.1.4.3 Class-F^{-1} PAE

In class-F^{-1} PA, a harmonic load network is designed to have high impedance at the second harmonic and low impedance at the third harmonic in order to shape current and voltage waveforms to achieve high efficiency possible. As shown in the previous section 4.1.3, the rectangular current and half-sinusoidal voltage waveforms are obtained to guarantee high efficiency achieved at the output of the amplifier. The load network of the PA is initially designed using the ideal passive components and later replaced with the real components for the final design. Fig 4.7 shows the peak PAE versus the input power level while Fig 4.8 illustrates the relationship between peak PAE and output power. Since there are losses in the load network as replacing the ideal components with the real components, the displays of efficiency for both cases are used for further analysis and comparison.

As the result, the PA achieves the peak PAE of 57.7 % with ideal components being used in the load network. The peak PAE decreases to about 45 % when all real components are replaced. The main reason for these losses is the use of low-Q passive components, leading to the parasitic resistances with both parallel and series path of the load network. This shows the importance of components selection in the design process. As mentioned, a custom made MOM capacitors are utilized to higher Q values to reduce power loss in the circuit.

The load pull simulation is also conducted to ensure that the highest PAE can be achieve and the optimum load as close to 50 Ω possible. Since there is a trade-off between

the maximum output power and the peak PAE, the goal is to determine the load impedance point where the PA can achieve the required output power and highest PAE as the same time.

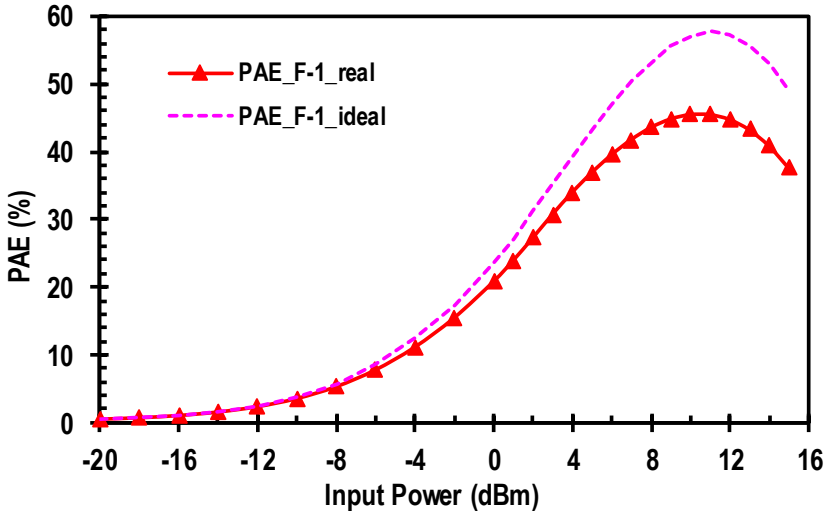

Fig. 4.7. Class-F^{-1} peak maximum efficiency (PAE) vs. P_{in} at 28 GHz.

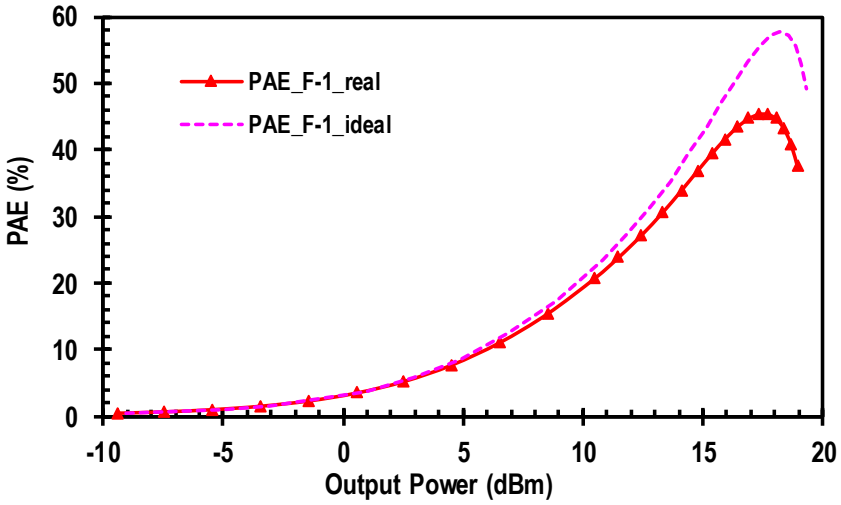

Fig. 4.8. Class-F^{-1} peak maximum efficiency (PAE) vs. P_{out} at 28 GHz.

4.2 Class-F Power Amplifier Performance

4.2.1 Class-F Small-signal and Large-signal Stabilities

4.2.1.1 Class-F Small-signal Stability

Small-signal stability is extremely important since the amplifier works at mm-wave frequency where the oscillation occurs frequently. With a careful design of the input and output networks, the stability factor (k) is guaranteed to be >1 at all frequencies as illustrated in Fig. 4.9.

4.2.1.2 Class-F Large-signal Stability

The purpose of large-signal stability test is to make sure the amplifier not only stable at all frequencies but also stable at all input power levels. Fig. 4.10 shows the large-signal stability factor as sweeping the input power from -20 dBm to 10 dBm with 1dB step. As having a closer look at the stability factor at low power level, both results from small-signal and large-signal stability tests are very close.

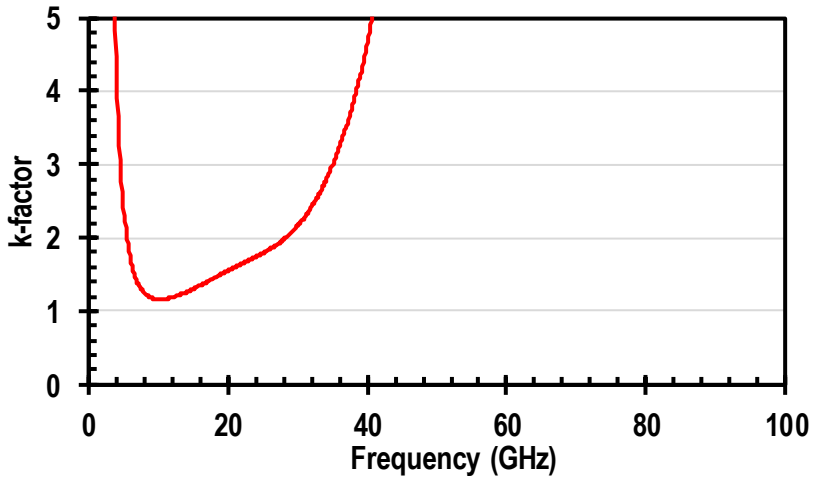

Fig. 4.9. Class-F small-signal stability factor k.

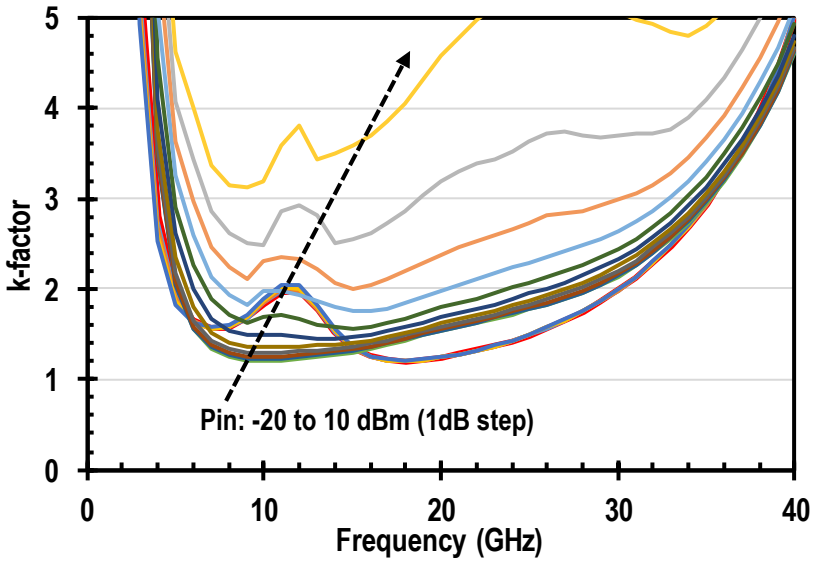

Fig. 4.10. Class-F large-signal stability factor k with P_{in} sweep.

4.2.2 Class-F Scattering Parameters

Using a conjugate matching for the input matching, 50-Ω match is obtained to ensure the maximum power delivered from the source to the transistor. At the output, the multi-resonance load network is utilized to bring to optimum load close to 50 Ω at the fundamental frequency (28 GHz). From the small-signal and large-signal simulation results, the S-parameters are captured with S_{11} <-10 dB @25-30.4 GHz, S_{22} <-10 dB @16.5-31 GHz, and S_{21} =9-10.7 dB @25-30 GHz in Fig. 4.11.

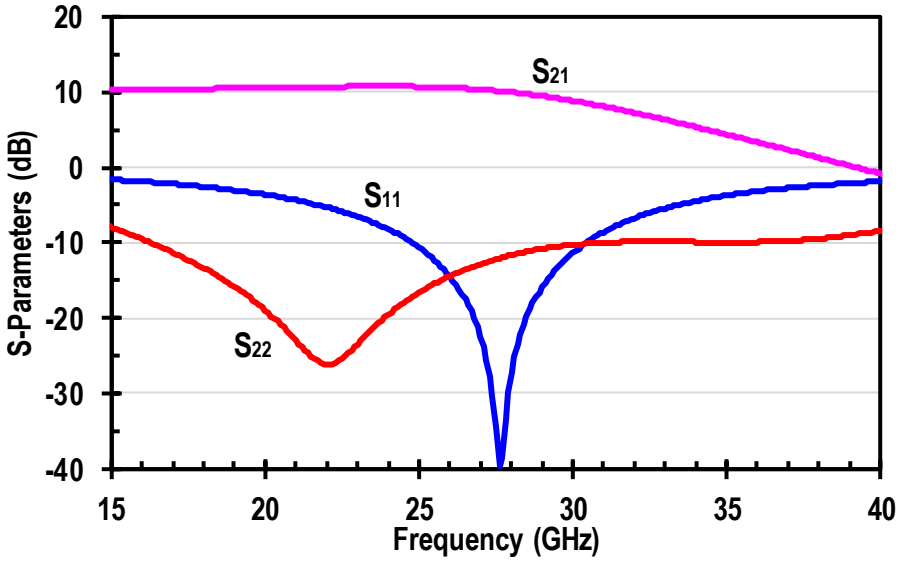

Fig. 4.11. Class-F S-parameters (gain, input and output matching).

4.2.3 Class-F Time-domain Simulation Waveform Analysis

The analysis on the time-domain waveforms for class-F is very similar to that of class-F^{-1}. In Fig. 4.12(a), AC load-line is displayed to show the relationship between collector current and voltage of class-F. The shape of the load-line shows the behavior of the class-F PA and looks a little different from class-F^{-1} case due to the limited voltage swing caused by the rectangular waveform.

Fig. 4.12(b) presents the time-domain IV waveforms in different color and patterns to show the difference between ideal and real fundamental current and voltage components. In class-F, the main goal is to obtain a rectangular voltage waveform and a half-sinusoidal current waveform to achieve highest efficiency possible. In Fig. 4.12(b), the dash grey line represents the theoretic current and voltage waveforms based on the expressions in (2.62) and (2.68). The dash line in green color shows the current and voltage waveforms when the PA has all ideal passive components in the load network. The solid red line and blue line represent the rectangular collector voltage waveform and the half-sinusoidal current waveform respectively when all real components are used in the load network of the class-F^{-1} PA. By observing three cases, the differences in the waveforms show how far the real design is from the theoretical estimation. There are some losses due to the real passive components not only in the load network but also in the input matching network, base DC feed network, etc. The process of selecting the passive components starts with the ideal components based on mathematic estimation and calculations. In order to maximize the magnitude of the current and voltage, a careful component selection and optimization is significantly needed.

Fig. 4.12. (c) and (d) are the spectrums of collector current and voltage respectively. As the results, the ratio v_3/v_1 is ~0.2 compared to the optimal value of ~0.1667, and the ratio i_2/i_1 is ~0.31 compared to the optimal value of ~0.354 from [17]. From the spectrum data, the collector efficiency becomes 64 %. Considering the power loss of P_{loss} = 0.908, the theoretical maximum collector efficiency is estimated as $\eta_{c,max} = 67.4\% \times P_{loss}$= 61.2 % while the actual collector efficiency is calculated to be η_c = 58 %.

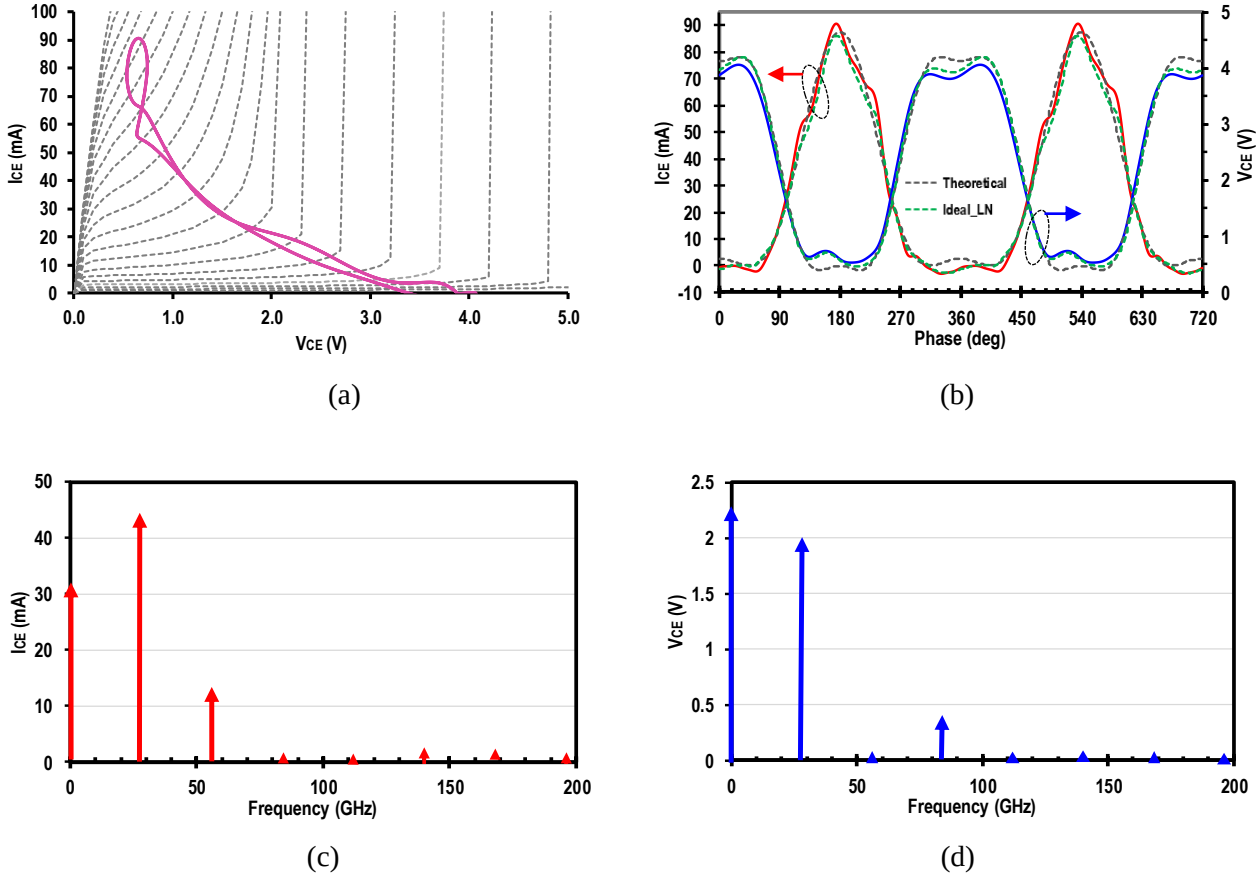

Fig. 4.12. Class-F simulated time domain results at 28 GHz: (a) AC load line, and (b) collector voltage and current waveforms, (c) collector current spectrum, and (d) collector voltage spectrum. In (b), green dash line is for ideal load network, solid lines are for real load network, and grey dash line is for theoretical estimation based on (2.62) and (2.68).

4.2.4 Class-F Power Gain, Output Power, and PAE

4.2.4.1 Class-F Output Power

Class-F PA operates at a class-AB bias point where the required output power can be achieved. Fig. 4.13 shows the output power of class-F PA versus the input power sweep from -20dBm to 15dBm at 28 GHz. The pink dash line is the output power curve of the class-F PA with all ideal components used in the load network, and the black line is the output power with all real components in the load network. As the result, the output power at 1 dB compression point (OP-1dB) is achieved with 14.5 dBm. At the peak PAE, the corresponding output power is estimated to be 16.5 dBm. The PA reaches the saturated output power P_{sat} of 17.9 dBm.

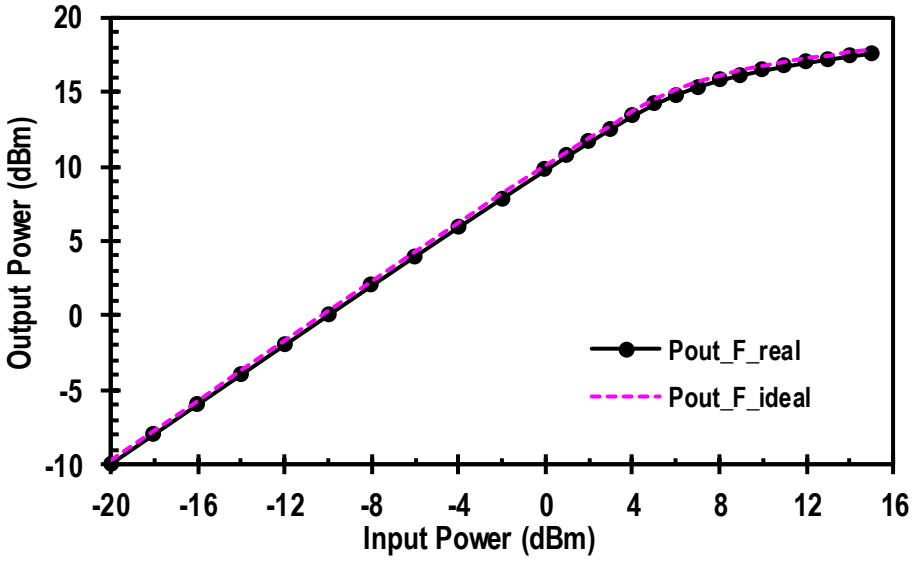

Fig. 4.13. Class-F output power (P_{out}) vs. P_{in} at 28 GHz.

4.2.4.2 Class-F Power Gain

Fig. 4.14. shows the simulated result of the power gain of the class-F PA with the ideal component load network (pink) and real component load network (blue). At 28 GHz, the PA achieves the power gain level of 10.3 dB. The peak PAE is achieved at the corresponding output power of 7.5 dB.

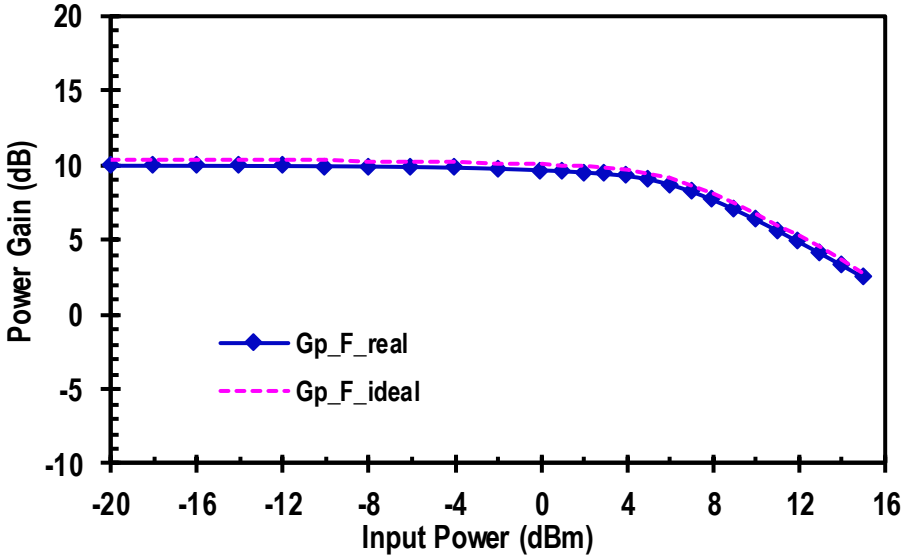

Fig. 4.14. Class-F power gain (G_P) vs. P_{in} at 28 GHz.

4.2.4.3 Class-F PAE

In class-F PA, a harmonic load network is designed to have high impedance at the second harmonic and low impedance at the third harmonic in order to shape current and voltage waveforms to achieve high efficiency possible. As shown in the previous section 4.2.3, the rectangular current and half-sinusoidal voltage waveforms are obtained to guarantee high efficiency achieved at the output of the amplifier. The load network of the PA is initially designed using the ideal passive components and later replaced with the real components for the final design. Fig 4.15 shows the peak PAE versus the input power level while Fig 4.16 illustrates the relationship between peak PAE and output power. Since there are losses in the load network as replacing the ideal components with the real components, the displays of efficiency for both cases are used for further analysis and comparison.

As the result, the PA achieves the peak PAE of 54.7 % with ideal components being used in the load network. The peak PAE decreases to about 45 % when all real components are replaced. The main reason for these losses is the use of low-Q passive components, leading to the parasitic resistances with both parallel and series path of the load network. This shows the importance of components selection in the design process. As mentioned, a custom made MOM capacitors are utilized to higher Q values to reduce power loss in the circuit.

The load pull simulation is also conducted to ensure that the highest PAE can be achieve and the optimum load as close to 50 Ω possible. Since there is a trade-off between the maximum output power and the peak PAE, the goal is to determine the load impedance point where the PA can achieve the required output power and highest PAE as the same time.

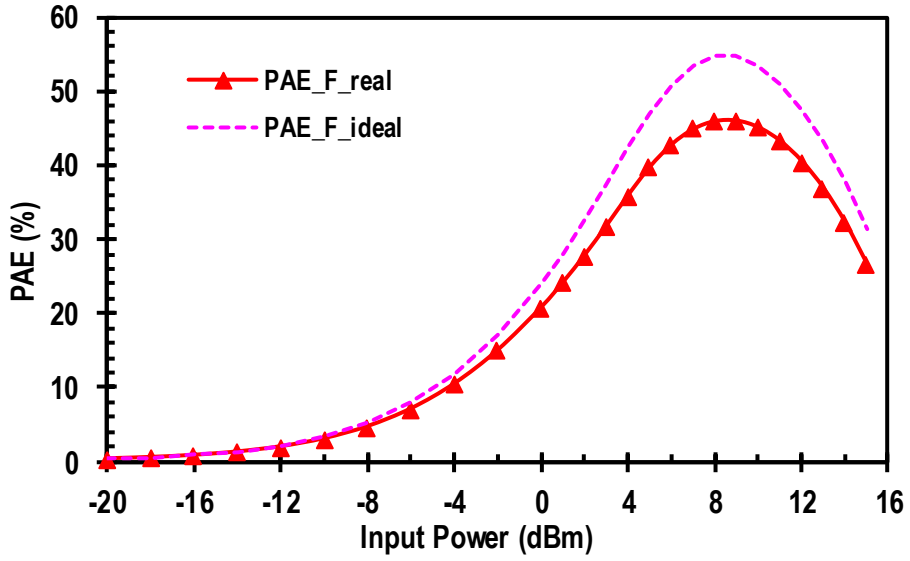

Fig. 4.15. Class-F peak maximum efficiency (PAE) vs. P_{in} at 28 GHz.

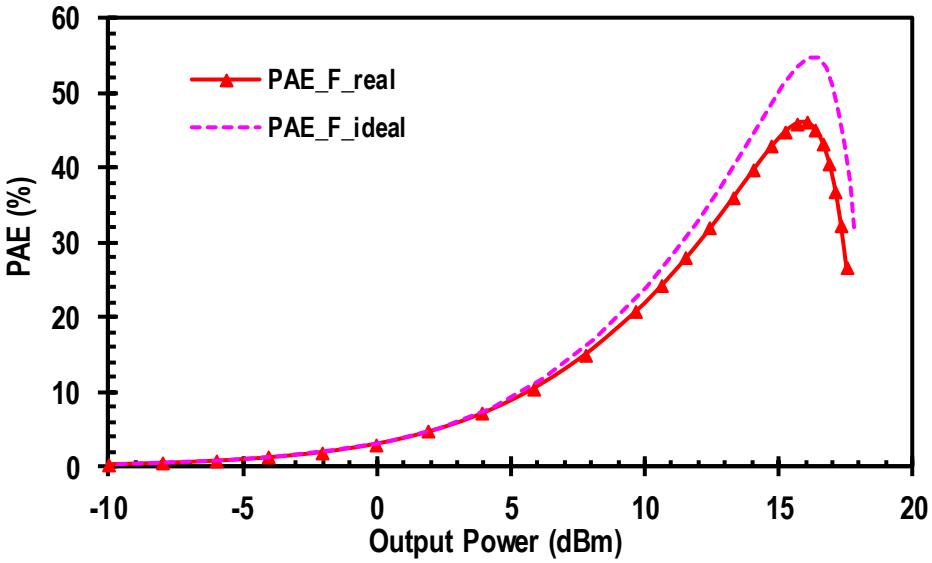

Fig. 4.16. Class-F^{-1} peak maximum efficiency (PAE) vs. P_{out} at 28 GHz.

4.3 Class-AB Power Amplifier Performance

4.3.1 Class-AB Small-signal and Large-signal Stabilities

4.3.1.1 Class-AB Small-signal Stability

Small-signal stability is extremely important since the amplifier works at mm-wave frequency where the oscillation occurs frequently. With a careful design of the input and output networks, the stability factor (k) is guaranteed to be >1 at all frequencies as illustrated in Fig. 4.17.

4.3.1.2 Class-AB Large-signal Stability

The purpose of large-signal stability test is to make sure the amplifier not only stable at all frequencies but also stable at all input power levels. Fig. 4.18 shows the large-signal stability factor as sweeping the input power from -20 dBm to 10 dBm with 1dB step. As having a closer look at the stability factor at low power level, both results from small-signal and large-signal stability tests are very close.

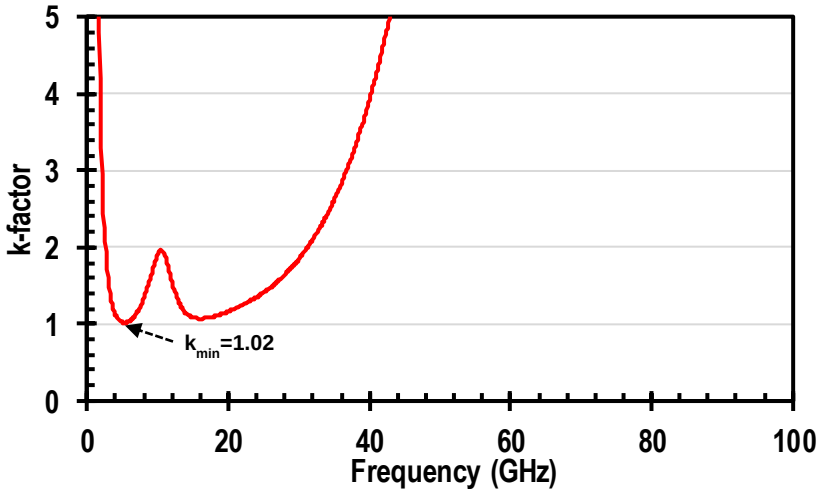

Fig. 4.17. Class-AB small-signal stability factor k.

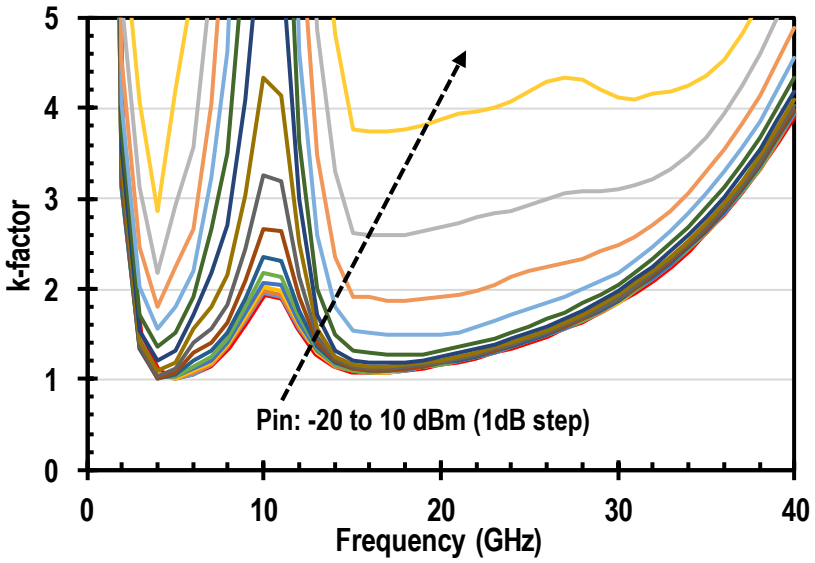

Fig. 4.18. Class-F large-signal stability factor k with P_{in}.

4.3.2 Class-AB Scattering Parameters

Using a conjugate matching for the input matching, 50-Ω match is obtained to ensure the maximum power delivered from the source to the transistor. At the output, the multi-resonance load network is utilized to bring to optimum load close to 50 Ω at the fundamental frequency (28 GHz). From the small-signal and large-signal simulation results, the S-parameters are captured with S_{11} <-10 dB @25-30.5 GHz, S_{22} <-8.2 dB @15-30 GHz, and S_{21} =9-11.4 dB @25-30.5 GHz in Fig. 19.

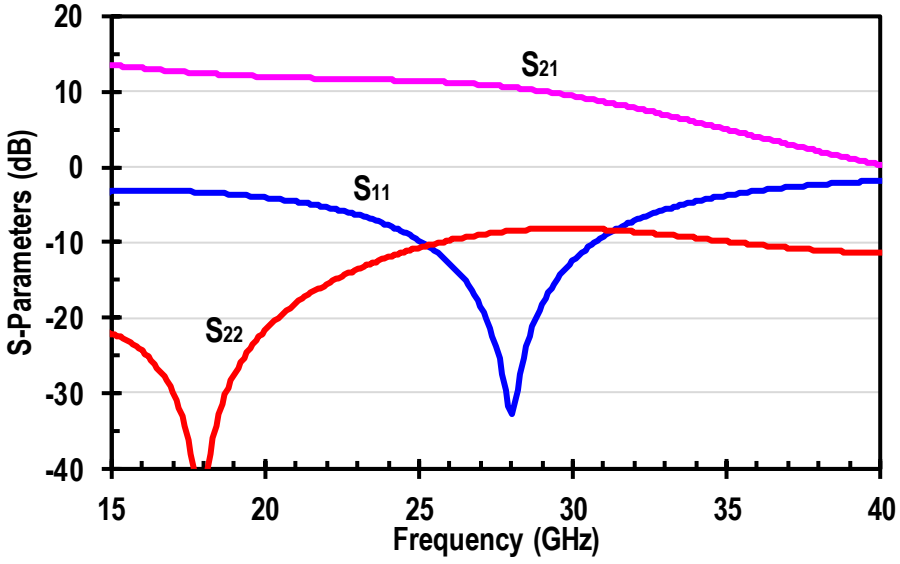

Fig. 4.19. Class-AB S-parameters (gain, input and output matching).

4.3.3 Class-AB Time-domain Simulation Waveform Analysis

In Fig. 4.20(a), AC load-line is displayed to show the relationship between collector current and voltage of class-AB. The shape of the load-line shows the behavior of the class-AB PA. Fig. 4.12(b) presents the time-domain IV waveforms. In class-AB, The collector voltage and current waveforms depends on the conduction angle α ($\pi < \alpha < 2\pi$). In Fig. 4.12(b), the solid red line and blue line represent the collector voltage waveform and the current waveform respectively.

Fig. 4.12. (c) and (d) are the spectrums of collector current and voltage respectively. From the spectrum of the current, the ratio I_1/I_{DC} is determined to be ~1.16 which can be used to estimate the conduction angle α based on the relationship between current components and the conduction angle in the Fig. 2.19. With a rough estimation, the conduction angle is ~ $13\pi/8$. Applying this conduction angle to the equation (2.76) the collector efficiency can be calculated to be η_c~56%.

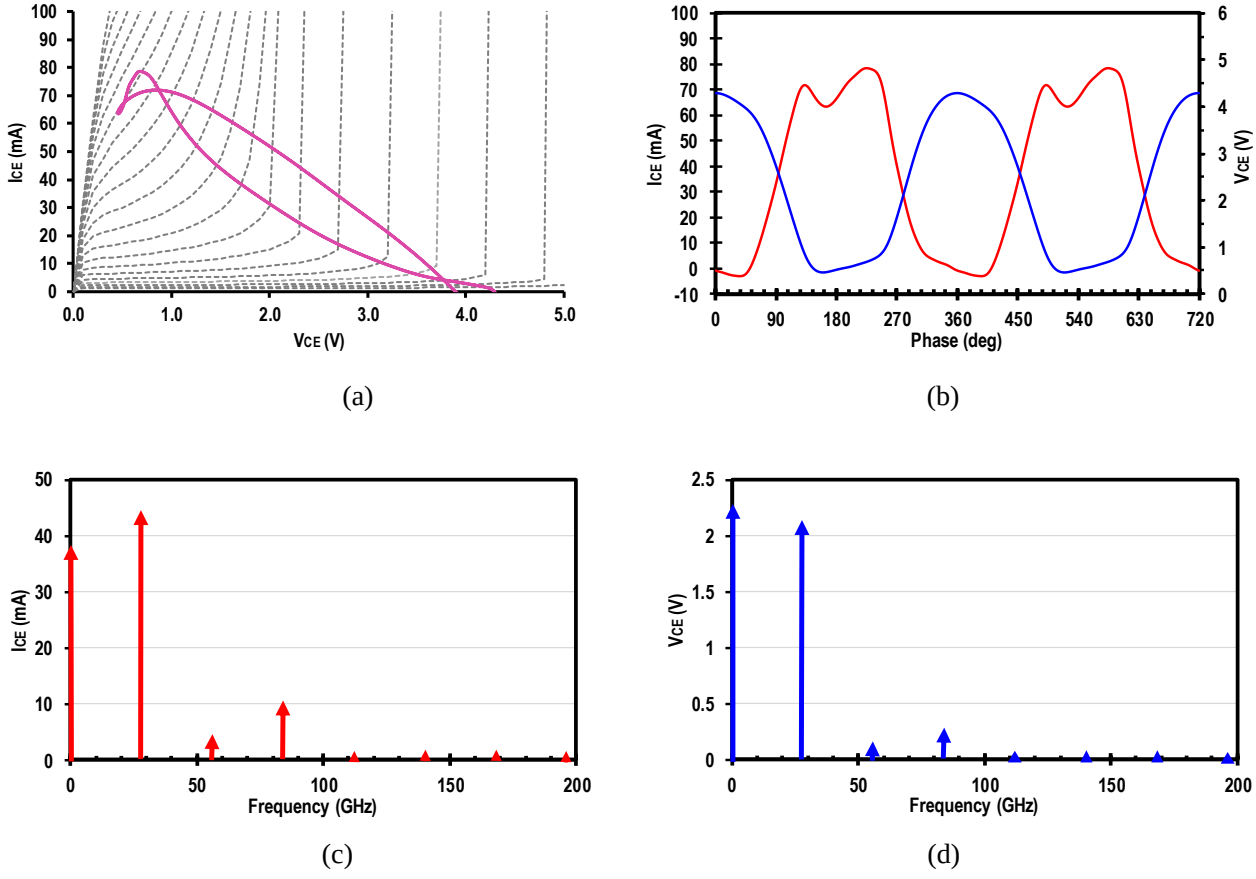

Fig. 4.20. Class-AB simulated time domain results at 28 GHz: (a) AC load line, and (b) collector voltage (blue) and current (red) waveforms, (c) collector current spectrum, and (d) collector voltage spectrum.

4.3.4 Class-AB Power Gain, Output Power, and PAE

4.3.4.1 Class-AB Output Power

Fig. 4.21 shows the output power of class-AB PA versus the input power sweep from -20dBm to 15dBm at 28 GHz. The pink dash line is the output power curve of the class-AB PA with all ideal components used in the load network, and the black line is the output power with all real components in the load network. As the result, the output power at 1 dB compression point (OP_{-1dB}) is achieved with 15.6 dBm. At the peak PAE, the corresponding output power is estimated to be 16.7 dBm. The PA reaches the saturated output power P_{sat} of >19 dBm.

4.3.4.2 Class-AB Power Gain

Fig. 4.22. shows the simulated result of the power gain of the class-AB PA with the ideal component load network (pink) and real component load network (blue) At 28 GHz, the PA achieves the power gain level of 10.9 dB. The peak PAE is achieved at the corresponding output power of 8.7 dB.

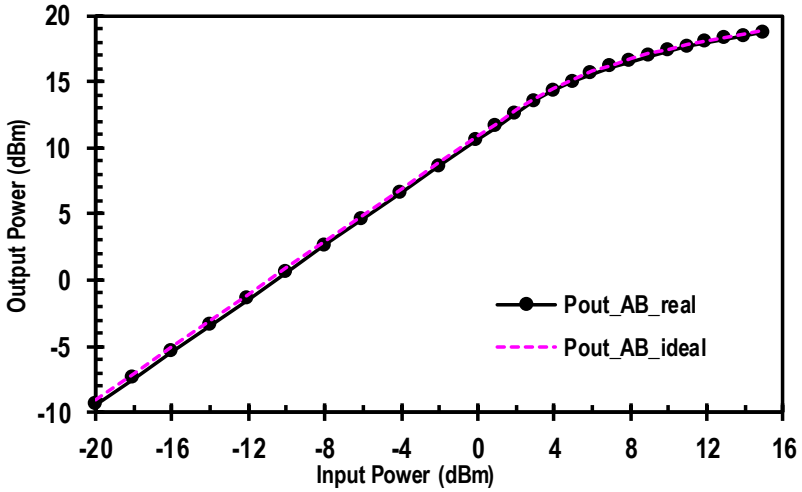

Fig. 4.21. Class-AB output power (P_{out}) vs. P_{in} at 28 GHz.

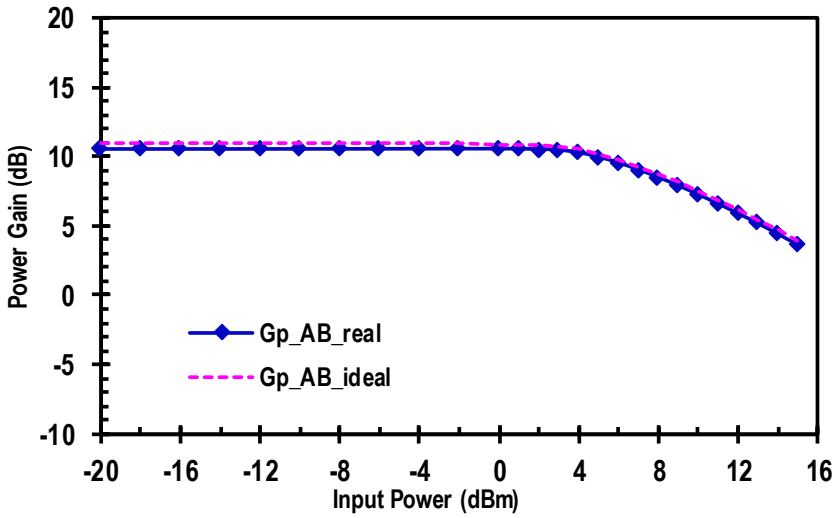

Fig. 4.22. Class-AB power gain (G_P) vs. P_{in} at 28 GHz.

4.3.4.3 Class-AB PAE

In class-AB PA, a harmonic load network is designed to have high impedance at the second harmonic and low impedance at the third harmonic in order to shape current and voltage waveforms to achieve high efficiency possible. As shown in the previous section 4.3.3, the rectangular current and half-sinusoidal voltage waveforms are obtained to guarantee high efficiency achieved at the output of the amplifier. The load network of the PA is initially designed using the ideal passive components and later replaced with the real components for the final design. Fig 4.23 shows the peak PAE versus the input power level while Fig 4.24 illustrates the relationship between peak PAE and output power. Since there are losses in the load network as replacing the ideal components with the real components, the displays of efficiency for both cases are used for further analysis and comparison.

As the result, the PA achieves the peak PAE of 48.5 % with ideal components being used in the load network. The peak PAE decreases to about 44 % when all real components are replaced. The main reason for these losses is the use of low-Q passive components, leading to the parasitic resistances with both parallel and series path of the load network. This shows the importance of components selection in the design process. As mentioned, a custom made MOM capacitors are utilized to higher Q values to reduce power loss in the circuit.

The load pull simulation is also conducted to ensure that the highest PAE can be achieve and the optimum load as close to 50 Ω possible. Since there is a trade-off between

the maximum output power and the peak PAE, the goal is to determine the load impedance point where the PA can achieve the required output power and highest PAE as the same time.

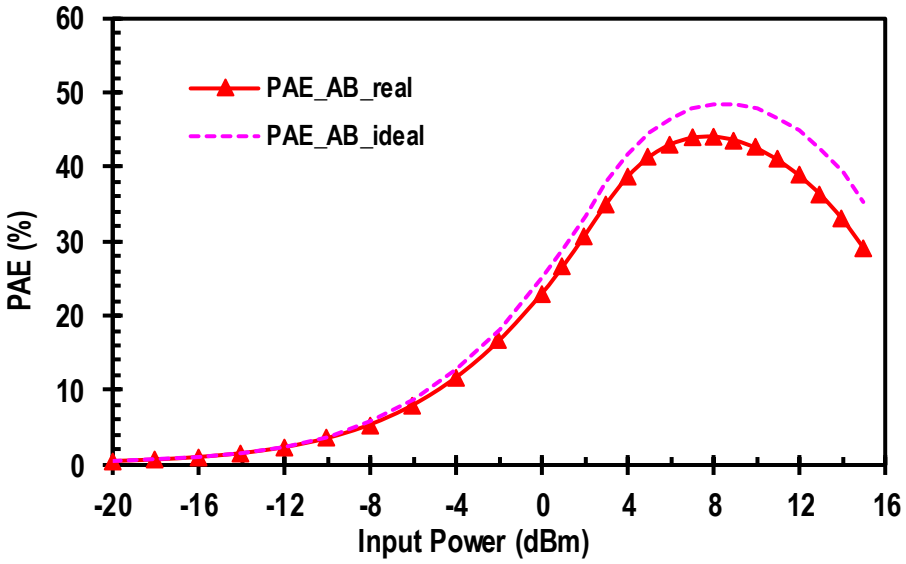

Fig. 4.23. Class-AB peak maximum efficiency (PAE) vs. P_{in} at 28 GHz.

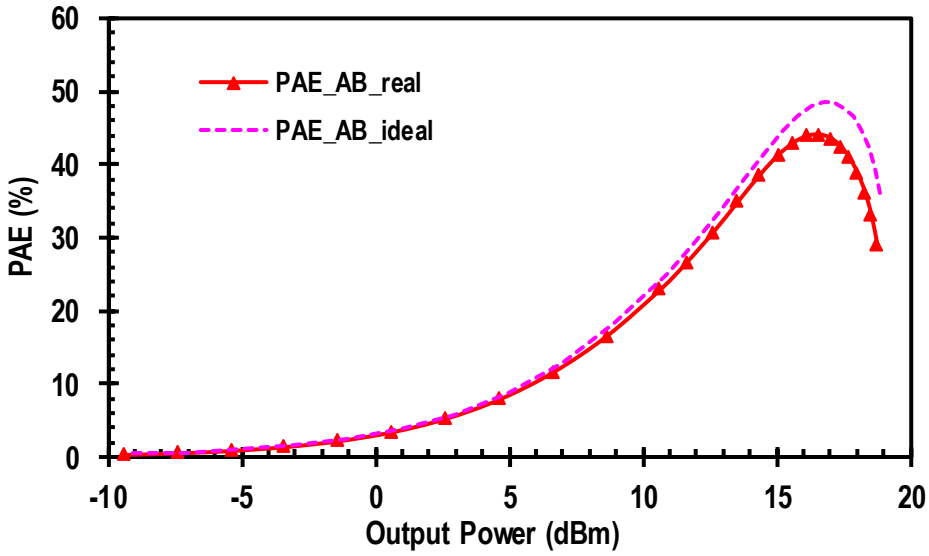

Fig. 4.24. Class-AB peak maximum efficiency (PAE) vs. P_{out} at 28 GHz.

4.4 Summary and Comparison

In general, all three classes achieve the performance results that are convincible and fairly satisfy the requirements of the system. The difference in load network design among three classes creates distinctive behavior and performance for each PA. The performance shows that three designs satisfy the stability requirement to have k-factor >1. The 1 dB compression powers are reached or very close to the expected value of 15 dBm. The PAs also achieve the power gain needed for the system. At 28 GHz, with the satisfaction of all other performance requirements, the results of the peak PAEs are obtained.

One of the two primary goals in thesis is to compare the maximum PAE among class-F, F^{-1}, and AB PAs at the same fundamental frequency of 28 GHz and at the same bias point of V_{CE}=2.3V and I_{CE}=12mA. Since the load networks are different, three classes achieve different the output powers and the peak PAEs as the result. In order to have a fair comparison, the output powers of the PAs are designed to be within 1dB difference. As mentioned in the previous sections, the load networks contain all ideal passive components initially, leading to the maximum PAE result versus output power as illustrated Fig. 4.25. After replaced by the real components, the maximum PAE for three classes are shown in Fig. 4.26.

As the results, the maximum PAEs of three PAs are fairly close to each other. Class-F PA achieves the highest maximum PAE among three classes with 46 %. The lowest maximum PAE with 44% belongs to class-AB PA. Finally, a 45 % maximum PAE is obtained by class-F^{-1} PA. In theory, class-F and class-F^{-1} PAs are expected to achieve higher efficiency than class-AB at the same bias condition and frequency. By observing the maximum PAEs in two figures, the result shows that the peak PAE of class-AB is only slightly lower than two other PAs. The reason that brings the maximum PAE performances of the PAs close to each other is the loss in the load networks. Class-F^{-1} PA has a complex load network with the most number of passive components (Fig. 3.11) comparing to two other classes. Therefore, the peak PAE of class-F^{-1} decreases >12% from 57.7% to 45% which is the most among three PAs. The second complex load network (Fig. 3.9) belongs to class-F PA which causes a big degradation in maximum PAE of >8% from 54.7% to 46%. Since the load network of class-AB PA contains the only inductor (Fig. 3.8), there is

only ~ 4% decrease in peak PAE from 48% to 44%. The results show how much effect of the loss in the load networks to the efficiencies.

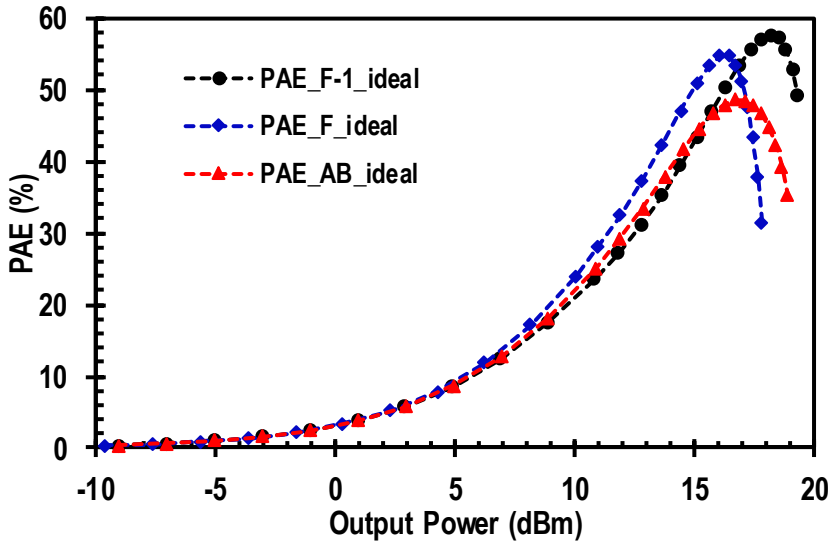

Fig. 4.25. Class-AB, F, and F^{-1} peak maximum efficiency (PAE) vs. P_{in} at 28 GHz.

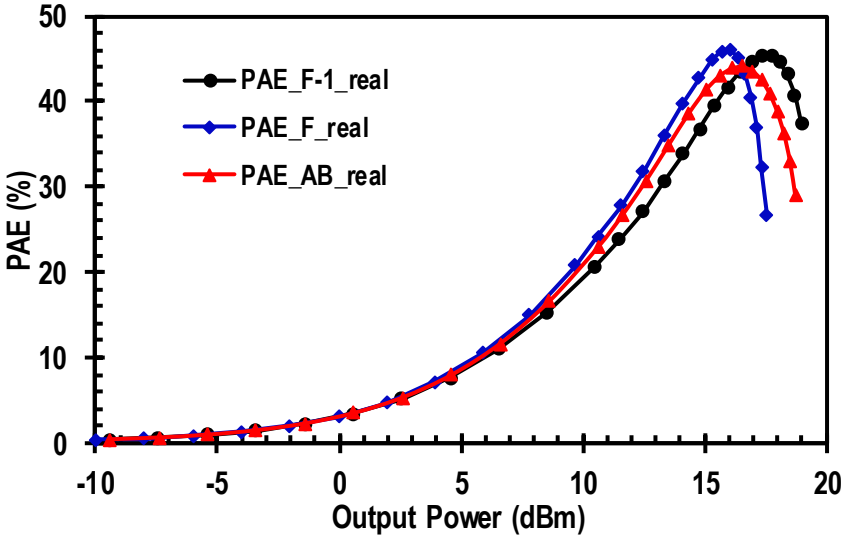

Fig. 4.26. Class-AB, F, and F^{-1} peak maximum efficiency (PAE) vs. P_{out} at 28 GHz.

Chapter 5

Linearization Analysis

Contents

5.1 Linearity on Class-F^{-1} Power Amplifier

5.1.1 Class-F^{-1} OP-$_{1dB}$ Estimation from Two-tone Simulation Data

The input signal is a two-tone excitation and expressed as:

$$v_i(t) = X_1 \cos(\omega_1 t) + X_2 \cos(\omega_2 t) \tag{5.1}$$

The output current of the PA is i_0 can be expressed in terms of currents as:

$$i_0(t) = \alpha_1 v_i + \alpha_2 {v_i}^2 + \alpha_3 {v_i}^3 + \cdots \tag{5.2}$$

Since the effect of higher order harmonic components is not significant, the output current expression is evaluated only up to the third harmonic for simplicity. As shown in (2.28), the IMD products are summarized and presented in Table 5.1 for the calculations of nonlinear coefficients.

In order to estimate the 1dB compression input and output powers using the nonlinear model (Volterra Series), a two-tone input signal is generated with power level of 0 dBm ($X_1 = X_2 = 0.634\ V$). Table 5.1 presents the result output currents and nonlinear coefficients at the upper side fundamental frequency (ω_2), the second IMD frequency ($\omega_2 + \omega_1$), and the third IMD frequency ($2\omega_2 - \omega_1$). Also, the nonlinear coefficients $\alpha_1, \alpha_2,$ and α_3 are estimated from these current components [10].

From the estimated nonlinear coefficients, the input, output powers, and gain at 1dB compression points can be calculated as follows:

Table 5.1. Class-F^{-1} IMD products, output currents, and nonlinear coefficients at the fundamental, second, and third IMD frequency at 1dB compression.

IMD Freq	IMD Products	i_0 (mA)	Coefficients (mm)
ω_2	$\alpha_1 X_1 + \left(\frac{3}{4}{X_1}^3 + \frac{3}{2}X_1{X_2}^2\right)\alpha_3$	19.613	$\alpha_1 = 30.93$
$\omega_2 + \omega_1$	$\alpha_2 X_1 X_2$	0.168	$\alpha_2 = 0$
$2\omega_2 - \omega_1$	$\frac{3\alpha_3 X_1 {X_2}^2}{4}$	0.866	$\alpha_3 = 4.5$

$$IP_{-1dB,2T} = 10\log\left[\frac{1}{8Z_0}(0.11)\frac{4}{9}\left(\frac{\alpha_1}{\alpha_3}\right)\right] + 30 \approx 0\ dBm \tag{5.3}$$

$$G_p = 20\log(2\alpha_1 * Z_0) = 9.81\ dB \tag{5.4}$$

$$OP_{-1dB,2T} = IP_{-1dB} + G_p = 0 + 9.81 = 9.8\ dBm \tag{5.5}$$

The results from (5.3), (5.4), and (5.5) are very close to the simulated results in Fig. 5.1. This clearly proves that the nonlinear model used in this analysis is valid and accurate to analyze the nonlinear behaviors of the power amplifier at 28 GHz.

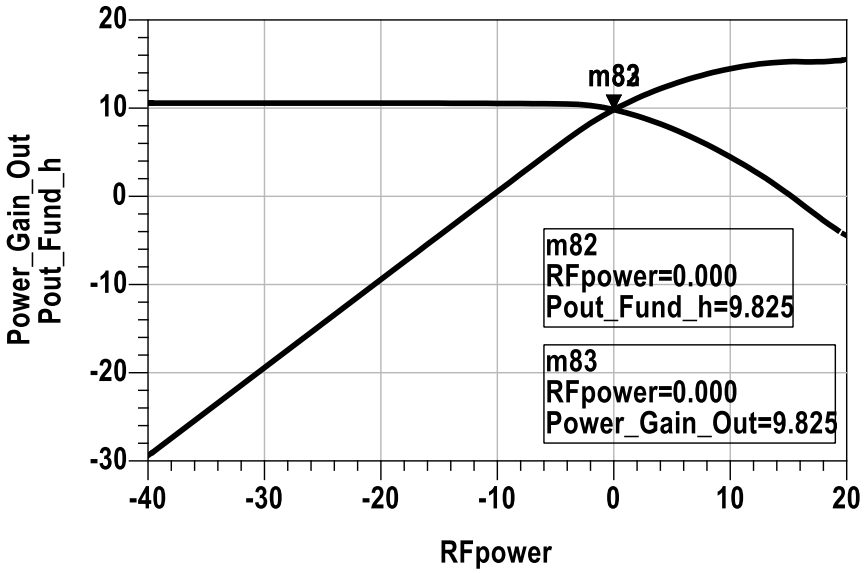

Fig. 5.1. Class-F^{-1} fundamental power and power gain vs. input power in two-tone simulation.

5.1.2 Class-F^{-1} IM3, IM5, and IIP3 Estimation from Two-tone Simulation Data

In power amplifier design, one of the most importance parameters is the intermodulation distortion. In order to analyze the linearity behaviors and performance, the difference between the fundamental component and the third order intermodulation component (IM3) is evaluated closely. The power amplifier that produces lower IM3 at a certain frequency range tends to have better linearity. IM3 can be estimated using the power curves as in Fig. 5.2. or the power spectrum as in Fig. 5.3. The estimation of IM3 can be expressed as:

$$IM3 = P(2\omega_2 - \omega_1) - P(\omega_2) \tag{5.6}$$

The results of IM3 is presented as a red curve in Fig. 5.4, showing the linearity performance of class-F^{-1} PA. In the output power (P_{out}) range from -10 to 10 dBm, class-F^{-1} IM3 are achieved from -75 to -44 dBc. The 5th IMD is considered to have some effects on the linearity of the amplifier. Thus, IM5 result is also obtained by applying the similar approach used for IM3 calculation (blue curve in Fig. 5.4).

A number of method can be used to determine the third order intercept point (IP3). One of methods is to use IM3 results. The third order intercept point is defined as the interception of the 3rd IMD power extended line (based on the linear region at low power) and the fundamental power extended line in Fig. 5.2. The input power chosen for the analysis is P_{in} = -30 dBm with corresponding P_{out} = -19.4 dBm. As in (2.31) and (2.32), the third order intercept can be expressed,

$$IIP3 = P_{in} + \frac{IM3}{2} = -30 + \frac{-19.4 + 107.8}{2} = 14.1\ dBm \tag{5.7}$$

$$OIP3 = P_{out} + \frac{IM3}{2} = -19.4 + \frac{-19.4 + 107.8}{2} = 24.7\ \text{dBm} \tag{5.8}$$

Table 5.2. Class-F^{-1} IMD products, output currents, and nonlinear coefficients at the fundamental, second, and third IMD frequency at low power (Pin=-30dBm).

IMD Freq	IMD Products	i_0 (mA)	Coefficients (mm)
ω_2	$\alpha_1 X_1 + \left(\frac{3}{4}{X_1}^3 + \frac{3}{2}X_1{X_2}^2\right)\alpha_3$	0.676	$\alpha_1 = 33.8$
$\omega_2 + \omega_1$	$\alpha_2 X_1 X_2$	$5.8 * 10^{-4}$	$\alpha_2 = 1.45$
$2\omega_2 - \omega_1$	$\frac{3\alpha_3 X_1 {X_2}^2}{4}$	$2.6 * 10^{-5}$	$\alpha_3 = 4.3$

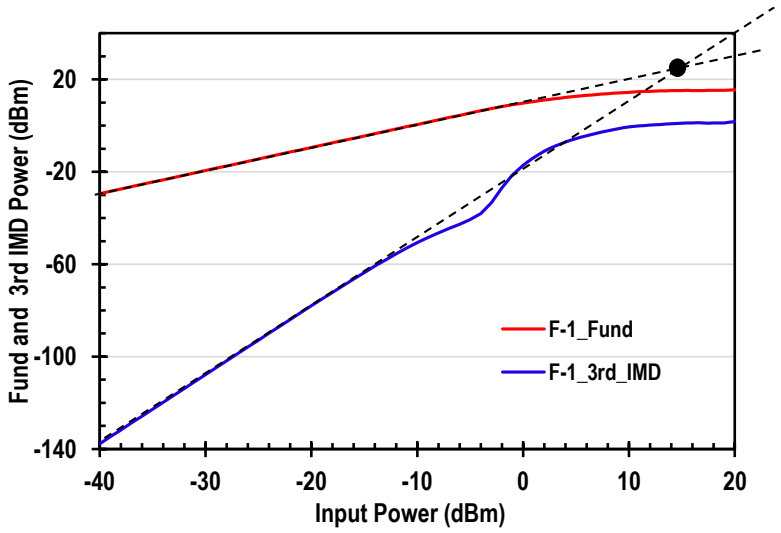

Fig. 5.2. Class-F^{-1} fundamental power and third-order distortion product

The second method involves into the nonlinear model as used in the estimation of 1dB compression. The input power chosen for the analysis is -30 dBm corresponding to the signal magnitude of $X_1 = X_2$ = 0.02 V. The coefficients are estimated from the output currents and the IMD products in Table 5.2. Then, the input and output third order intercept powers are calculated in the 50-Ω system as:

$$IIP3 = 10\log\left[\frac{1}{8Z_0}\frac{4}{3}\left(\frac{\alpha_1}{\alpha_3}\right)\right] + 30 = 14.1\ dBm \tag{5.9}$$

$$G_p = 20\log(2\alpha_1 * Z_0) = 10\ dB \tag{5.10}$$

$$OIP3 = IIP3 + G_p = 10 + 14.1 = 24.1\ dBm \tag{5.11}$$

Fig. 5.2. shows the intercept point results (black dot) which match with the calculated values from (5.9), (5.10), and (5.11) and from the first method (5.7) and (5.8).

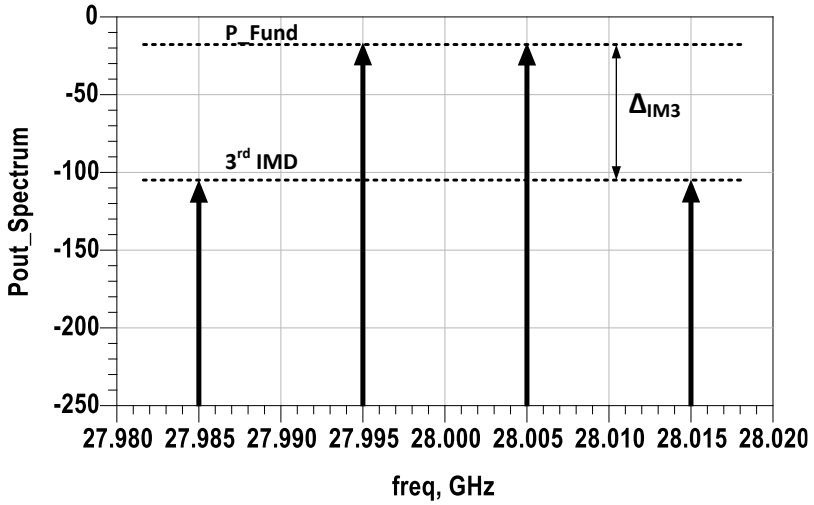

Fig. 5.3. Class-F^{-1} spectrum of the fundamental power and third-order distortion product.

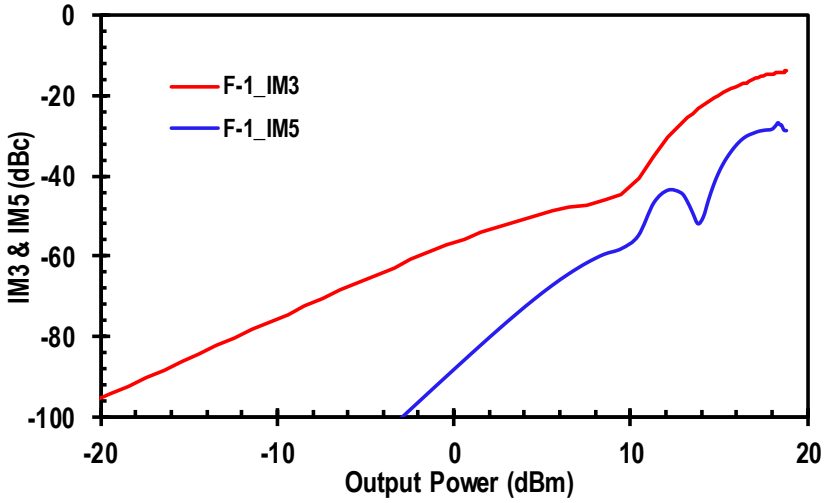

Fig. 5.4. Class-F^{-1} 3rd and 5th IMD harmonic suppressions.

5.1.3 Class-F^{-1} ACPR Result from Modulated Signal Simulation

In order to characterize the linearity of class-F^{-1} PA, the modulated input signals with various modulation schemes (QPSK, 16QAM, 64QAM, and 256QAM) are applied to the PA. The modulated signal has a 13.5 MHz available bandwidth after a raised cosine filtering with 0.35 roll-off factor as a system requirement. The symbol rate used in this simulation is 10 MHz.

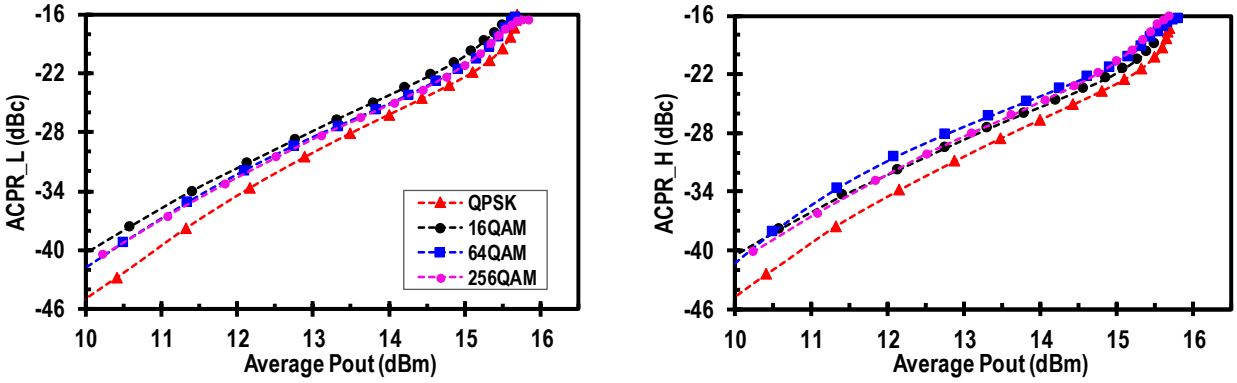

(a) (b)

Fig. 5.5. Class-F^{-1} lower side ACPR in (a) and higher side ACPR in (b) vs. average output power of modulated signals: QPSK, 16QAM, 64QAM, and 256QAM at 28 GHz.

Fig. 5.5 shows the ACPR values of all four modulation schemes for both lower and higher sides. As the results, QPSK scheme gives the best ACPRs with -43→-19.4 dBc in the average output power range of -10→15.5 dBm. In the same power range, ACPR results of the other modulation schemes are -39→-17 dBc for 16 QAM, -42→-18 dBc for 64QAM, and -41→-18 dBc for 256QAM. At 28 GHz, the results show that QPSK has better ACPRs (red line) than other schemes for all power level.

5.1.4 Class-F^{-1} EVM Result from Modulated Signal Simulation

To further analyze linearity behavior of the designed class-F^{-1} PA, the simulation of EVM is conducted to see how much nonlinearity of the amplifier affects the constellations of different modulation schemes: QPSK, 16QAM, 64QAM, and 256QAM. As the system requirements, the EVM percentage is preferred to below 5.5%. The average output power for < 5.5% EVM is >16 dBm for QPSK, and 12.7 dBm for 16QAM, 64QAM, and 256QAM as illustrated in Fig. 5.6. Among the modulated signal schemes, QPSK gives the lowest EVM with <2% all power level.

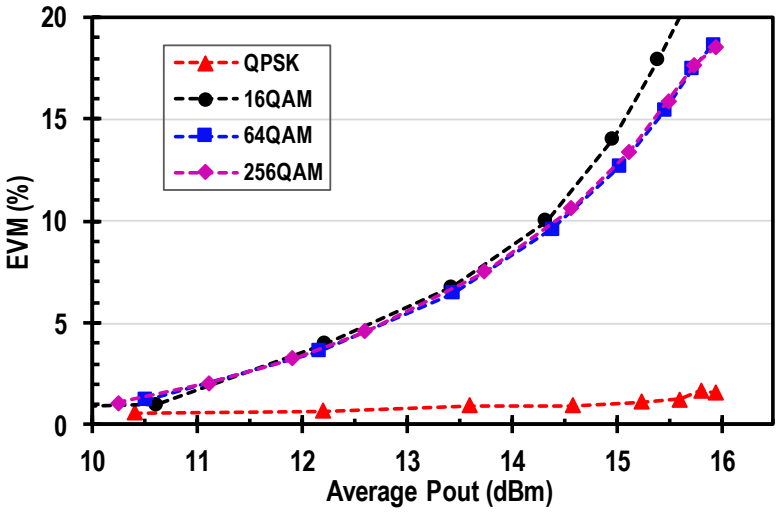

Fig. 5.6. Class-F^{-1} EVM versus average output power of modulated signals: QPSK, 16QAM, 64QAM, and 256QAM at 28 GHz.

5.2 Linearity on Class-F Power Amplifier

5.2.1 Class-F IP_{1dB} Estimation from One-tone and Two-tone Data

In order to estimate the 1dB compression input and output powers using the nonlinear model (Volterra Series), a two-tone input signal is generated with power level of 0.5 dBm ($X_1 = X_2 = 0.664\,V$). Table 5.3 presents the result output currents and nonlinear coefficients at the upper side fundamental frequency (ω_2), the second IMD frequency ($\omega_2 + \omega_1$), and the third IMD frequency ($2\omega_2 - \omega_1$). Also, the nonlinear coefficients $\alpha_1, \alpha_2,$ and α_3 are estimated from these current components.

Table 5.3. Class-F IMD products, output currents, and nonlinear coefficients at the fundamental, second, and third IMD frequency at 1dB compression.

IMD Freq	IMD Products	i_0 (mA)	Coefficients
ω_2	$\alpha_1 X_1 + \left(\frac{3}{4}{X_1}^3 + \frac{3}{2}X_1{X_2}^2\right)\alpha_3$	18.986	$\alpha_1 = 28.593$
$\omega_2 + \omega_1$	$\alpha_2 X_1 X_2$	0.28	$\alpha_2 = 0$
$2\omega_2 - \omega_1$	$\frac{3\alpha_3 X_1 {X_2}^2}{4}$	0.599	$\alpha_3 = 2.73$

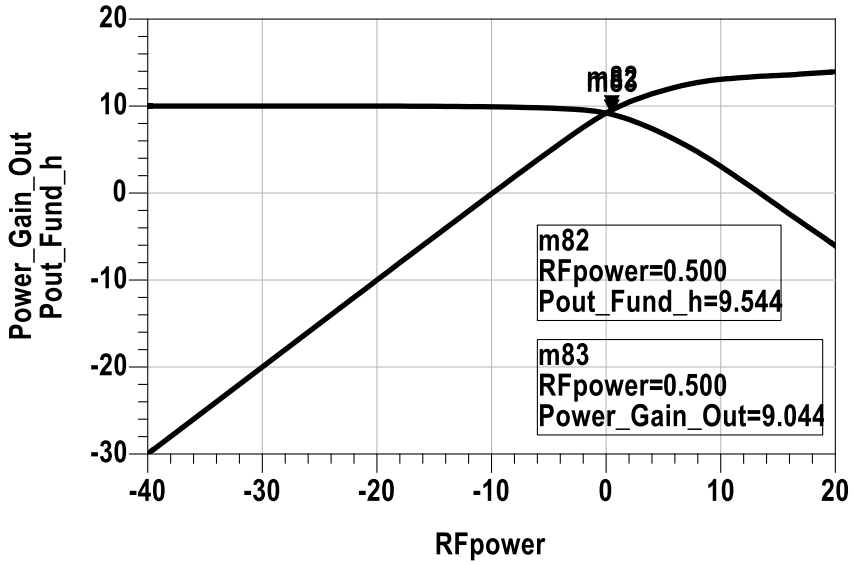

Fig. 5.7. Class-F^{-1} fundamental power and power gain vs. input power in two-tone simulation.

From the estimated nonlinear coefficients, the input, output powers, and gain at 1dB compression points can be calculated as follows:

$$IP_{-1dB,2T} = 10\log\left[\frac{1}{8Z_0}(0.11)\frac{4}{9}\left(\frac{\alpha_1}{\alpha_3}\right)\right] + 30 \approx 1\ dBm. \tag{5.12}$$

$$G_p = 20\log(2\alpha_1 * Z_0) = 9.12\ dB \tag{5.13}$$

$$OP_{-1dB} = IP_{-1dB} + G_p = 1 + 9.12 = 10.12\ dBm \tag{5.14}$$

The results from (5.12), (5.13), and (5.14) are very close to the simulated results in Fig. 5.7. This clearly proves that the nonlinear model used in this analysis is valid and accurate to analyze the nonlinear behaviors of the power amplifier at 28 GHz.

5.2.2 Class-F IM3, IM5, and IIP3 Estimation from Two-tone Simulation Data

In order to analyze the linearity behaviors and performance of the PA, the difference between the fundamental component and the third order intermodulation component (IM3) is evaluated closely. The power amplifier that produces lower IM3 at a certain frequency range tends to have better linearity. IM3 can be estimated using the power curves as in Fig. 5.8. or the power spectrum as in Fig. 5.9 with the expression (5.6).

Table 5.4. Class-F IMD products, output currents, and nonlinear coefficients at the fundamental, second, and third IMD frequency at low power (Pin=-30dBm).

IMD Freq	IMD Products	i_0 (mA)	Coefficients
ω_2	$\alpha_1 X_1 + \left(\frac{3}{4}{X_1}^3 + \frac{3}{2}X_1{X_2}^2\right)\alpha_3$	0.633	$\alpha_1 = 31.65$
$\omega_2 + \omega_1$	$\alpha_2 X_1 X_2$	$3.5 * 10^{-4}$	$\alpha_2 = 0.875$
$2\omega_2 - \omega_1$	$\frac{3\alpha_3 X_1 {X_2}^2}{4}$	$1.8 * 10^{-5}$	$\alpha_3 = 3$

The results of IM3 is presented as a red curve in Fig. 5.10, showing the linearity performance of class-F PA. In the output power (P_{out}) range from -10 to 10 dBm, class-F IM3 are achieved from -77 to -44 dBc. The 5th IMD is considered to have some effects on the linearity of the amplifier. Thus, IM5 result is also obtained by applying the similar approach used for IM3 calculation (blue curve in Fig. 5.10).

A number of method can be used to determine the third order intercept point (IP3). One of methods is to use IM3 results. The third order intercept point is defined as the interception of the 3rd IMD power extended line (based on the linear region at low power) and the fundamental power extended line in Fig. 5.7. The input power chosen for the analysis is P_{in} = -30 dBm with corresponding P_{out} = -20 dBm. As in (2.31) and (2.32), the third order intercept can be expressed,

$$IIP3 = P_{in} + \frac{IM3}{2} = -30 + \frac{-20 + 111}{2} = 15.5\ dBm \tag{5.15}$$

$$OIP3 = P_{out} + \frac{IM3}{2} = -20 + \frac{-20 + 111}{2} = 25.5\ \text{dBm} \tag{5.16}$$

The second method involves into the nonlinear model as used in the estimation of 1dB compression. The input power chosen for the analysis is -30 dBm corresponding to the signal magnitude of $X_1 = X_2$ = 0.02 V. The coefficients are estimated from the output currents and the IMD products in Table 5.4. Then, the input and output third order intercept powers are calculated in the 50-Ω system as:

$$IIP3 = 10\log\left[\frac{1}{8Z_0}\frac{4}{3}\left(\frac{\alpha_1}{\alpha_3}\right)\right] + 30 = 15.5\ dBm \tag{5.17}$$

$$G_p = 20\log(2\alpha_1 * Z_0) = 10\ dB \tag{5.18}$$

$$OIP3 = IIP3 + G_p = 10 + 14.1 = 25.5\ dBm \tag{5.19}$$

Fig. 5.8. shows the intercept point results (black dot) which match with the calculated values from (5.17), (5.18), and (5.19) and from the first method (5.15) and (5.16).

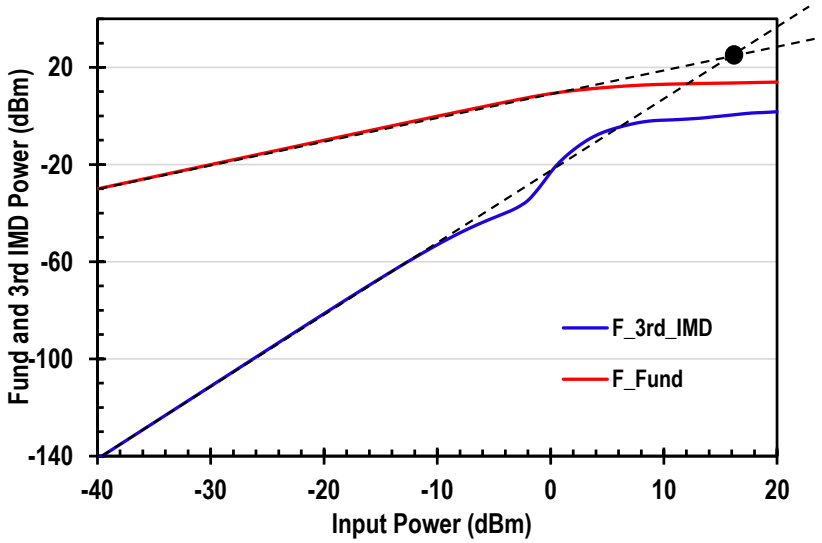

Fig. 5.8. Class-F fundamental power and third-order distortion product.

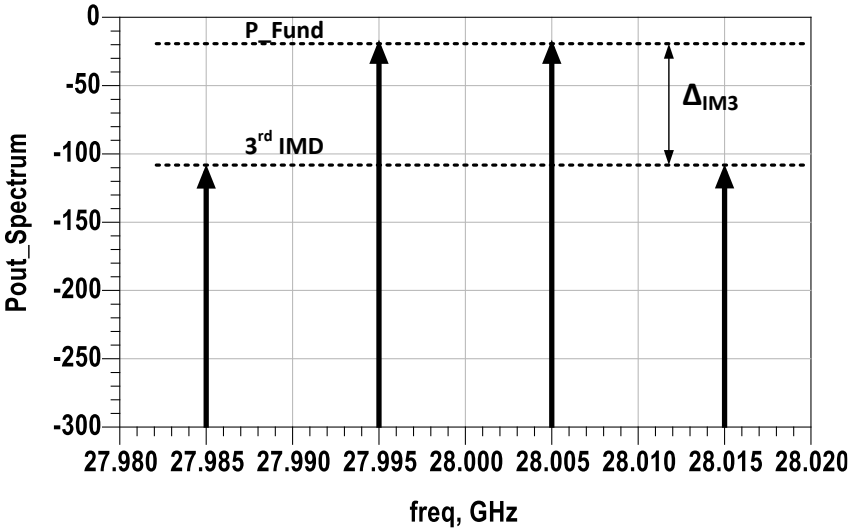

Fig. 5.9. Class-F spectrum of the fundamental power and third-order distortion product.

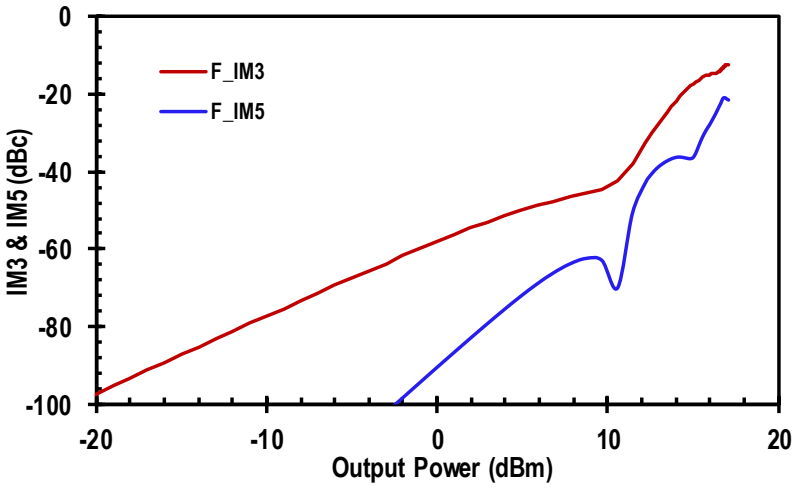

Fig. 5.10. Class-F 3rd and 5th IMD harmonic suppressions.

5.2.3 Class-F ACPR Result from Modulated Signal Simulation

In order to characterize the linearity of class-F PA, the modulated input signals with various modulation schemes (QPSK, 16QAM, 64QAM, and 256QAM) are applied to the PA. The modulated signal has a 13.5 MHz available bandwidth after a raised cosine filtering with 0.35 roll-off factor as a system requirement. The symbol rate used in this simulation is 10 MHz.

Fig. 5.11 shows the ACPR values of all four modulation schemes for both lower and higher sides. As the results, QPSK scheme gives the best ACPRs with -45→-18.5 dBc in the average output power range of -10→15.5 dBm. In the same power range, ACPR results of the other modulation schemes are -40→-17 dBc for 16 QAM, -42→-17.3 dBc for 64QAM, and -40→-17.3 dBc for 256QAM. At 28 GHz, the results show that QPSK has better ACPRs (red line) than other schemes for all power levels.

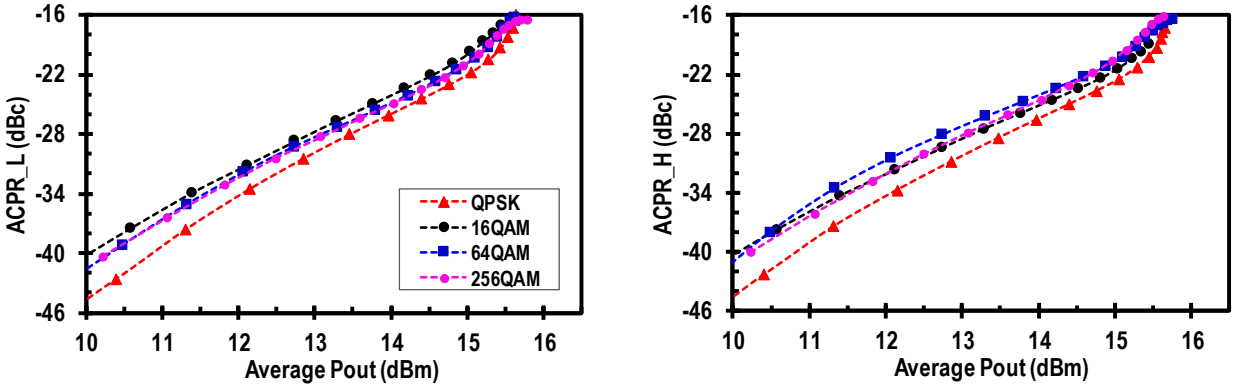

(a) (b)

Fig. 5.11. Class-F lower side ACPR in (a) and higher side ACPR in (b) vs. average output power of modulated signals: QPSK, 16QAM, 64QAM, and 256QAM at 28 GHz.

5.2.4 Class-F EVM Result from Modulated Signal Simulation

To further analyze linearity behavior of the designed class-F PA, the simulation of EVM is conducted to see how much nonlinearity of the amplifier affects the constellations of different modulation schemes: QPSK, 16QAM, 64QAM, and 256QAM. As the system requirements, the EVM percentage is preferred to below 5.5%. The average output power for < 5.5% EVM is >16 dBm for QPSK, and 12.7 dBm for 16QAM, 64QAM, and 256QAM as illustrated in Fig. 5.12. Among the modulated signal schemes, QPSK gives the lowest EVM with <2% all power levels.

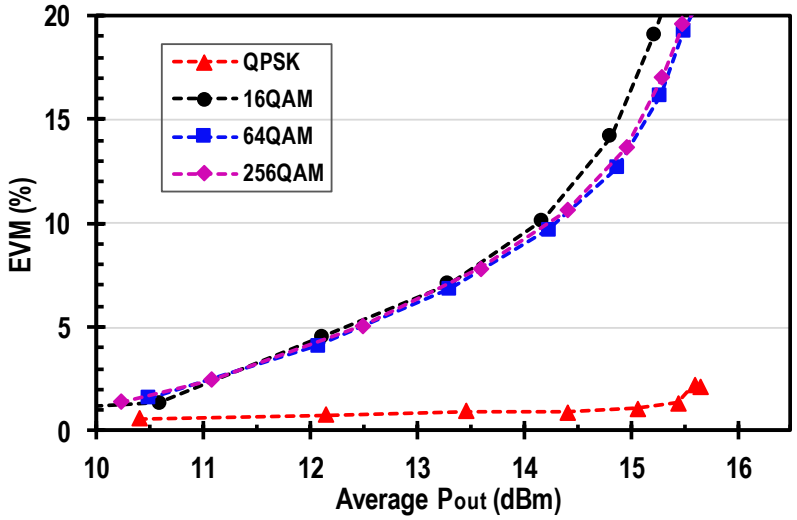

Fig. 5.12. Class-F EVM versus average output power of modulated signals: QPSK, 16 QAM, 64 QAM, and 256 QAM at 28 GHz.

5.3 Linearity on Class-AB Power Amplifier

5.3.1 Class-AB IP_{1dB} Estimation from One-tone and Two-tone Simulation Data

In order to estimate the 1dB compression input and output powers using the nonlinear model (Volterra Series), a two-tone input signal is generated with power level of 0 dBm ($X_1 = X_2 = 0.618\,V$). Table 5.5 presents the result output currents and nonlinear coefficients at the upper side fundamental frequency (ω_2), the second IMD frequency ($\omega_2 + \omega_1$), and the third IMD frequency ($2\omega_2 - \omega_1$). Also, the nonlinear coefficients α_1, α_2, and α_3 are estimated from these current components.

From the estimated nonlinear coefficients, the input, output powers, and gain at 1dB compression points can be calculated as follows:

$$IP_{-1dB,2T} = 10\log\left[\frac{1}{8Z_0}(0.11)\frac{4}{9}\left(\frac{\alpha_1}{\alpha_3}\right)\right] + 30 \approx 0\ dBm \tag{5.20}$$

$$G_p = 20\log(2\alpha_1 * Z_0) = 10.23\ dB \tag{5.21}$$

$$OP_{-1dB,2T} = IP_{-1dB} + G_p = 0 + 10.23 = 10.23\ dBm \tag{5.22}$$

The results from (5.20), (5.21), and (5.22) are very close to the simulated results in Fig. 5.13. This clearly proves that the nonlinear model used in this analysis is valid and accurate to analyze the nonlinear behaviors of the power amplifier at 28 GHz.

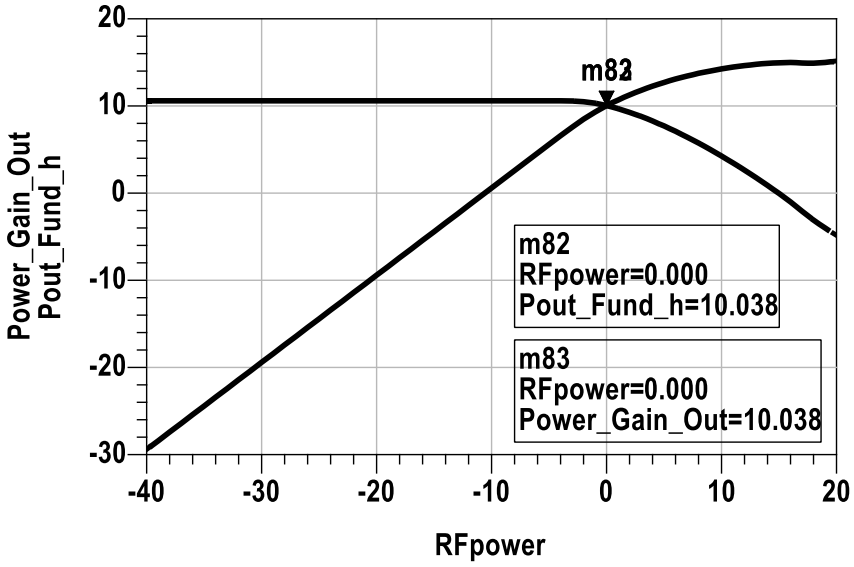

Fig. 5.13. Class-AB fundamental power and power gain vs. input power in two-tone simulation.

Table 5.5. Class-AB IMD products, output currents, and nonlinear coefficients at the fundamental, second, and third IMD frequency at 1dB compression.

IMD Freq	IMD Products	i_0 (mA)	Coefficients
ω_2	$\alpha_1 X_1 + \left(\frac{3}{4}{X_1}^3 + \frac{3}{2}X_1{X_2}^2\right)\alpha_3$	20.09	$\alpha_1 = 32.5$
$\omega_2 + \omega_1$	$\alpha_2 X_1 X_2$	1.287	$\alpha_2 = 3.37$
$2\omega_2 - \omega_1$	$\frac{3\alpha_3 X_1 {X_2}^2}{4}$	0.825	$\alpha_3 = 4.66$

5.3.2 Class-AB IM3, IM5, and IIP3 Estimation from Two-tone Simulation Data

The results of IM3 is presented as a red curve in Fig. 5.15, showing the linearity performance of class-AB PA. In the output power (P_{out}) range from -10 to 17 dBm, class-AB IM3 are achieved from -86 to -52 dBc. The 5th IMD is considered to have some effects on the linearity of the amplifier. Thus, IM5 result is also obtained by applying the similar approach used for IM3 calculation (blue curve in Fig. 5.16).

A number of method can be used to determine the third order intercept point (IP3). One of methods is to use IM3 results. The third order intercept point is defined as the interception of the 3rd IMD power extended line (based on the linear region at low power) and the fundamental power extended line in Fig. 5.14. The input power chosen for the analysis is P_{in} = -30 dBm with corresponding P_{out} = -19.4 dBm. As in (2.31) and (2.32), the third order intercept can be expressed,

$$IIP3 = P_{in} + \frac{IM3}{2} = -30 + \frac{-19.4 + 118}{2} = 19.3\ dBm \tag{5.23}$$

$$OIPn = P_{out} + \frac{IM3}{2} = -19.4 + \frac{-19.4 + 118}{2} = 29.9\ \text{dBm} \tag{5.24}$$

The second method involves into the nonlinear model as used in the estimation of 1dB compression. The input power chosen for the analysis is -30 dBm corresponding to the signal magnitude of $X_1 = X_2$ = 0.02 V. The coefficients are estimated from the output currents and the IMD products in Table 5.6. Then, the input and output third order intercept powers are calculated in the 50-Ω system as:

Table 5.6. Class-F^{-1} IMD products, output currents, and nonlinear coefficients at the fundamental, second, and third IMD frequency at low power (Pin=-30dBm).

IMD Freq	IMD Products	i_0 (mA)	Coefficients
ω_2	$\alpha_1 X_1 + \left(\frac{3}{4}{X_1}^3 + \frac{3}{2}X_1{X_2}^2\right)\alpha_3$	0.677	$\alpha_1 = 33.85$
$\omega_2 + \omega_1$	$\alpha_2 X_1 X_2$	0.0041	$\alpha_2 = 0.1$
$2\omega_2 - \omega_1$	$\frac{3\alpha_3 X_1 {X_2}^2}{4}$	$8 * 10^{-6}$	$\alpha_3 = 1.33$

$$IIP3 = 10\log\left[\frac{1}{8Z_0}\frac{4}{3}\left(\frac{\alpha_1}{\alpha_3}\right)\right] + 30 = 19.3\ dBm \tag{5.25}$$

$$G_p = 20\log(2\alpha_1 * Z_0) = 10.6\ dB \tag{5.26}$$

$$OIP3 = IIP3 + G_p = 10.6 + 19.3 = 29.9\ dBm \tag{5.27}$$

Fig. 5.14. shows the intercept point results (black dot) which match with the calculated values from (5.25), (5.26), and (5.27) and from the first method (5.23) and (5.24).

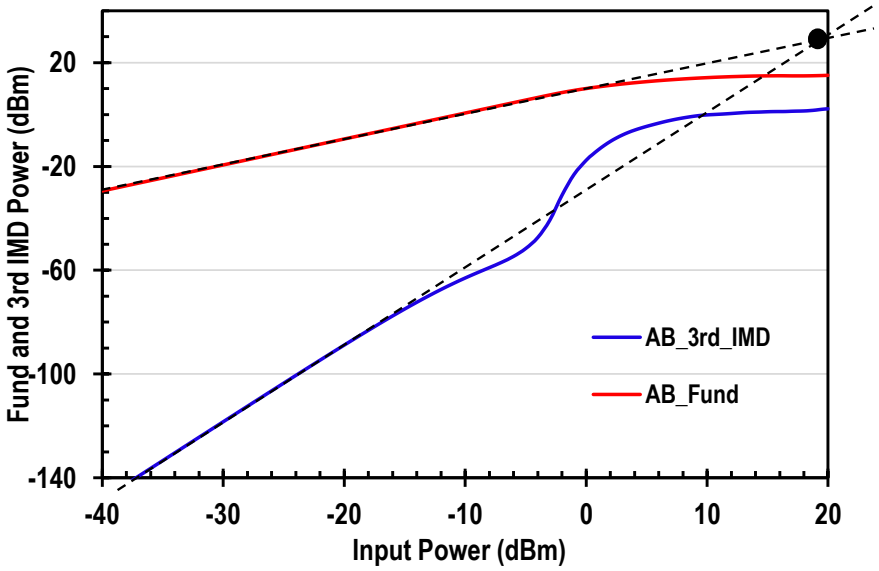

Fig. 5.14. Class-AB fundamental power and third-order distortion product.

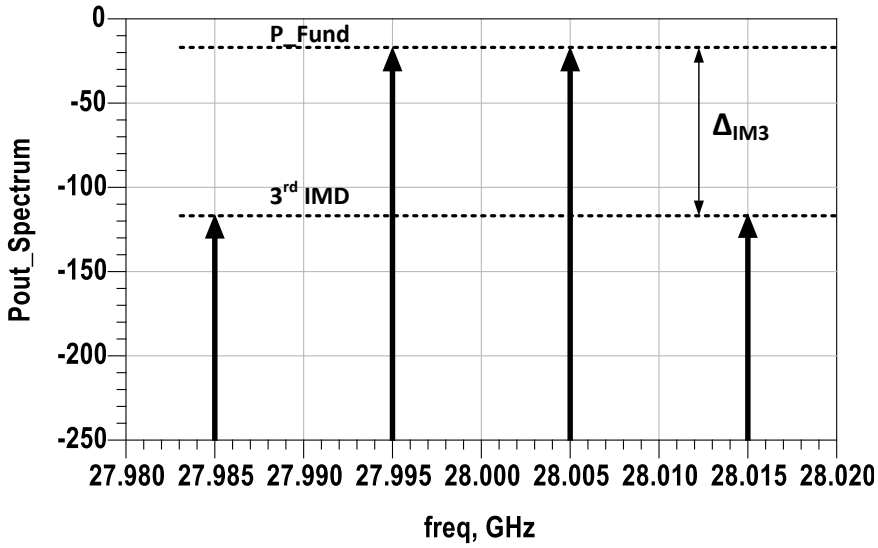

Fig. 5.15. Class-AB spectrum of the fundamental power and third-order distortion product.

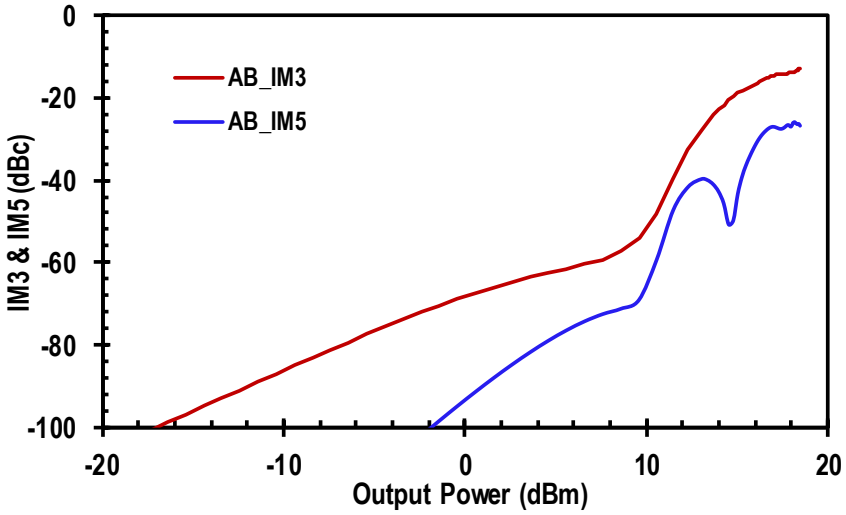

Fig. 5.16. Class-AB 3rd and 5th IMD harmonic suppressions at 28 GHz.

5.3.3 Class-AB ACPR Result from Modulated Signal Simulation

In order to characterize the linearity of class-F^{-1} PA, the modulated input signals with various modulation schemes (QPSK, 16QAM, 64QAM, and 256QAM) are applied to the PA. The modulated signal has a 13.5 MHz available bandwidth after a raised cosine filtering with 0.35 roll-off factor as a system requirement. The symbol rate used in this simulation is 10 MHz.

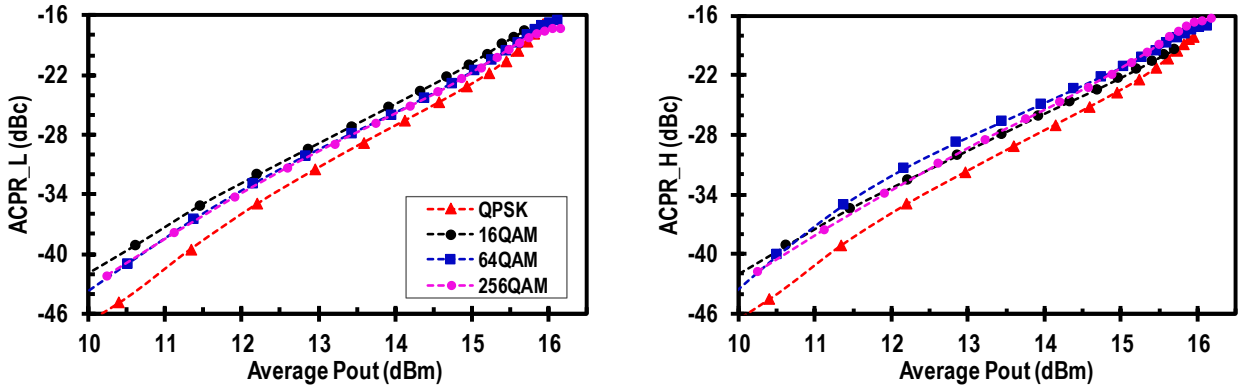

(a) (b)

Fig. 5.17. Class-AB lower side ACPR in (a) and higher side ACPR in (b) vs. average output power of modulated signals: QPSK, 16QAM, 64QAM, and 256QAM at 28 GHz.

Fig. 5.17 shows the ACPR values of all four modulation schemes for both lower and higher sides. As the results, QPSK scheme gives the best ACPRs with -47→-19.4 dBc in the average output power range of -10→15.5 dBm. In the same power range, ACPR results of the other modulation schemes are -42→-18.5 dBc for 16 QAM, -44→-19 dBc for 64QAM, and -41→-19.4 dBc for 256QAM. At 28 GHz, the results show that QPSK has better ACPRs (red line) than other schemes for all power levels.

5.3.4 Class-AB EVM Result from Modulated Signal Simulation

To further analyze linearity behavior of the designed class-F^{-1} PA, the simulation of EVM is conducted to see how much nonlinearity of the amplifier affects the constellations of different modulation schemes: QPSK, 16QAM, 64QAM, and 256QAM. As the system requirements, the EVM percentage is preferred to below 5.5%. The average output power for < 5.5% EVM is >16 dBm for QPSK, and 13 dBm for 16QAM, 64QAM, and 256QAM as illustrated in Fig. 5.18. Among the modulated signal schemes, QPSK gives the lowest EVM with <2% all power levels.

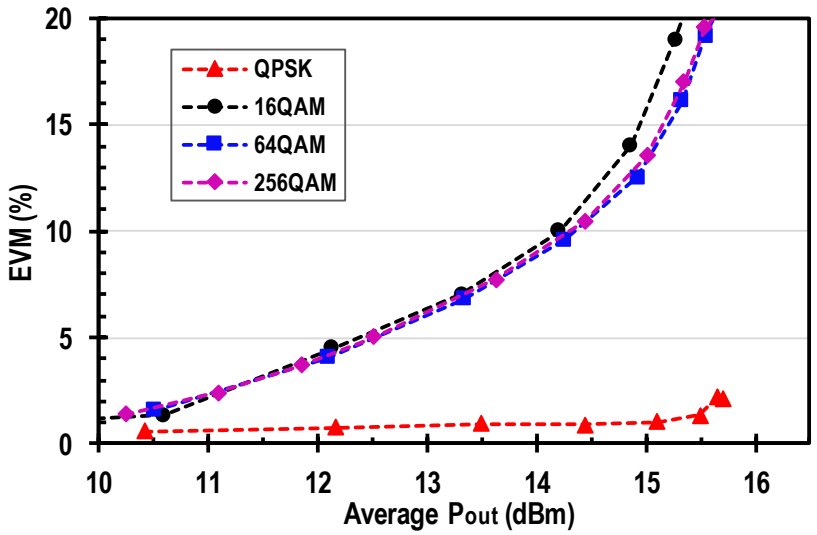

Fig. 5.18. Class-AB EVM versus average output power of modulated signals: QPSK, 16 QAM, 64 QAM, and 256 QAM at 28 GHz.

5.4 Summary and Comparison

In this chapter, two different types of input signals are applied to class-F^{-1}, class-F, and class-AB PAs to characterize the linearity behaviors. In order to evaluate the linearity of the PAs, important linearity parameters are captured and estimated from the simulation results. The nonlinear model with Volterra Series is used to estimate the 1dB compression and the third order intercept points. The results of these estimations match with the simulation results shown in the plots and the calculations using the output power spectrum. To further analyze the linearity effects on the PAs, the modulated input signals with four different modulation schemes (QPSK, 16QAm, 64QAM, and 256 QAM) are applied. As the results, ACPR and EVM values are obtained and analyzed to determine the suitability of the PA to the system.

To compare the linearity of the PAs, the analysis of IM3, ACPR, and EVM are conducted. Using the identical input networks (input matching, base bias, and base stability networks), three PAs achieve the output power of 16-17 dBm and the power gain of ~10 dB. In Fig. 5.19, the simulated IM3 of three PAs are obtained and plotted for the comparison. The results show that class-AB has > 10 dB IM3 higher in absolute values than two other classes in a wide range of the output powers from -20 to 10 dBm. Class-F and class-F^{-1} IM3 results are fairly close to each other, it is hard to determine which amplifier gives better IM3 or linearity in term of IM3 estimations. Fig. 5.21 shows a

comparison of the fifth harmonic suppressions (IM5) of all three classes. Again, class-AB shows a little better IM5 results than others.

In order to have more information to the linearity comparison of three PAs, ACPR results are closely evaluated. Four different plots in Fig. 5.20 shows the simulated ACPR results of three PAs for different modulation schemes. By observing these plots, class-AB ACPRs (red line) are > 5 dB high than other classes in term of absolute values over the average output power range from 10 dBm to 15.5 dBm, and the results are consistent throughout four modulation schemes. Comparing class-F and F^{-1} PAs, the simulated ACPRs of class-F^{-1} (pink line) are slightly better than class-F's (blue line) in Fig. 5.20.

Finally, one of the most important parameters in the linearity analysis of amplifiers is error vector magnitude (EVM). As the results shown in Fig. 5.22, the simulated EVM results of three classes are plotted over the average output power range from 10 dBm to 15.5 dBm for comparison purpose. Similar to the ACPR analysis and comparison, there are four separate plots representing the EVM results of four different modulation schemes for three PAs. The results show that QPSK gives the best EVM values comparing to other schemes, and class-AB has better results than other classes. In Fig. 5.22(ii), (iii), and (iv), EVM curves of class-AB (red) shows the best values while class-F^{-1}'s are slightly better results than class-F's.

After the analysis and comparison of three classes, the conclusion of which PA has better linearity performance can be drawn. Based on the estimation and comparison plots, class-AB power amplifier has an advantage of having higher linearity than two other PAs. Even though it is very hard to distinguish the difference in the linearity performance between class-F and class-F^{-1}, the linearity of class-F^{-1} PA still shows slightly better results than class-F. As looking back to the efficiency performances of three PA classes, there exists a level of consistency in describing the trade-off between efficiency and linearity. In conclusion, class-AB with the lowest peak PAE (44%) among three has the highest linearity; class-F^{-1} with 45% peak PAE has slightly better linearity than class-F; finally, class-F has the worst linearity while it gives the highest peak PAE among three classes of PAs.

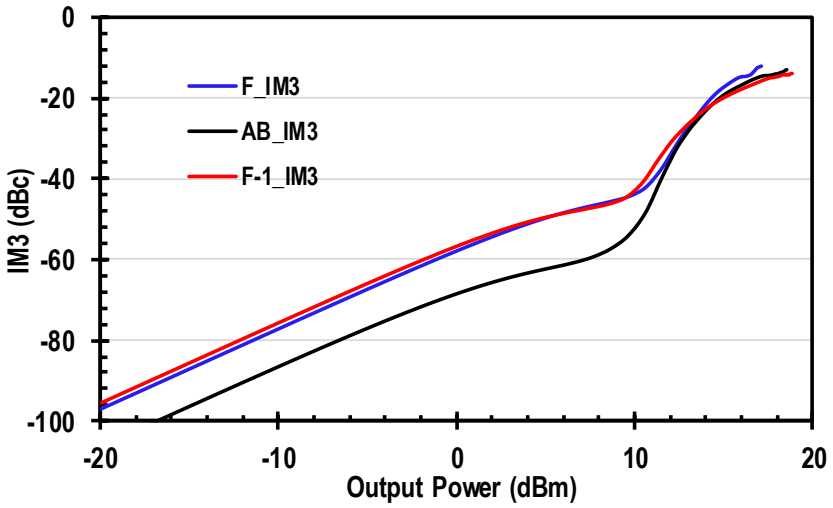

Fig. 5.19. Class-AB, F, and F^{-1} 3rd IMD harmonic suppressions at 28 GHz.

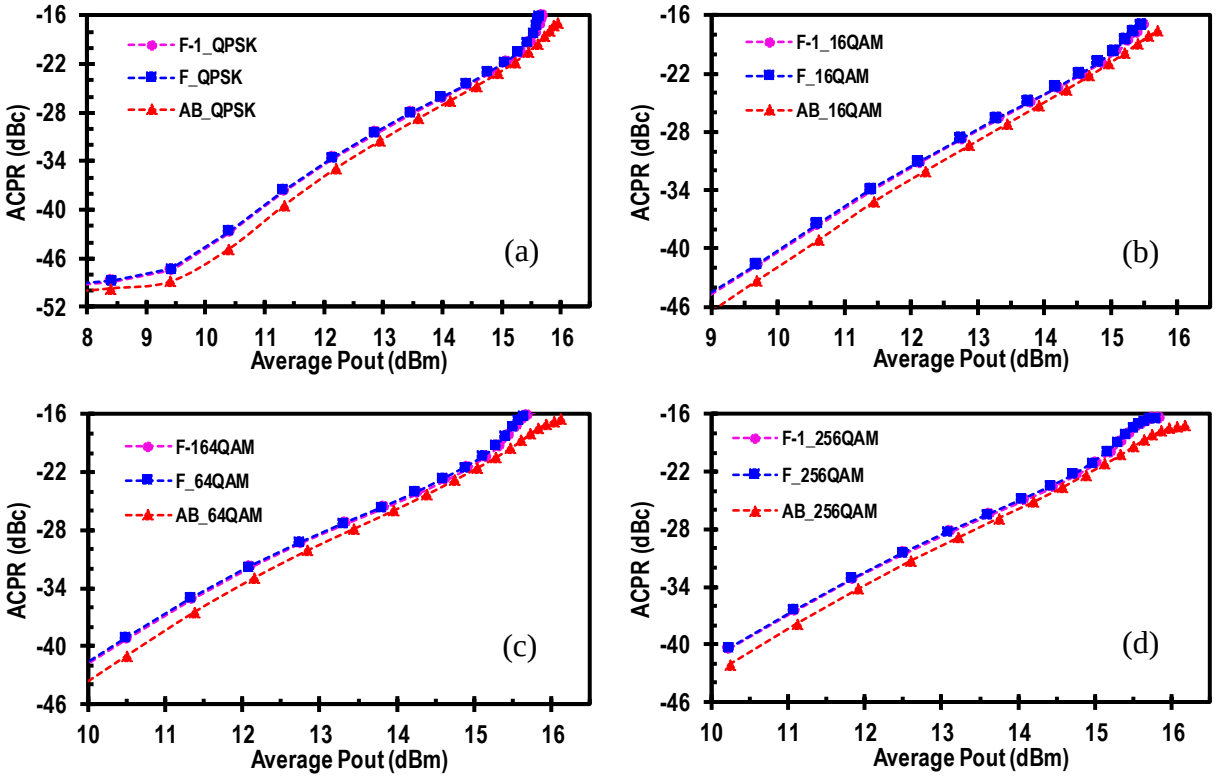

Fig. 5.20. Class-AB, F and F^{-1} simulated ACPR vs. average output power of modulated signals: (a) QPSK, (b) 16QAM, (c) 64QAM, and (d) 256QAM at 28 GHz.

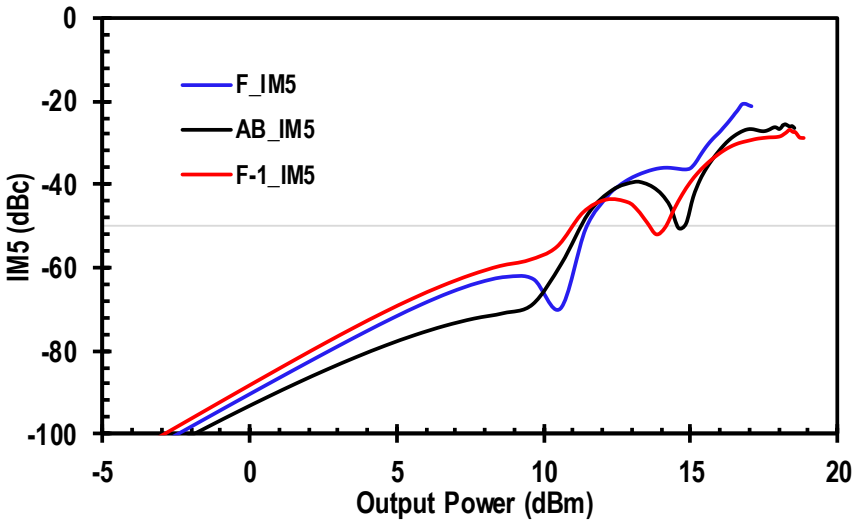

Fig. 5.21. Class-AB, F, and F^{-1} 5th IMD harmonic suppressions at 28 GHz

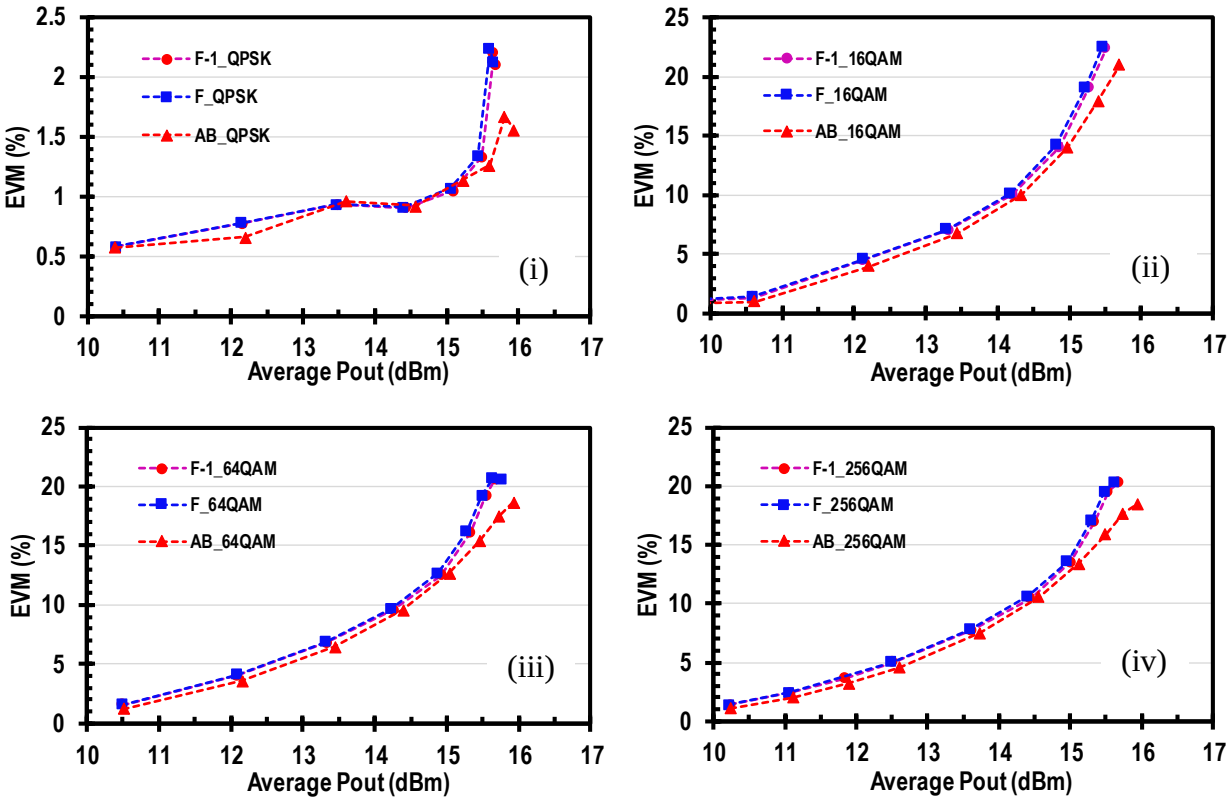

Fig. 5.22. Class-AB, F and F^{-1} simulated EVM vs. average output power of modulated signals: (i) QPSK, (ii) 16QAM, (iii) 64QAM, and (iv) 256QAM at 28 GHz.

Chapter 6

Conclusion

Contents

6.1 Conclusion

A power amplifier is a very essential component in many microwave and millimeter-wave systems. The need for high output power levels is the main driver in the selection of the active devices composing PAs. PA design is typically the result of a trade-off between either linearity and efficiency or high output power level and low distortion. The design approach to be selected depends on operating frequency and bandwidth, available device technology, application, and many other factors. This leads to the consideration of what PA classes can fulfill most of the requirements.

In this thesis, three PAs: class-AB, class-F, class-F^{-1} are the great examples for an in-depth analysis on both efficiency and linearity. In order to conduct a fair comparison among three PA classes, the input networks are designed to be identical and the load networks are different for each PA. The input matching network is a 50-Ω conjugate matched network which is a pi-type LC network with one series inductor and two shun capacitors. A bias DC feed network (current mirror) is utilized to provide base DC current to the transistor. This bias network path also provides DC resistance of <250 to reduce the effect of negative resistance at the input as well as creates a harmonic trap to mitigate the sub-harmonic from the circuit to improve stability. The last part of the input networks is the network (a capacitor in parallel to a resistor) connected directly to the base of the transistor to ensure the stability for all frequencies.

The load network of class-AB PA is simply composed of a single inductor and a parasitic capacitor, creating a parallel resonance at the fundamental frequency (28 GHz). The load network of class-F is more complex with a parallel and a series networks, creating a multi-resonance load network. The parallel network contains one LC tank and a series

inductor with the parasitic capacitor in parallel, which can provides 50-Ω optimum impedance at the ω_o-band, low impedance at the $2\omega_o$-band, and high impedance at the $3\omega_o$-band. In the series network, a $3f_o$ –resonance LC tank is utilized to provide high impedance at the $3\omega_o$-band, and a series capacitor creates a series resonance with the inductive impedance from the LC tank at the ω_o-band. With similar ideas to class-F, the parallel network of class-F^{-1} PA is the most complex network with two LC tanks and a series inductor. This parallel network can provides 50-Ω optimum impedance at the ω_o-band, high impedance at the $2\omega_o$-band, and low impedance at the $3\omega_o$-band. The series network consists of a $2f_o$ –resonance LC tank for providing high impedance at the $2\omega_o$-band and a series capacitor for creating a series resonance with the inductive impedance from the LC tank at the ω_o-band to bring the impedance to 50 Ω.

As the results, three PAs achieve the output powers in the range from 16-17 dBm and 10 dB power gain both cases of using ideal and real passive components for the load networks. With the ideal components used in the load networks, the class-F^{-1} PA achieves the highest peak PAE with 57%, class-F gives the second highest peak PAE of 54%, and class-AB gives the lowest peak PAE of 48%. However, this order changes after replacing the ideal components with the real ones in the load networks. The peak PAEs of the PAs are achieved with the highest 46% for class-F, 45% for class-F^{-1}, and 44% for class-AB. The main reason for this degradation of the peak PAEs is the loss in the load network. Even though the class-F^{-1} PA can achieves the highest efficiency among three classes with the ideal components used in the load network (with the most number of components), the loss from the real and low Q components causes the peak PAE to drop >12% from 57% to 45%. Class-F PA with a less number of components in the load network than class-F^{-1}, the reduction in the peak PAE is >8% from 54% to 46% after replacing the real components. Since class-AB load network contains a single inductor, the peak PAE only decreases ~4% from 48% to 44%.

Besides efficiency, linearity is considered to meet the requirements of the system. The comparison on linearity is also conducted using the simulation results of IM3 (in two-tone signal simulation), ACPR, and EVM (modulated signal simulation). After analyzing the results very carefully, the class-AB shows much better linearity than two other classes. Also, class-F^{-1} gives slightly better linearity than class-F.

In conclusion, the peak PAEs of class-F^{-1} and class-F are much higher than class-AB's when ideal passive components are utilized in the load networks. However, in reality, the achieved efficiencies of three classes are very close to each other due to losses in the load networks. From the linearity analysis of three classes, class-AB shows much better linearity than other two classes while class-F^{-1} has a slightly better linearity than class-F. By observing both efficiency and linearity performances, class-AB PA can have more advantage at 28 GHz based on the results. This shows how critical the load network design is. In order to achieve the highest efficiency possible from class-F and class-F^{-1} at this high frequency, the load network design requires good techniques and a carefulness in component selection to avoid losses.

References

[1] nxp.com. (2016). *RF Generic Front-End*. [Image] Available: http://www.nxp.com/pages/rf-generic-front-end:RF-GENERIC-FRONT-END

[2] M. A. M. Albreem, "5G wireless communication systems: Vision and challenges," *2015 International Conference on Computer, Communications, and Control Technology (I4CT)*, Kuching, 2015, pp. 493-497.

[3] T. S. Rappaport et al., "Millimeter Wave Mobile Communications for 5G Cellular: It Will Work!," *in IEEE Access*, vol. 1, no. , pp. 335-349, 2013.

[4] J. D. Cressler, "Emerging SiGe HBT reliability issues for mixed-signal circuit applications," *in IEEE Transactions on Device and Materials Reliability*, vol. 4, no. 2, pp. 222-236, June 2004.

[5] K. Datta, and H. Hashemi, "Performance Limits, Design and Implementation of mm-Wave SiGe HBT Class-E and Stacked Class-E Power Amplifiers," *IEEE JSSC*, vol.49, no.10, pp.2150-2171, Oct. 2014.

[6] O. A. Gouba and Y. Louët, "Theoretical analysis of the trade-off between efficiency and linearity of the high power amplifier in OFDM context," *European Wireless 2012; 18th European Wireless Conference 2012*, Poznan, Poland, 2012, pp. 1-7.

[7] J. D. Cressler and G. Niu. Silicon-Germanium Heterojunction Bipolar Transistors. Artech House, 1st edition, 2003.

[8] A. Farahat. (Sept. 2015). *SiGe HBT Technology:The SiGe Heterojunction Bipolar Transistor*. [Image] Available: http://www.engineering-bachelors-degree.com/electronic-components/uncategorized/sige-hbt-technologythe-sige-heterojunction-bipolar-transistor/

[9] Y. Y. Woo, Y. Yang and B. Kim, "Analysis and experiments for high-efficiency class-F and inverse class-F power amplifiers," *in IEEE Transactions on Microwave Theory and Techniques*, vol. 54, no. 5, pp. 1969-1974, May 2006.

[10] P. Colantonio, F. Giannini, and E. Limiti, High efficiency RF and microwave solid state power amplifiers, 1st ed. The Atrium, Southern Gate, Chichester, West Sussex, United Kingdom: John Wiley & Sons Ltd, 2009.

[11] L. Dunleavey. (Aug. 2009). *S-parameters.* Available: http://www.uvm.edu/~muse/modules/RFH/MUSE_S-parameters_081003.pdf

[12] S. Long. (Dec. 2007). *S-parameters.* Available: http://www.uvm.edu/~muse/modules/RFH/MUSE_S-parameters_081003.pdf

[13] S. C. Cripps, RF Power Amplifiers for Wireless Communications, 2nd ed. Norwood, MA, USA: Artech House, 2006.

[14] C. Bowick, J. Blyler, and C. Ajluni. RF Circuit Design. Newnes, 2nd edition, 2007.

[15] F. H. Raab, “Class-F power amplifiers with maximally flat waveforms,” *IEEE Trans. Microw. Theory Techn.*, vol. 45, no. 11, pp. 2007–2012, Nov. 1997

[16] S. Y. Mortazavi and K. J. Koh, "Integrated Inverse Class-F Silicon Power Amplifiers for High Power Efficiency at Microwave and mm-Wave," in *IEEE Journal of Solid-State Circuits*, vol. 51, no. 10, pp. 2420-2434, Oct. 2016.

[17] F. H. Raab, "Maximum efficiency and output of class-F power amplifiers," *IEEE Trans. Microw. Theory Techn*., vol. 49, no. 6, pp. 1162–1166, Jun. 2001.

[18] S. Y. Mortazavi and K.-J. Koh, "A 28-GHz inverse class-F power amplifier with coupled-inductor based harmonic impedance modulator," in *Proc. IEEE Custom Integr. Circuits Conf. (CICC)*, Sep. 2015, pp. 1–4.

[19] S. Y. Mortazavi and K.-J. Koh, "A 38 GHz inverse class-F power amplifier with 38.5% peak PAE, 16.5 dB gain, and 50 mW psat in 0.13-mm SiGe BiCMOS," *Proc. IEEE Radio Freq. Integr. Circuits Symp. (RFIC)*, May 2015, pp. 211–214.

[20] A. Sarkar and B. Floyd, "A 28-GHz class-J power amplifier with 18-dBm output power and 35% peak PAE in 120-nm SiGe BiCMOS," in *Proc. IEEE Silicon Monolithic Integr. Circuits Rf Syst. (SiRF)*, Jan. 2014, pp. 71–73.

[21] H.-T. Dabag, J. Kim, L. E. Larson, J. F. Buckwalter, and P. M. Asbeck, "A 45-GHz SiGe HBT amplifier at greater than 25% efficiency and 30 mWoutput power," in *Proc. IEEE Bipolar/BiCMOS Circuits Technol. Meeting (BCTM)*, Oct. 2011, pp. 25–28.

[22] K. Datta and H. Hashemi, "Performance Limits, Design and Implementation of mm-Wave SiGe HBT Class-E and Stacked Class-E Power Amplifiers," in *IEEE Journal of Solid-State Circuits*, vol. 49, no. 10, pp. 2150-2171, Oct. 2014.

[23] S. Shakib, H. C. Park, J. Dunworth, V. Aparin and K. Entesari, "A Highly Efficient and Linear Power Amplifier for 28-GHz 5G Phased Array Radios in 28-nm CMOS," in *IEEE Journal of Solid-State Circuits*, vol. 51, no. 12, pp. 3020-3036, Dec. 2016.

[24] BiCMOS8HP Design Manual. Globalfoundries.

[25] S. Y. Mortazavi and K.-J. Koh, "A class F-1/F 24-to-31GHz power amplifier with 40.7% peak PAE, 15dBm OP1dB, and 50mW Psat in 0.13μm SiGe BiCMOS," in *Proc. IEEE Int. Solid-state Circuits Conf. (ISSCC)*, Feb. 2014, pp. 254–255.